Emission Reduction and Assisted Combustion Strategies for Compression Ignition Engines with Subsequent Testing on a Single-Cylinder Engine

By

J. Colter Ragone

Submitted to the graduate degree program in Mechanical Engineering and the Graduate Faculty of the University of Kansas in partial fulfillment of the requirements for the degree of Master of Science.

Chair: Dr. Christopher Depcik

Dr. Ronald L. Dougherty

Dr. Edward Peltier

Defended: July 26, 2012

The Thesis Committee for Colter Ragone certifies that this is the approved version of the following thesis:

Emission Reduction and Assisted Combustion Strategies for Compression Ignition Engines with Subsequent Testing on a Single-Cylinder Engine

By

J. Colter Ragone

Chair: Dr. Christopher Depcik

Acceptance Date

Accepted: July 27, 2012

Abstract

Due to increasingly stringent regulations set forth by the Environmental Protection Agency, engine researchers and manufacturers are testing and developing various emission reduction strategies for compression ignition engines. This thesis contains three sections where the author details two separate strategies for emission reduction and assisted combustion.

Combustion resulting from compression ignition diesel engines contains high levels of nitrogen oxides (NO_x) due to their lean operating characteristics. A common NO_x reduction strategy used by most automotive manufactures involves the use of cooled EGR (exhaust gas recirculation) to reduce combustion temperatures. However, a downfall to this method is the formation of particulate matter (PM) from the reduced combustion temperatures. This reduction in NO_x emissions with resulting increasing PM emissions describes the well-known NO_x-PM tradeoff. Typically, a reduction in one of the emissions will result in an increase in the other. Chapter two documents the construction and testing of a cooled EGR system for a single cylinder diesel engine along with subsequent performance and emission analysis. The result of the cooled EGR system demonstrates a reduction in brake specific NO_x due to reduced combustion temperatures, while decreasing brake specific PM due to increased turbulence. Resulting performance calculations displayed a slight increase in fuel consumption.

Chapter three analyzes the effects of ozone-assisted combustion on a single cylinder diesel engine. This work starts with a summarization of the literature in the field, which supports the simplified combustion model for determination of trends. Experimentation results demonstrate the addition of ozone causes a decrease in

ignition delay, which produces slightly higher in-cylinder temperatures. Due to the elevated temperatures and ozone decomposition, NO_x production increases, while PM decreases through radial atomic oxygen chemistry. Additionally, carbon monoxide emissions increase while hydrocarbon levels decrease. The changes in fuel consumption resulting from ozone injection are negligible. Of additional importance, this work verifies findings in the literature that demonstrate the effects of adding more ozone is negligible above a certain level of ozone injection (20 ppm in this effort). This is due to high concentrations of ozone facilitating its own destruction during the compression process of the engine.

Table of Contents

Table of Figures

CHAPTER 2: The Effects of Cooled Exhaust Gas Recirculation on Exhaust Emissions for a Single Cylinder Compression Ignition Research Engine

CHAPTER 3: The Influence of Ozone on Combustion of a Single-Cylinder Diesel Engine

Table of Tables

CHAPTER 2: The Effects of Cooled Exhaust Gas Recirculation on Exhaust Emissions for a Single Cylinder Compression Ignition Research Engine

CHAPTER 3: The Influence of Ozone on Combustion of a Single-Cylinder Diesel Engine

Nomenclature

Variable	Description	Units
a	Engine Crank Radius	(m)
A	Arrhenius Expression	(m^3/mol-s)
b	Engine Cylinder Bore	(m)
$bsfc$	Brake Specific Fuel Consumption	(g/kW-hr)
C	Molar Concentration	(mol/L)
c_v	Constant Volume Specific Heat	(J/kg-s)
E	Activation Energy	(kJ/mol)
EGR	Exhaust Gas Recirculation	(%)
e	Internal Energy of Individual Species	(J)
k	Rate Constant	(m^3/mol-s)
ℓ	Engine Connecting Rod Length	(m)
L	Number of Iterations	(-)
m	Temperature Dependency	(-)
$\dot{m}$	Mass Flow Rate	(g/s)
$\dot{m}_a$	Air Mass Flow Rate	(g/s)
$\dot{m}_f$	Fuel Mass Flow Rate	(g/s)
$\dot{m}_j$	Mass Flow of Exhaust Constituents	(g/s)
N	Engine Speed	(rpm)
P	Engine Output Power	(kW)

P_b	Engine Brake Power	(kW)
p	Pressure	(bar)
p_{intake}	Intake Pressure	(bar)
p_{amb}	Ambient Pressure	(bar)
Q_{lhv}	Lower Heating Value	(kJ/kg)
R_1	Reaction Rate for Reaction 1	(mol/m^3-s)
R_2	Reaction Rate for Reaction 2	(mol/m^3-s)
R	Gas Constant	(J/kg-K)
R_{amb}	Gas Constant of Air	(J/kg-K)
R_{air}	Gas Constant of Air	(J/kg-K)
R_u	Universal Gas Constant	(J/mol-K)
s	Engine Stroke	(m)
T	Temperature	(K)
T_{amb}	Ambient Temperature	(K)
V, $\mathbb{V}$	Cylinder Volume	(m^3)
V_d	Engine Displacement Volume	(m^3)
W	Molecular Weight	(g/mol)
x	Distance	(m)

X	Mole Fractions	(-)
Y	Mass Fractions	(-)
η_c	Combustion Efficiency	(%)
η_f	Fuel Conversion Efficiency	(%)
η_t	Thermal Conversion Efficiency	(%)
η_v	Volumetric Efficiency	(%)
$\dot{\omega}$	Reaction Rates	(mol/m^3-s)
ρ	Density	(kg/m^3)
ρ_a	Ambient Air Density	(kg/m^3)
θ	Engine Crank Angle	(º)
Subscripts		
1	Reaction 1	
2	Reaction 2	
amb	Ambient	
ex	Exhaust	
f	Fuel	
in	Intake	
j	Exhaust Species	
mix	Mixture	

1.1 Introduction

The use of diesel engines in passenger vehicles is constantly rising in the United States due to increasing fuel prices. Diesel engines contain several characteristics that provide advantages over typical gasoline fueled spark ignition (SI) engines. The first significant difference between compression ignition (CI) and SI engines is the lack of a spark plug. CI engines operate on lean mixtures and rely on injecting fuel into a highly compressed cylinder, to facilitate combustion. By using high air-to-fuel ratios, the fuel consumption of CI engines is noticeably lower than SI engines, and the ratio assists in the reduction of certain emissions such as particulate matter (PM) and hydrocarbons (HC) [1]. Mixing fuel and air does not occur before entering the cylinder, which removes the concern of engine knock for CI engines. Engine knock occurs in SI engines when the air and fuel mix inside the cylinder and combust under pressure before the desired time. This causes a loss in performance and can increase emissions resulting from partial combustion. CI engines only compress air inside the cylinder, which prevents engine knock from occurring. However, with the lean air-to-fuel ratios, power reduction is evident when directly compared to SI engines. In order to increase the power output, the addition of a turbocharger can increase the engine output power [1]. High amounts of boost are achievable since engine knock is not an issue.

With the addition of turbochargers and high compression ratios, CI engines operate under high cylinder pressures and temperatures. As a result, nitrous oxide (NO_x) emissions are of concern as high temperatures facilitate the formation of NO_x. In order to reduce these emissions, one approach is to alter run-time properties of the engine such as the injection timing, which alters the combustion temperatures and

pressures. A main concern stemming from these methods is the NO_x-PM tradeoff [2]. Generally, methods to reduce one emission results in the increase in the other and vice versa. This thesis will discuss the effects of cooled exhaust gas recirculation (EGR) as a NO_x reducing method, as well as the effects of ozone injection on the performance and emissions of the single cylinder diesel engine.

1.2 Single Cylinder Engine Test Cell and Prior Efforts

The engine implemented for testing at The University of Kansas is a Yanmar L100V single-cylinder, direct-injection diesel engine. In order to simulate engine loading, the engine was previously connected by driveshaft to a NorthStar AC electric generator. Load was applied to the engine through four resistance heating elements, each representing a 25% load. The resulting torque from the applied load was measured using a FUTEK (model #TRS605) transducer located between the engine and generator. Prior studies using this design, including work involving hydrogen injection and biodiesel blends, have led to publications in academic journals [3, 4].

This configuration was redesigned to accommodate updated equipment. The electric generator was replaced with a Dyne Systems, Inc. Dymond Series 12 horsepower air-cooled regenerative Alternating Current (AC) dynamometer. A Dyne Systems, Inc. Inter-Loc V OCS controller is utilized to control the dynamometer up to a maximum speed of 7500 revolutions per minute (RPM). The FUTEK torque sensor was replaced with a more robust model (model #TRS-605) which is connected between the engine and dynamometer shafts providing torque readings up to 200 N-m. As fuel consumption is a critical parameter for engine testing, a Micro-Motion Coriolis fuel flow meter (model #CMF010M) is used. The engine intake airflow is measured using a

laminar flow element (model #50MW20). In-cylinder pressure measurements are recorded by a Kistler 6052C piezoelectric transducer with a range from 0 to 250 bar with a minimal error of 0.5%. A Kistler 2614B1 encoder is used in conjunction with the transducer is bolted directly to the flywheel of the engine. An analog signal is sent by the encoder, which is converted to a digital crank angle via a Kistler signal converter (model #2614B2). Adjustment of the encoder angle is made possible by a Kistler pulse multiplier (model #2614B4). Pressure transducers and thermocouples are used throughout the test cell to record various temperatures and pressures, which in turn are recorded through a National Instruments-based data acquisition system using LabView.

Along with the installation of the engine dynamometer, upgrades include the installation of improved emission equipment. For previous studies, a Semtech-DS Mobile Emissions Analyzer (Sensors, Inc.) was used to measure carbon monoxide (CO), carbon dioxide (CO2), oxygen (O2), nitrogen oxide (NO), nitrogen dioxide (NO2), and total hydrocarbon (HC) concentrations from the engine exhaust. This unit was replaced with an AVL SESAM Fourier Transform Infrared Spectroscopy (FTIR) emissions analyzer. The FTIR retrieves a gas sample from the engine exhaust through a heated line in order to prevent condensation. The sample stream passes through a heated prefilter to eliminate particulates from entering the analyzing equipment. After the prefilter, the sample diverges into three separate components for measurement. These components include the FTIR analyzer, the Flame Ionization Detector (FID) which measures total hydrocarbons, and the Magnos 106 for oxygen measurement as the FTIR cannot measure diatomic molecules. Previously, particulate matter was captured using a Dekati PM10 low-pressure cascade impactor. This utilized 25 mm

polycarbonate filters, in 13 stages, which would collect particles ranging from 0.031 to 30 micrometers.

Exhaust flow was collected at a rate of 10 liters/minute by a Sogevac Leybold vacuum pump connected to the impactor. The filter masses were recorded prior to, and after, PM testing in a controlled temperature and humidity environment. The PM measurements would require an additional hour long emission test in order to provide sufficient data. This configuration was replaced by an AVL 415S Variable Sampling Smoke Meter. A volume of exhaust gas is sampled through a probe connected to the exhaust pipe. This volume is drawn through a filter paper with subsequent measurement using an orifice flow meter. The blackening of the filter paper is recorded as a Filtration Soot Number (FSN) and as a soot concentration in mg/m^3. The sample time required for this equipment ranges between 6 and 180 seconds as opposed to 60 minutes with the previous setup. As different amounts of PM are generated by the engine under varying loads, the sample time is adjusted in order to generate a blackening number between 1 and 6 for accuracy. For this study, a blackening number of 4 was desired, leaving the sample time to be adjusted accordingly.

1.3 Yanmar Limitations

Emission data is displayed on a brake specific basis in order to provide a direct comparison with larger production engines. However, there are limitations of the Yanmar, which create difficulty for that comparison. The next few paragraphs will discuss these restrictions and the actions moving forward in order to assess them.

The Yanmar engine is limited to an operating speed of 3600 RPM. This limitation is due to the controlling of the direct injection system by a mechanical fuel pump and

governor. The engine was originally paired with a NorthStar AC generator, whose 60 Hz electric generation matched the 3600 RPM of the engine. For research purposes, this is not ideal for comparison between larger production vehicle engines, as engine performance at multiple speeds and injection timings are not possible. Effort is currently being applied to address the issue by upgrading the system to an electronic rail pressure system. This configuration provides subsequently higher injection pressure, intended to more effectively mimic the high pressures utilized in modern production engines. The electronic injection will allow the operator to control the speed of the engine, as well as injection timing in order to gain a greater understanding of performance and emission characteristics.

As previously mentioned, CI engines benefit greatly from the addition of a turbocharger. In fact, most current production vehicle diesel engines come equipped with a turbocharger. As the Yanmar is naturally aspirated, this leads to significantly different operating conditions and efficiencies as compared to production engines. However, there is ongoing collaboration with a local turbocharger company to provide an appropriately sized turbocharger for the Yanmar. Following installation, the data obtained from the turbocharged engine will be shared with the local company for possible future upgrades and modifications.

1.4 Thesis Focus

As previously discussed, diesel engine emissions are a major cause for the low percentage of on road diesel vehicles in the United States. This study focuses on two separate methods for emission reduction as well as assisting the combustion process. A common method of reducing NO_x emissions by engine manufacturers is using EGR.

This recycles the hot exhaust gas back into the intake of the engine where it acts as a heat sink. The exhaust gases do not facilitate the combustion process, but merely take up volume inside the cylinder, resulting in lower temperature combustion. As the influence of temperature on NO_x generation is significant, EGR effectively reduces these harmful emissions. The implemented Yanmar engine did not have an EGR system prior to this study, resulting in the need for the design, fabrication, and testing of a system. As found in the literature, which will be discussed in Chapter 2, cooling the exhaust gases before they enter the cylinder increases the efficiency of NO_x reduction. The author took this information and implemented a complete cooled EGR system for the Yanmar engine.

Modification of the Yanmar exhaust by implementing a control ball valve allows the operator to control EGR flow to the engine. As CO_2 concentrations in ambient air are minimal, calculation of the percentage of EGR is done by comparing the ratio of CO_2 in engine intake air to the amount in the exhaust resulting from combustion [5-8]. For these measurements, two K-33 ICB 30% CO_2 sensors measure samples from the exhaust and the intake. The sensors are mounted inside a protective case with a pump to supply a constant flow of 1.5 L/min to the sensors. Collection and viewing of real time data is possible with DAS100. This is a data acquisition program developed by CO_2 Meter, Inc. and displays readings at a rate of 0.5 Hz. The exhaust gas passes through a series of filters before reaching the CO_2 sensors in order to prevent water and particulates from altering the sensor readings. The filters include a 200 micron PM filter, water trap, and a 0.22 micron hydrophobic filter. To reduce the exhaust gas temperature, the exhaust passes through a heat exchanger with cooling fans, each

moving air at 133.6 cubic feet per minute (CFM). For this study, both fans operate at maximum speed, however, the system was designed with future work in mind, as the fan speeds can be adjusted to produce a desired temperature of EGR. This will allow for future work and the investigation of the differences between "hot" and "cool" EGR. Exiting the heat exchanger, the exhaust gas passes through a second ball valve (left full open for this study) before entering the mixing chamber where the EGR and fresh intake air collide. The second ball valve is in place for future use with a stepper motor to allow for automated and transient flow with engine loading.

Chapter 3 covers the influence of ozone on combustion through a literature review, kinetic model, and engine testing. The model uses necessary decomposition equations found in the literature to simulate the effects on combustion in the Yanmar engine. With results from the model, the necessary equipment was assembled in order to supply ozone to the intake of the engine. The system includes an Absolute Ozone ATLAS 30 Ozone Generator, which provides 30 g/hr maximum ozone output with 14% ozone concentration by weight. An AirSep Onyx Plus Oxygen Concentrator supplies pure oxygen to the ozone generator as a source gas. Using pure oxygen eliminates impurities from the air, resulting in efficient ozone generation. Ozone injection occurs at the intake of the engine, with sampling occurring downstream to measure the ozone concentration of the intake. A 2B Technologies Ozone Concentration Monitor (model #106-M) measures the ozone concentration up to 1000 ppm (parts per million) with 2% accuracy. The current ozone generation system provides up to 430 ppm ozone, which falls into the range of the monitor.

References

1. Heywood, J.B., *Internal Combustion Engine Fundamentals*1988, New York: McGraw-Hill, Inc.
2. Abd-Alla, G., *Using exhaust gas recirculation in internal combustion engines: a review.* Energy Conversion and Management, 2002. **43**(8): p. 1027-1042.
3. Cecrle, E., et al., *An Investigation of the Effects of Biodiesel Feedstock on the Performance and Emissions of a Single-Cylinder Diesel Engine.* Energy & Fuels.
4. Cecrle, E.D., *Controls and Measurements of KU Engine Test Cells for Biodiesel, SynGas, and Assisted Biodiesel Combustion.* 2011.
5. Agrawal, A.K., et al., *Effect of EGR on the exhaust gas temperature and exhaust opacity in compression ignition engines.* Sadhana, 2004. **29**(3): p. 275-284.
6. Lim, G., et al., *Effects of HPL and LPL EGR Gas Mixed Supply on Combustion and Emissions in Automotive Diesel Engine.* SAE International, 2011.
7. Bihari, B., et al., *Diagnostics for Combustion Metrics in Natural Gas Fuelled Reciprocating Engines.* 2011.
8. Yoshimura, T., M. Miyai, and H. Nakamura, *Transient Exhaust Gas Recirculation Ratio Measurement Utilizing Heated NDIR Method*, 2012, SAE International.

CHAPTER 2: The Effects of Cooled Exhaust Gas Recirculation on Exhaust Emissions for a Single Cylinder Compression Ignition Research Engine

Christopher Depcik[1], Michael Mangus[1], Colter Ragone*[1]

[1] University of Kansas, Department of Mechanical Engineering

1530 W. 15th Street, Lawrence, KS 66045-4709

* Corresponding author: colterragone@gmail.com

2.1 Abstract

The high emission levels of nitrogen oxides (NO_x) from lean combustion involving direct injection hinder the use of Compression Ignition (CI) or diesel engines in passenger vehicles. In order to address this species, most automotive manufacturers include cooled EGR in order to reduce combustion temperatures. However, as combustion temperatures decrease, particulate matter (PM) emissions increase causing the well-known NO_x-PM tradeoff. Typically, a reduction in one of the emissions will result in an increase in the other. This work documents the construction of a cooled EGR system for a single cylinder diesel engine in order to update the engine to be more representative of modern combustion systems. Moreover, this effort analyzes the resulting effects on performance and emissions. The results of the manufactured cooled EGR system illustrate a decrease in brake specific NO_x through reduced temperatures, while the increased turbulence also reduces PM emissions. The resulting performance calculations indicate a slight increase in fuel consumption.

2.2 Introduction

Compression Ignition (CI) or diesel engines operate with relatively high air to fuel ratios as compared to Spark Ignition (SI) engines. Without the use of spark plugs, the start of combustion relies on high compression ratios producing elevated temperatures in order to achieve auto-ignition. Because of the resulting ratio of specific heats and the increase in expansion work, CI engines obtain higher thermal efficiencies than SI engines. However, the abundance of oxygen and high flame temperatures leads to significant emissions of nitrogen oxides (NO_x), which are mostly comprised of nitrogen monoxide (NO) and nitrogen dioxide (NO_2) [1]. A common and effective method of reducing NO_x in diesel engines is with Exhaust Gas Recirculation (EGR) [2-4]. This method works by throttling the engine and recycling exhaust gases back into the intake of the engine. The products being re-circulated include carbon dioxide (CO_2), water (H_2O), carbon monoxide (CO), hydrogen (H_2), oxygen (O_2), NO_x, nitrogen (N_2), unburned hydrocarbons (HC) and particulate matter [1, 5]. Over 99% of diesel exhaust is comprised of CO_2, H_2O, N_2, and O_2 with the remaining 1% being emissions pollutants which are typically harmful to the environment and humans [1]. These gases are inert and act as a heat sink inside the cylinder since they typically do not participate in the combustion event. Moreover, EGR occupies space inside the cylinder leading to less volume of fresh air needed for combustion. Hence, the addition of EGR reduces the oxygen concentration [1, 6-8]. These conditions decrease combustion temperatures that in turn reduce NO_x emissions largely through reducing the chemical kinetic rates of the thermal NO mechanism [5].

The use of EGR in production vehicles has been around since 1973, leading to an extensive amount of available literature on the subject. As regulations from the EPA (Environmental Protection Agency) changes constantly requiring cleaner emissions, EGR as a system has also been evolving. As mentioned previously, the goal of EGR is to decrease flame temperatures in the combustion chamber in order to reduce NO_x emissions. However, exhaust gas temperatures can reach over 700 °C for some vehicles [9]. As a result, using hot exhaust gas to reduce in-cylinder temperatures is still effective, as the exhaust constituents do not facilitate the combustion process; however, the exhaust gas raises the temperature of the intake mixture slightly mitigating the heat sink effect while facilitating a hotter combustion chamber. Alternatively, cooled EGR more effectively reduces cylinder component temperatures and wall heat losses while largely eliminating any rise in intake temperatures [9]. For this topic, conducting a brief literature review over the recent applications of EGR systems helps provide a relevant understanding of the material and leads the exploration within this paper.

In 1998, Zelenka et al. investigated the effects of cooled EGR on turbocharged diesel engines. They determined that lower EGR rates, around 12%, were ideal for high engine loads; whereas, rates up to nearly 30% at low load were effective [10]. The reason for high ratios of EGR under low engine loads, and low ratios of EGR for higher loads relates to the amount of CO_2 and H_2O returning to the intake. In particular, at high loads the concentrations of these species increased leaving less room for oxygen and efficient combustion. These conditions reduced NO_x emissions in their study to as low as 2 g/kW-hr with the use of cooled EGR. In order to optimize EGR performance, they modified their turbocharger layout resulting in an increase in brake specific fuel

consumption (*bsfc*) of about 2 to 3%. Alongside the decrease in NO_x emissions, they observed a progressive increase in particulate matter (PM) emissions. This NO_x-PM "trade-off" is a widespread phenomenon regarding the use of EGR and other emission reduction strategies. Generally, a characteristic change leading to the reduction of NO_x will result in an increase in PM, and vice versa. The balancing act between these emissions increases the difficulty in finding an ideal method of reducing emissions to meet EPA standards.

In Zelenka et al.'s effort, they utilized an EGR-cooler in order to reduce the temperatures of the exhaust gas. The maximum cooling capabilities required 30 kW, which was approximately 15% of the rated engine power. As a result, one negative impact of the addition of an EGR cooling loop is the power draw required to reduce the EGR temperatures. Other areas of possible concern comprise fouling or leaking of the system, as well as condensation building up within the cooler.

In 2002, Abd-Alla investigated the potential of EGR to reduce NO_x emissions. The discussion in this paper mentions further the tradeoff between NO_x and PM with EGR aggravating this trend, especially at high loads. Results in this paper demonstrate a maximum EGR percentage of up to 30% before the desired results begin to diminish and engine combustion becomes unstable; e.g., too much inert products interfering with oxygen finding the fuel. Results from their testing determined that hot EGR improves the thermal efficiency of the engine due to an increased intake charge temperature and the re-burning of the unburned combustion products resulting in a faster heat release. Compared to hot EGR, cooled EGR resulted in a lower thermal efficiency, but had a greater influence on the reduction of NO_x emissions [2]. Observing the trends of hot and

cold EGR, the cold EGR shifted the NO_x-PM tradeoff toward the lower end of NO_x emissions while the hot EGR shifted in the other direction comparatively.

At the same time, McGeehan et al. investigated the wear characteristics resulting from diesel engines using cooled EGR. This work states that the most influential variable influencing NO_x is peak cylinder temperature because of the thermal kinetic mechanism of NO production [3]. They note that two methods work to decrease NO_x emissions, cooled EGR or delayed injection timing. Their work illustrates that EGR is the more favorable option since it provides a 10% increase in fuel economy over delayed timing. Furthermore, their research indicates that using ranges from 5-25% of cooled EGR can produce reductions in NO_x formation of 30-75%. For control of the EGR temperature, they employed an air-to-air intercooler that reduced the temperature from 210°C to 43°C.

In the following year, Agrawal et al. investigated the effect of EGR on exhaust gas temperatures and opacities for diesel engines. Measuring the opacity of the exhaust provides a metric for PM calculations since the more opaque the exhaust, the more PM is present in the exhaust gas. They mention that a simple method for NO_x reduction occurs with late injection of fuel (delayed injection) into the combustion chamber. This delayed injection reduces combustion temperature, but will increase fuel consumption by 10-15% [4]. They find that EGR is more effective for NO_x control since the fuel consumption does not decrease at that drastic a rate. They tested a range of EGR from 0-21% under eight different engine loads. Similar to the other literature, NO_x decreases with EGR addition and the NO_x-PM tradeoff was evident as PM emissions increased especially at higher loads. Agrawal et al. mention that diesel engines

generally excel in characteristics such as fuel consumption and CO emissions, with their main drawback being NO_x emissions. As a result, controlling the engine for NO_x with regard to the tradeoff is a preferred option since manufacturers can treat the increase in PM with particulate traps and adequate regeneration methods. Furthermore, EGR did not significantly influence the calculated thermal efficiency and fuel consumption.

In 2004, Zheng et al. compiled an extensive review of diesel engine exhaust gas recirculation. They discussed the effectiveness of using EGR as a NO_x reduction method while illustrating that it will increase the amount of PM. Their test results indicated that cooled EGR reduces NO_x more effectively than hot EGR because of the added reduction in intake charge temperatures resulting in lower flame temperatures [1]. They also note that diesel engines tend to generate more PM with higher load since there is a reduction of oxygen as compared to low loads. As a result, the addition of EGR at high loads effectively generates more PM since it provides a second reduction factor on the amount of available oxygen. Hence, the use of EGR at high loads was determined to be ineffective for altering the NO_x-PM tradeoff. Therefore, one should delay the fuel injection for these instances in lieu of EGR for NO_x control.

The next year found Kim and Lee investigating the effects of cooled EGR on emissions of a Homogeneous Charge Compression Ignition (HCCI) engine. Their testing indicated that EGR led to a slower combustion rate and later combustion phasing, resulting in lower peak pressures and combustion temperatures [11]. These conditions led to a decrease in NO_x but increased the amount of PM. Moreover, EGR suppressed the sharp increase of heat release at high temperatures, making ignition more stable at high loads.

In 2007, Kawano et al. studied two forms of EGR on a turbocharged CI engine using biodiesel. Aftertreatment devices included a Diesel Particulate NO_x Reduction (DPNR) system which acted as both as a Diesel Particulate Filter (DPF) and a NO_x Storage Reduction (NSR) catalyst. The methods of incorporating EGR involved separation into a high-pressure loop (HPL) and low-pressure loop (LPL). The HPL system circulated the EGR directly from the exhaust manifold back to the intake. The LPL passes through the turbo, the DPNR, and then back into the engine intake. Of importance, an increase in the level of EGR for the HPL reduced NO_x without elevating the amount of PM [12]. They explained this suppression of PM formation as being due to the oxygen content in the rapeseed oil methyl ester (RME) used for testing. In addition, the EGR from HPL produced lower HC, PM, and fuel consumption than LPL but higher CO emissions. The LPL EGR resulted in a higher cylinder pressure than HPL EGR due to its interaction with the turbocharger. The HPL system resulted in a loss of boost pressure, whereas the LPL did not. Note that biodiesel in general acts to reduce PM emissions [13]; hence, one must be careful when comparing trends for PM emissions when using different fuels. In addition, their LPL system provided cooler temperatures (112°C vs. 34°C). Moreover, from their location of the sampling, the LPL preserved boost pressure. Hence, their efforts demonstrate a number of non-linear effects.

The subsequent year Kruger et al. investigated the effects of cooled EGR systems with the hopes of meeting future exhaust regulations. Through their experiments, they concluded that a two stage low temperature EGR system provides the most desirable results and is a significant step toward achieving cleaner emissions

with lower fuel consumption [14]. The first stage in their setup cooled the exhaust gas using coolant from the main engine circuit. The second stage reduced exhaust gas temperature further using coolant from a separate low temperature circuit. This method provided cooler EGR temperatures before mixing with the intake air, thus lowering the charge temperatures. They found a 2% improvement in fuel consumption with cooled EGR over hot EGR with the two-stage low cooling system reducing NO_x levels to 0.85 g/kW-hr. They achieved this improvement in fuel consumption by setting an earlier start of fuel injection for the engine; e.g., cooled EGR worked to reduce NO_x more effectively allowing the operator to adjust injection timing to match hot EGR NO_x levels while improving fuel economy.

More recently, similar to Kawano et al. [12], Lim et al. studied the EGR effects of HPL and LPL on diesel engine emissions. Their results indicated an increase in CO and HC emissions, which were stated to be attributed to the low intake air temperatures as LPL EGR increased [15]. They concluded that a low temperature intake charge produced incomplete combustion, resulting in increased CO and HC even though these emissions largely relate to excess air levels (e.g., amount of oxidizer typically plays a larger role than intake temperature). Both systems successfully reduced NO_x while they additionally saw an improvement in PM emissions with the increase of LPL EGR resulting from the homogeneous charge. The LPL EGR had significantly more time for mixing with fresh air due to the physical layout of the system. These characteristics created a more homogeneous mixture that decreased PM emissions.

As the literature illustrates, CI engines employ EGR for NO_x control; therefore, any research engine requires the addition of an EGR loop in order for the results to

remain pertinent. Moreover, given the prevalence of cooled EGR in production engines today, the experimental setup must also cool this EGR loop effectively. Therefore, the goal of this study is to construct and analyze a cooled EGR system for a single-cylinder diesel research engine. This will involve analysis of a few of the pertinent phenomena as found from the literature discussed in this section:

- EGR participates in the NO_x-PM trade-off leading to higher PM emissions and lower NO_x emissions while potentially increasing CO and HC emissions through a reduction in combustion efficiency
- However, the mixing of EGR and the intake can lead to higher levels of mixing potentially offsetting this NO-PM trade-off
- Hot EGR may lead to a higher thermal efficiency over cooled EGR because of the increase in cylinder temperatures; however, generally the use of EGR may lower thermal efficiency by reducing the rate of combustion (e.g., less constant volume combustion)
- Cooled EGR as opposed to hot EGR results in a more significant reduction in NO_x because it reduces the intake (over hot EGR) and cylinder wall temperatures more effectively leading to a relatively colder combustion
- One should use high ratios of EGR under low engine loads, and low ratios of EGR for higher loads since at higher engine loads, the amount of CO_2 and H_2O returning to the intake increases, resulting in lower oxygen levels that subsequently reduce the combustion efficiency

- EGR often results in an increase in the fuel consumption of the engine due to both a lower combustion efficiency and thermal efficiency through slower combustion rates
- EGR is advantageous over delayed injection timing for controlling NO_x because of a smaller increase in fuel consumption

The following sections describe the installation of the required equipment for a cooled EGR loop. Of importance, prior to this study the single-cylinder engine in the advisors laboratory did not include EGR, resulting in the construction of a complete system.

2.3 Equipment Installation

This study required the design and installation of a complete cooled EGR system for the single-cylinder Yanmar CI engine, as shown in Figure 1. In particular, this involved the installation of two K-33 ICB 30% CO_2 sensors in order to determine the amount of exhaust gas returning to the intake. With the capability of measuring up to 30% CO_2, these sensors are within the operating range for this work, as well as any future testing where CO_2 emissions might increase.

The amount of carbon dioxide in the ambient air is minimal, which leads to a relatively simple method of monitoring the amount of EGR by measuring the CO_2 concentration in the intake of the engine [1, 16-19]. By comparing the ratio of CO_2 in the intake to the exhaust, a representation of EGR can be measured as follows [1]:

$$EGR(\%) = \frac{[CO_2]_{in}}{[CO_2]_{ex}} \times 100 \quad (1)$$

where the *in* and the *ex* nomenclature represents the intake and exhaust, respectively.

Since there is a small amount of CO_2 in the ambient air, and the hardware used has the capability to measure low concentrations, a more accurate reading of EGR can be made by taking into account the ambient CO_2 [4, 15, 20, 21]:

$$EGR(\%) = \frac{[CO_2]_{in} - [CO_2]_{amb}}{[CO_2]_{ex} - [CO_2]_{amb}} \times 100 \quad (2)$$

where the *amb* nomenclature represents the ambient air.

The first sensor samples the midstream exhaust gas in order to determine the concentration of CO_2 exiting the engine. The exhaust sample then travels through a set of filters including a 200-micron PM filter, a water trap, and finally a 0.22-micron hydrophobic filter before entering the sampling case as shown in Figure 2.

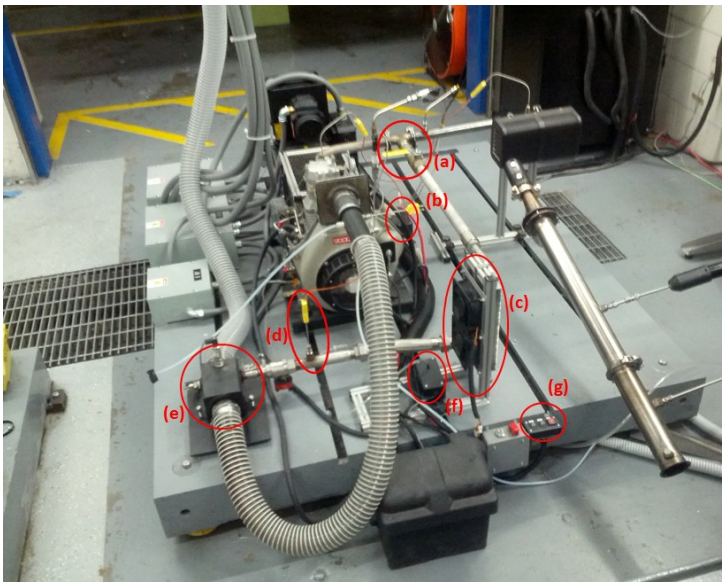

Figure 1. Picture of the Locations of the (a) EGR Valve, (b) Exhaust CO_2 Sensor, (c) Heat Exchanger and Cooling Fans, (d) Cooled EGR Thermocouple, (e) Mixing Chamber, (f) Intake CO_2 Sensor, and (g) Control Switch for CO_2 and Cooling Fans.

Figure 2. Filtration System for CO_2 Sensors. Top: PM Filter (200 micron), Middle: Water Trap, Bottom: Hydrophobic Filter (0.22 micron).

Located inside the sampling case is a pump that pulls from the sample line and feeds the CO_2 sensor with a constant flow of 1.5 L/min as shown in Figure 3. A USB connection sends the CO_2 reading to a computer where the software program DAS100 monitors concentration at a rate of 0.5 Hz. DAS100 is developed by CO_2 Meter, Inc. and allows viewing of real-time data while storing testing logs. The control of the flow rate of EGR happens using a manual control ball valve located on the exhaust as shown in Figure 1(a). The exhaust gas then flows through the heat exchanger with cooling fans, each moving air at 133.6 CFM shown in Figure 4.

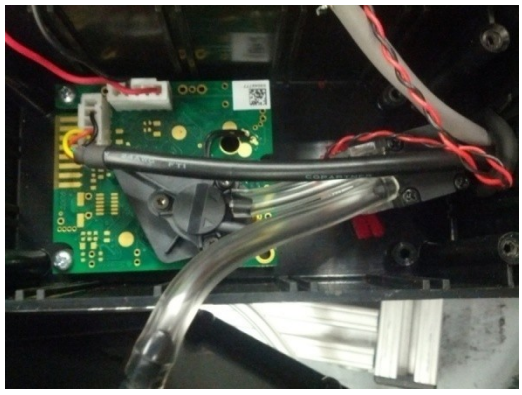

Figure 3. K-33 ICB CO_2 Sensor on the Left with Pump Sensor on the Right.

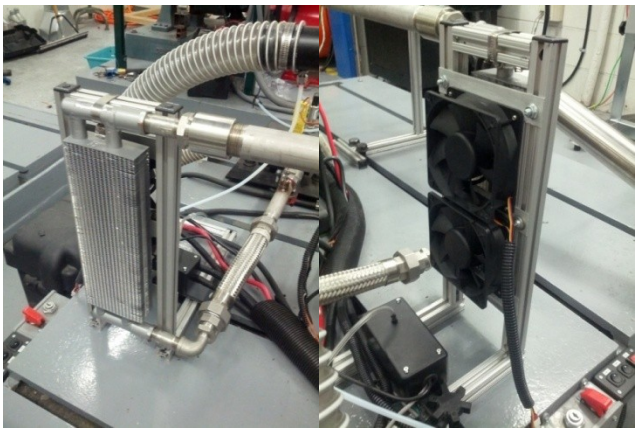

Figure 4. Heat Exchanger on the Left and Cooling Fans on the Right.

Figure 5.Toggle Switches for Fans and CO_2 Measurement.

The goal of this effort is to demonstrate the maximum capabilities of the cooled EGR setup. As a result, the testing efforts presented later utilized both fans running at maximum speed. The setup employs toggle switches for these fans alongside the power switch for the CO_2 sensors in Figure 5. The ability to toggle the fans will create opportunities for future testing with respect to different levels of cooled EGR. Moreover, the system allows for the installation of a control system in order to monitor EGR temperatures and adjust fan speed respectively. Both fans operate at the top speed of 3000 RPM. For future testing, students can add a potentiometer to the yellow power

wire of each fan allowing for a variable voltage adjustment. This will allow the user to adjust the fan RPM in order to achieve variable cooling results.

After exiting the heat exchanger, the exhaust gas traverses into a mixing chamber where it will premix with intake air before entering the engine. The addition of a thermocouple directly before the mixing chamber allows for measurement of the temperature of the EGR before interacting with ambient intake air as seen in Figure 6. In addition, the inclusion of a secondary control valve before the mixing chamber with the ability to pair with a stepper motor and control system allows future researchers to adjust the EGR flow rate automatically without having to manually step into the test cell. In addition, this leaves the possibility for investigating transient EGR flow as a function of engine loading in future testing. Calculation of the EGR fraction required the installation of second CO_2 sensor sample line directly before the mixed air enters the engine in order to determine the amount of exhaust gas re-entering the engine.

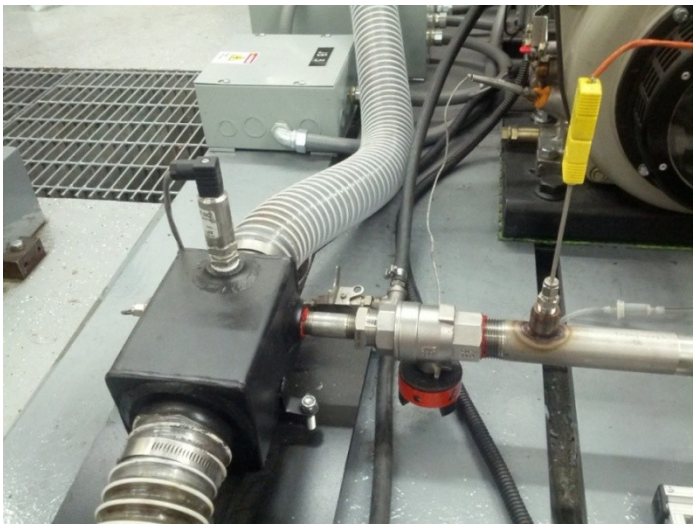

Figure 6. EGR and Intake Flow into Mixing Chamber with Secondary Control Valve and Thermocouple.

Preliminary testing of the system resulted in a maximum flow of approximately 10% EGR. A greater pressure drop from the engine to the muffler was evident, as compared to the pressure drop of the exhaust from the engine to the EGR system. In order to increase the flow rate of EGR, either the exhaust or intake needed to be throttled as elucidated by the literature [1, 10, 12, 20]. Since throttling of production engines for vehicles is a common occurrence, the installation of a throttle valve results in a closer relationship between the test cell engine and real world applications. Due to the high temperatures of the exhaust, it was more reasonable to find a throttle and install it on the intake of the engine. This increases the pressure drop between the exhaust and the intake resulting in a higher flow rate. A throttle valve, shown in Figure 7, was installed downstream of the laminar flow element in order to retain a laminar intake flow through this element for calculation of airflow rates. The resulting addition of the throttle valve allowed for a flow of roughly 25% EGR across all engine loads.

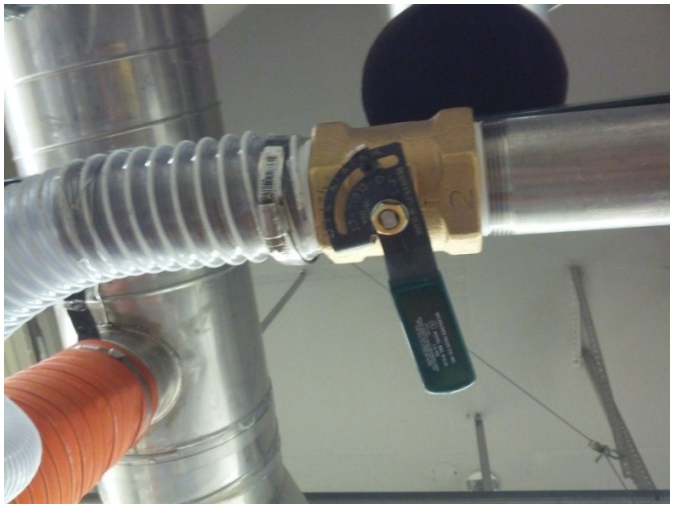

Figure 7. Intake Throttle Valve Downstream of the Laminar Flow Element that Measures Intake Air Flow Rates.

2.3.1 Emissions

For emission data collection, this work employs a Vetronix PXA-1100 five-gas analyzer that measures of HC, CO, CO_2, O_2, and NO_x (NO and NO_2). While other emissions analyzers are available in the laboratory, since the primary analyzer used in the past (Semtech DS) was out for repair, and the new analyzer was not ready for usage (AVL FTIR), the choice of this five-gas analyzer allowed for project completion given time commitments. The Non-Dispersive Infrared (NDIR) Gas Measurement Bench utilized by this equipment meets or exceeds BAR90 and OIML Class 1 standards. The emissions analyzer interfaced with TechView software used on a dedicated laptop for data storage and analysis as shown in Figure 8.

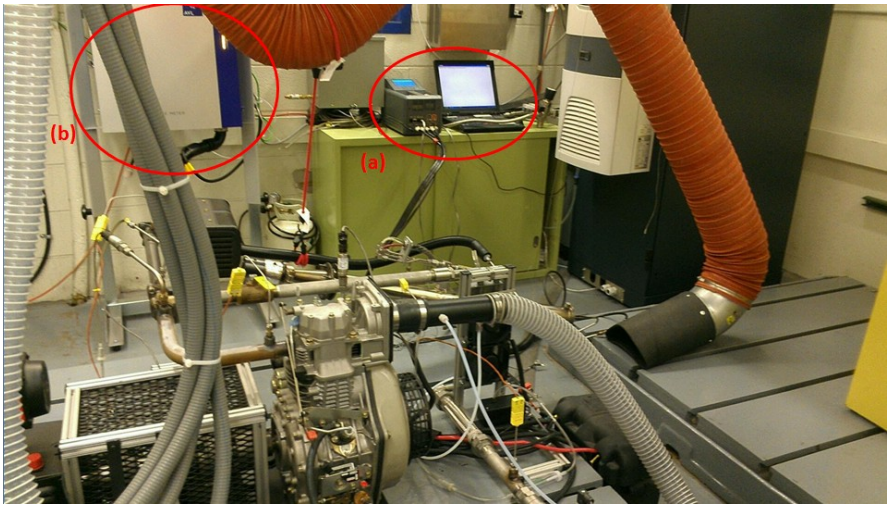

Figure 8. Emission Analysis Equipment (a) PXA-1100 5-Gas Analyzer and Laptop along with (b) AVL Smoke Meter.

Particulate matter is measured with an AVL 415S Variable Sampling Smoke Meter. Through a probe built into the exhaust of the Yanmar, the device samples a volume of exhaust. Calculation of an effective length is done by drawing this volume through a filter paper with subsequent measurement using an orifice flow meter. Detection of the blackening of the filter paper due to PM occurs through use of an

optical reflectometer head. From the filter paper blackening and effective length values, the software calculates a Filtration Soot Number (FSN) and soot concentration in mg/m^3. Note that the operator adjusts the sample time according to the level of filter paper blackening. This is because different run-time conditions of the engine can produce a wide range of PM measurements. If the sampling volume remains constant for all conditions, the filter paper may blacken completely, resulting in inaccurate data. Ideal operating conditions specified by the manufacturer lie in-between the range of one to six for filter paper blackening. For repeatability, the paper blackening number remained at four for this set of testing.

2.4 Experimental Setup

In order to generate reliable and repeatable results, this effort employs a single-cylinder engine for testing. The use of a single-cylinder engine eliminates the non-linearity in fluid mechanics and heat transfer of multi-cylinder engines allowing for a clearer identification of trends from ozone injection [13, 23]. The single-cylinder engine for this experiment is a direct-injected Yanmar L100V diesel engine (see Table 1 for specifications). A Dyne Systems, Inc. Dymond Series 12 horsepower air-cooled regenerative Alternating Current (AC) dynamometer acts as the load upon the engine with a maximum speed of 7500 rpm while utilizing a Dyne Systems, Inc. Inter-Loc V OCS controller. A FUTEK rotary torque sensor (model #TRS-605) connected between the engine and dynamometer shafts provide torque readings for the system and can measure from 0-200 N-m. This range of readings eliminates any limiting factors from the torque sensor on the engine, including signal saturation due to torque spikes, while allowing for possible future testing under a higher power output.

Table 1: Engine and Dynamometer Specifications [13]

Engine	Value
Manufacturer and Model	Yanmar L100V
Type	Vertical Direct-Injection Compression Ignition
Engine Intake	Naturally Aspirated
Cooling	Air-Cooled
Cycle	4-Stroke
Displacement	435 cc
Number of Cylinders	1
Number of Valves	1 Intake, 1 Exhaust
Bore	86 mm
Stroke	75 mm
Connecting Rod Length	0.118 m
Crank Radius	0.038 m
Clearance Volume	2.1611×10^{-5} m^3
Cylinder Head/Piston Area	0.0058088 m^2
Compression Ratio	21.2
Injection Timing	15.5 (+/- 0.5) degrees BTDC
Intake Valve Close	122 degrees BTDC
Exhaust Valve Open	144 degrees ATDC
Continuous Rated Output	8.3 hp SAE
	6.2 kW
Rated Speed	3600 RPM
Injector Pressure	19.6 MPa
Aftertreatment	None
Engine Oil Used	Shell 15W-40
Dynamometer	
Manufacturer and Model	Dyne Systems, Inc.Dymond Series 12
Continuous Torque	21.1 ft-lbs
Continuous Power	12 hp
Speed Range	0-7500
Voltage	480 V
Phase	Three-phase
Frequency	60 Hz
Controller	Dyne Systems, Inc. Inter-Loc V OCS

Instrumentation for the engine includes thermocouples for ambient air temperature, engine intake temperature, exhaust port temperature, and downstream exhaust temperature. A Kistler 6052C piezoelectric transducer measures the pressure inside the cylinder of the diesel engine and is calibrated to measure from 0 to 250 bar

with a minimal error of 0.5%. A Kistler2614B encoder is used in conjunction with the transducer, and is bolted directly to the flywheel of the engine. The encoder sends an analog signal that is converted to digital crank angle and TDC signals via a Kistler signal converter (model #2614B2). Employing a Kistler pulse multiplier (model #2614B4) allows adjustment of the encoder angle resolution from 0.1º to 6º. A National Instruments-based data acquisition system using LabView records these digital crank angle and pressure signals. This allows for highly accurate pressure readings at 0.5 degree increments. A Micro-Motion Coriolis flow meter (model #CMF010M) provides the mass flow and density measurements of the fuel. A Merriam laminar flow element (model #50MW20-2) paired with an Omega differential pressure transducer (model #PX277-30D5V) calculates the airflow readings. Additional sensors include ambient and exhaust pressure along with the relative humidity of the test cell environment.

2.5 Test Strategy

The effects of four different separate concentrations of EGR (approximately 0%, 10%, 20%, and 25%) were tested at five engine-loading conditions during the same day at the same engine speed (3600 rpm): 0.5 N-m, 4.5 N-m, 9.0 N-m, 13.5 N-m, and 16.75 N-m. Note that the current engine equipment limits engine speed to 3600 rpm because of the mechanical unit injector system and speed governor employed. Future efforts include replacing this system with a rail injection system for complete control of the injection event for testing under different engine speeds. In order to produce comparable results for the no load cases, a minimal load of 10 W was applied in order to provide corresponding values for brake specific fuel consumption (*bsfc*) and emission data in g/kW-hr [22]. As mentioned in the prior section, an AC dynamometer applied

the load during each test. The experimental data was captured once the engine and EGR flow reached steady state, which was taken to be the time when the temperature of the downstream exhaust port and intake CO_2 concentration changed less than one percent per minute. Collection time for emissions on each load was five minutes, with a sample rate of one sample per second. Sample time for particulates varied between 30 and 120 seconds. In particular, in order to produce accurate and repeatable results, a blackening number of four was targeted. Hence, the adjustment of sample times for different engine loads achieved the desired blackening number. Sampling commenced only when reaching steady-state under each load and specific EGR addition. Taking engine performance metrics for two minutes during the emission testing at a rate of ten samples per second provided low experimental error. Moreover, the LabView setup records in-cylinder pressure traces concurrently to the performance and emissions data. The sample rate for pressure readings occurred at a 0.5-degree crank angle resolution, and the results presented later are composed of an average of 60 thermodynamic cycles. Experimental error analysis includes calculation of the relative standard error for each data point. Furthermore, the plots within the results and discussion section provide linear trend lines, in some circumstances, in order to help with the visual identification of the trends.

2.6 Results and Discussion

The goal of this study was to find a simple method of obtaining the coolest EGR possible in order to reduce NO_x emissions. During testing, use of a thermal infrared camera (FLIR E40) allowed for a visual illustration of the cooling process occurring within the system. Figure 9 provides for a comparison of the engine and exhaust

temperatures along the cooled EGR system. The thermal imaging offers a clear, visual understanding of the heat loss along the exhaust and through the heat exchanger. Figures 9 (c) and (d) show a comparison between the heat exchanger with no EGR and full EGR. The images demonstrate a well-defined temperature gradient moving through the heat exchanger. The result is that the return line for the cooled EGR to the mixing chamber is nearly the same temperature as the ambient surroundings.

One of the main concerns of this study was the reduction of EGR temperature before entering the intake. Figure 10 (a) presents the EGR temperature before interacting with the intake air in the mixing chamber, and the temperature of the engine intake air before entering the cylinder. Figure 10 (a), as well as the thermal imaging pictures, illustrates cooling of the EGR to nearly the ambient temperature (Figure 10(c)) before entering the mixing chamber. For some cases, the system lowers the EGR temperature a few degrees Kelvin below the ambient intake temperature, which is measured at a higher physical location in the test cell. Since heat rises in the test cell, the air circulation system pulls through the ceiling (facilitating convection), and temperatures increase notably during long testing, this is indeed a possible outcome. In particular, the ambient temperature does vary throughout the testing. A noticeable increase is evident between the 10 W test and the other trials. The 10 W test was conducted first, resulting in a cooler test cell since the engine was not running previously adding heat to the room; hence, this helps validate the reasoning behind why the EGR temperature may be below the intake temperature.

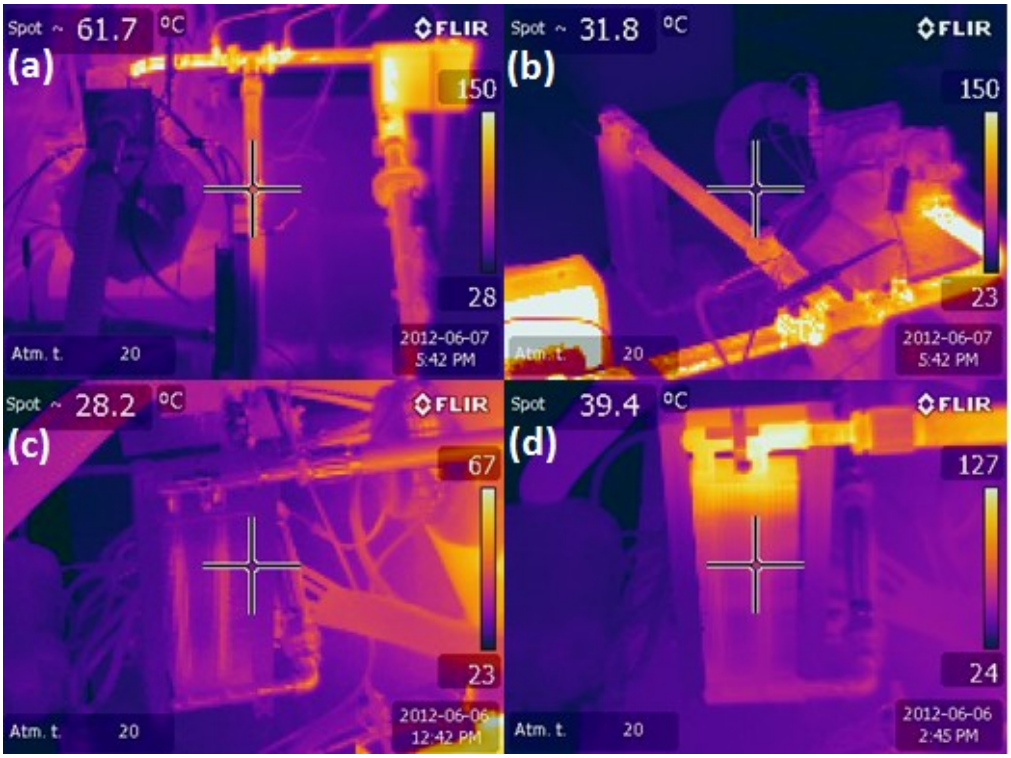

Figure 9. Thermal Imaging Taken of Testing Components including (a) Yanmar Engine and Exhaust with EGR Cooling in Foreground, (b) Yanmar Engine and Exhaust with EGR Cooling in Background, (c) EGR Cooling Heat Exchanger with No Flow through EGR System, and (d) EGR Cooling with Maximum Flow.

As illustrated in Figure 10 (b), the EGR system employed did not appreciably increase the engine intake temperature (measured closer to the engine and hotter due to convection around the engine and radiation from the exposed engine cooling fins). This result is ideal since the goal of EGR is to reduce NO_x emissions by decreasing the temperature of combustion. As previously discussed, the use of EGR provides a heat sink inside the cylinder during combustion by acting as a diluent. In production vehicles, the exhaust gas temperature can reach up to 450 °C in passenger vehicles and up to 700 °C in commercial vehicles [9]. By sending exhaust gases at those levels of elevated temperatures back into the cylinder, the intake air temperature rises, facilitating the production of NO_x; e.g., if combustion starts hotter, it will end hotter. The diluent effect offsets this thermal rise component; however, thermal rise still leads to some NO_x

production. By adding cooled EGR at ambient temperatures, not only are the gases inert and not participating in the combustion process, but they do not provide a thermal energy component.

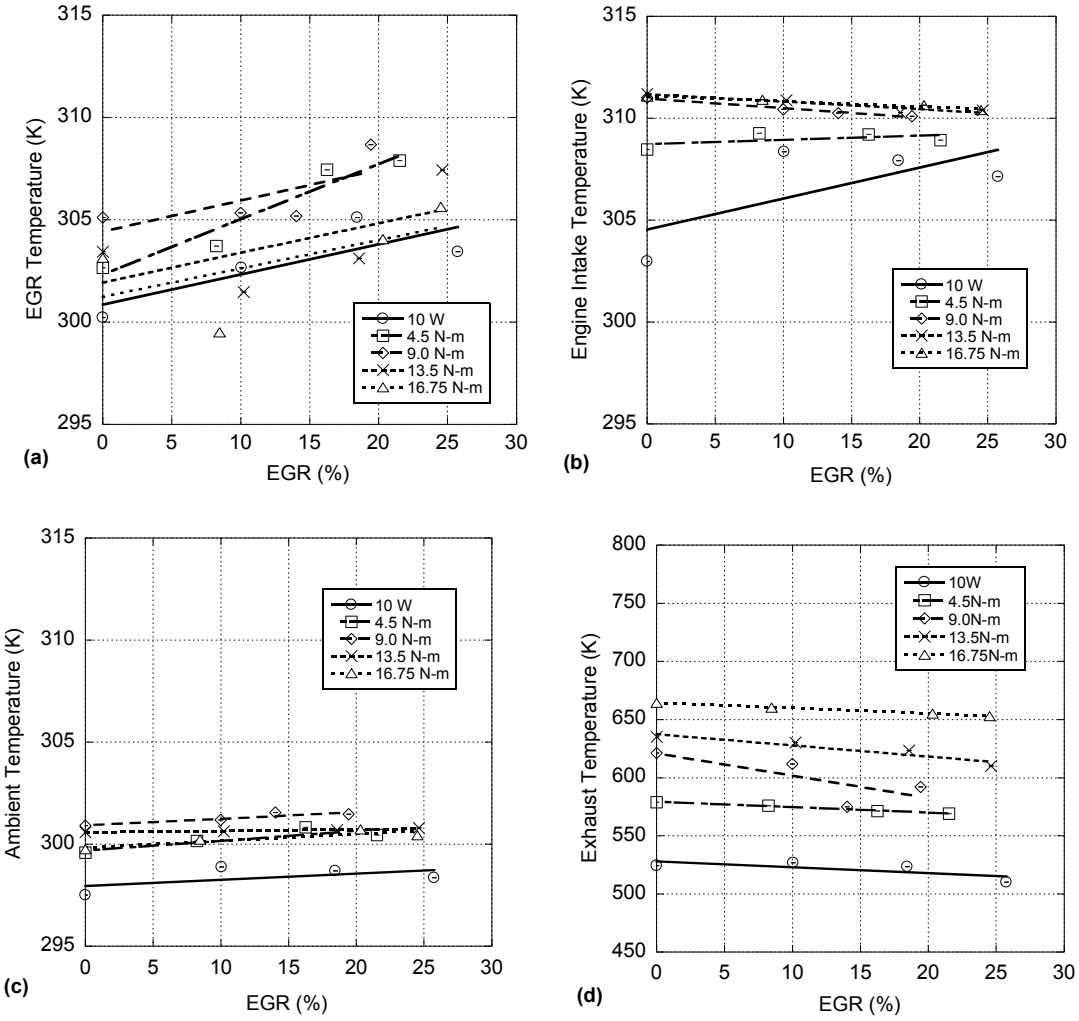

Figure 10. Temperatures Resulting from EGR Percentage of (a) Cooled Exhaust Gas, (b) Engine Intake Before Entering Cylinder, (c) Ambient Air Temperature, and (d) Exhaust Temperature.

As Figure 10 (d) depicts, increasing engine load causes the exhaust temperature to rise. More of fuel entering the engine leads to a greater energy release and hotter combustion temperatures (illustrated through the in-cylinder pressure plots discussed next) resulting in augmented exhaust temperatures. In conjunction with this effect, the

EGR temperature for the most part increases slightly with loading, as the hotter exhaust gas is relatively harder to cool (some of the deviation through load will be discussed later as a function of volumetric efficiency). Moreover, EGR temperature increases with the level of EGR added, since more of the hot exhaust gas is circulating through the system making it relatively harder to cool. However, this change is less than 1% of the overall temperature. Observing the trends in exhaust temperature with increasing EGR, it is evident that the temperature decreases with more EGR. This is expected since relatively colder combustion happens from the heat sink effect along with the fact that there is less fresh air in the cylinder to facilitate combustion.

In-cylinder pressure traces provide valuable information when attempting to understand the effects of altering run-time properties. Figure 11 presents the in-cylinder pressure profiles for increasing cooled EGR percentages at different loads with the average EGR percentage for each test given in the legend. Observing the changes in ignition delay (time between the fuel injection event that is held constant by the injection system and the start of combustion indicated by a rapid pressure rise) and peak pressure assists the analysis of the influence of cooled EGR on emission characteristics. For these reasons, the plots present results between -10° to +15° after top dead center (ATDC) in order to provide a snapshot of the combustion initiation process. From Figure 11, the addition of cooled EGR generates a clear trend for all engine loads by increasing the ignition delay. This relates to the fact that EGR is largely inert and does not significantly contribute to the combustion process. Hence, it becomes harder to initiate the combustion process since the inert mixture that draws in available energy surrounds the fuel rather than an oxidizer. As a result, the adiabatic

flame temperature drops when introducing EGR. Furthermore, combustion now happens later in the expansion process when the piston is acting to expand the working fluid. This adds an additional pressure reduction component since combustion is happening away from an ideal situation; e.g., TDC where pressures and temperatures are highest after compression.

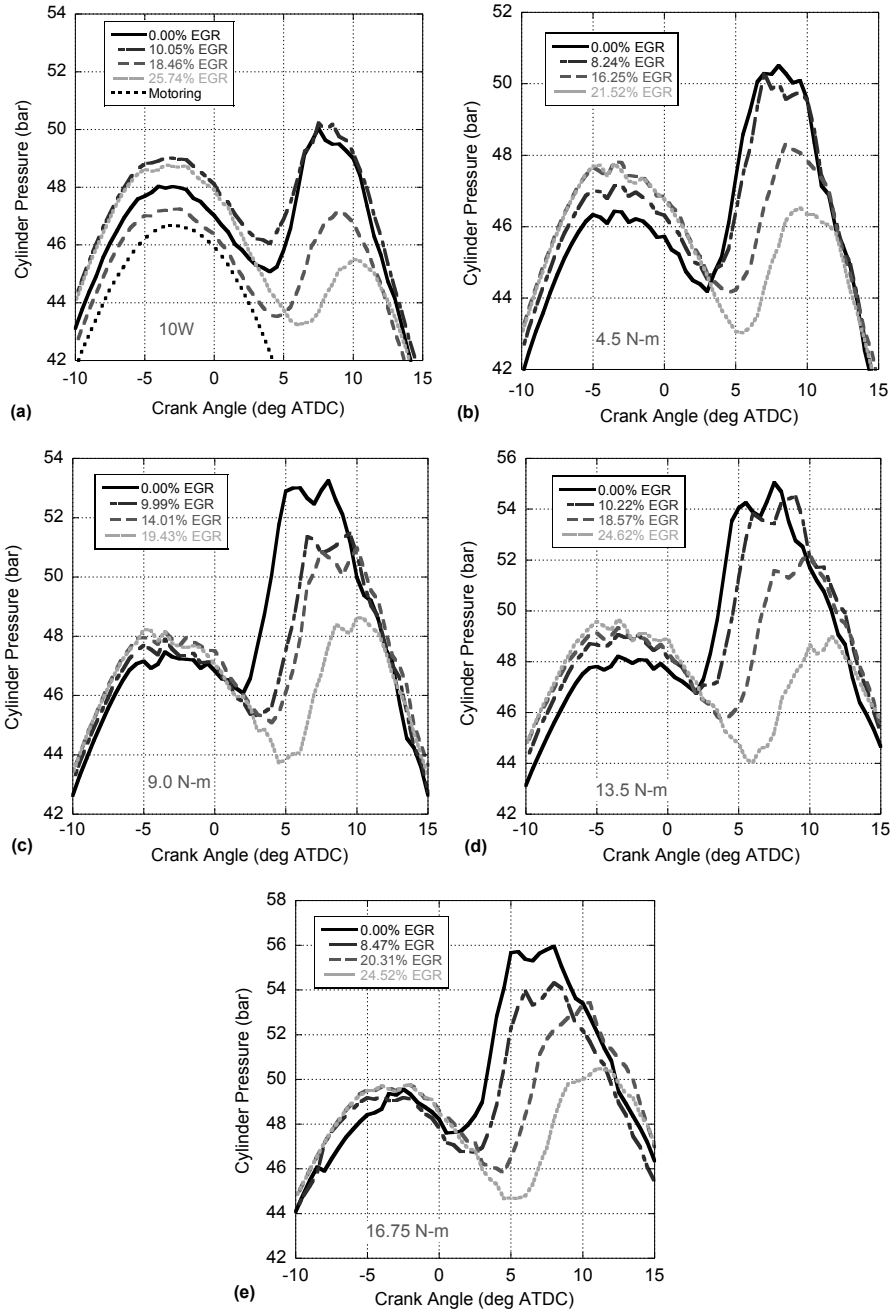

Figure 11. In-cylinder Pressure Traces at (a) 10W, (b) 4.5 N-m, (c) 9.0 N-m, (d) 13.5 N-m, and (e) 16.75 N-m as a Function of Increasing EGR.

Interestingly, adding EGR increases the cylinder pressure during the compression process leading to higher pressures at TDC. Since EGR comes from an unthrottled loop (exhaust is unthrottled unlike intake) that includes the high-pressure exhaust blow down process, this mixing effect increases the pressure during the intake

process (Figure 12) leading to a higher compression pressure. Moreover, this pressure drop between the intake and exhaust increases the level of turbulence in the intake. Note that because compression is exponential in nature, a small increase in initial conditions (less than a percent) leads to a significant pressure rise at TDC. Finally, with respect to engine loading, the pressures and ignition delays follow the expected trends; e.g., higher pressures, and shorter delays with increasing load. This relates to the increased level of combustion temperatures because of a larger energy release.

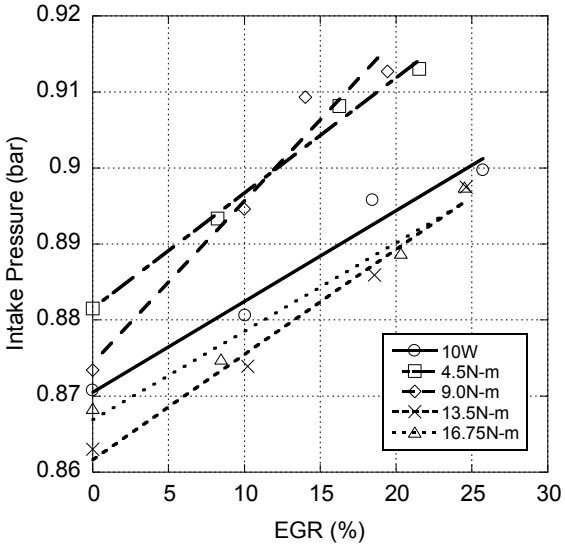

Figure 12. Intake Pressure as a Function of EGR Percentage and Engine Load.

The inverse relationship between NO_x and cooled EGR flow in Figure 13 is approximately linear showing a reduction in NO_x of over 70% for most cases with maximum EGR. As mentioned previously, the reduction of NO_x is a result of three properties of cooled EGR. The first is the thermal diluent effect that decreases the thermal NO mechanism kinetic rates. The second is a lower temperature of combustion due to a reduction of intake air. In other words, less oxidizer is available to produce a hot burn. Finally, combustion phasing plays a role as in-cylinder pressures and temperatures decrease as more combustion happens later in the expansion process.

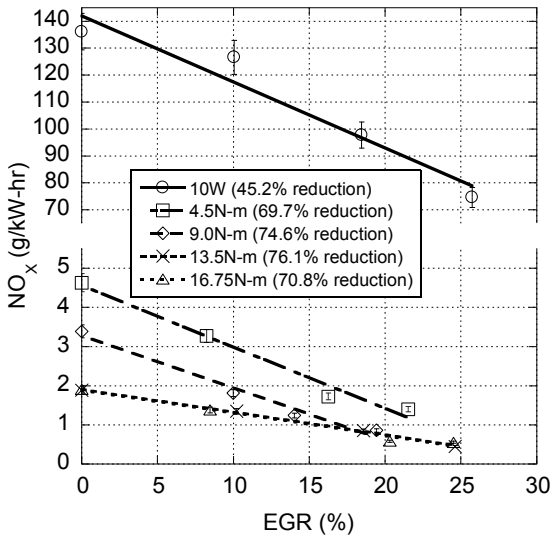

Figure 13.Influence of EGR and Engine Load on NO_x Emissions.

Observing NO_x production trends with respect to engine loading, a decrease is evident. As load is applied, combustion temperatures increase promoting the production of NO_x. However, the engine operates more efficiently (presented later), resulting in the use of less fuel for the required power increase. With the results on a brake specific scale, the NO_x levels decrease with an increase in engine load as the resulting power output from the engine outweighs the temperature influence on NO_x production. Recalling the literature, high ratios of EGR are beneficial for low engine loads, and conversely low ratios of EGR for higher engine loads, as the amount of CO_2 and H_2O returning to the intake increases, resulting in lower oxygen levels. Figure 13 provides the percentage decrease in NO_x from no EGR to the highest EGR in the legend. From a strictly NO_x reduction standpoint, high levels of EGR still appear to be effective at high engine loads for this particular engine. Further testing at higher loads may help illustrate the limit of the oxidizer-to-CO_2/H_2O ratio.

Calculation of the volumetric efficiency illustrates the influence of EGR on the intake air level. This variable characterizes how effectively the engine brings in air in

relation to the volume displaced by the piston. A poor volumetric efficiency would be a result of the engine pulling in a low amount of air, and not displacing the piston to its full capability. The calculation of volumetric efficiency (η_v) follows as:

$$\eta_v = \frac{\dot{m}_a}{2 \cdot \rho_a \cdot N \cdot V_d} \times 100 \quad (3)$$

where $\dot{m}_a$ is the air mass flow rate, ρ_a is the ambient air density, N is engine speed, and V_d is the engine displacement volume. Use of the ideal gas law allows for calculation of the ambient air density:

$$\rho_a = \frac{p_{amb}}{R_{air} \cdot T_{amb}} \quad (4)$$

where p_{amb} is the ambient pressure of the test cell, R_{air} is the gas constant specific to air, and T_{amb} is the ambient air temperature of the test cell. Furthermore, from the bore and stroke of the engine, one can compute the displacement volume from the bore (*b*) of the engine and its stroke (*s*):

$$V_d = \frac{\pi b^2}{4} s \quad (5)$$

As mentioned previously, the recycled exhaust gas takes up space that could be occupied by fresh air. Therefore, since exhaust gases contain a relatively smaller fraction of O_2 than ambient air, there is less oxidizer available for combustion. Figure 14 demonstrates this influence as the volumetric efficiency decreases with an increase in EGR, similar to Abd-Alla [2]. However, with respect to loading there is no defined trend. In particular, Figure 14 shows a distinct difference in volumetric efficiency for two of the test loads.

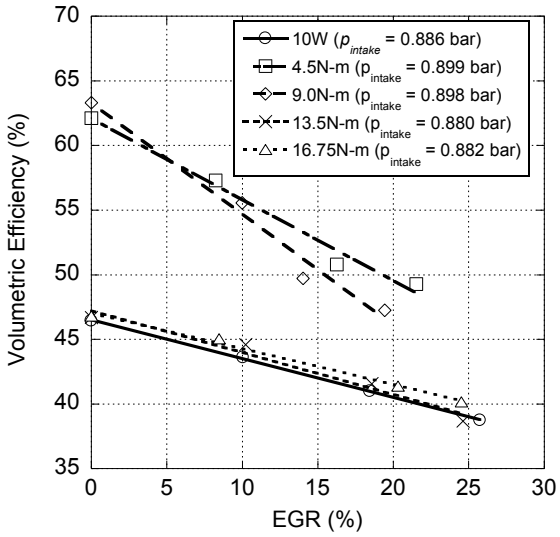

Figure 14.Volumetric Efficiency as a Function of EGR Percentage and Engine Load.

Due to conditions beyond the authors' control, changing of the throttle valve location was necessary in order to insure safe operating conditions of the equipment. In particular, completed tests began with the 10 W, 16.75 N-m and 13.5 N-m loads. However, halfway through the 9.0 N-m test, a weld on the exhaust broke. After fixing this the next day, testing commenced; however, upon startup of the engine, the throttle valve closed causing the vibration chamber (barrel) to collapse. After fixing this chamber, the researchers moved the throttle valve from between the laminar flow element and chamber to between the engine and the chamber. This is because keeping the throttle in the original position caused the chamber to flex. Hence, the experimental setup did change, and this will require retesting of the results generated in this work before subsequent publication. Due to time commitments and the fact that the goal of this effort was to explore the cooled EGR system, Dr. Depcik agreed that the results presented here are sufficient for thesis completion. Further testing can explore the influence of volumetric efficiency with load. Although the magnitude of volumetric

efficiency changed, the EGR trends are still clear, with volumetric efficiency decreasing as a function of increased EGR. Note that this also explains the difference in intake pressures as a function of load in Figure 12.

Further explaining the reduction in NO_x emissions with load requires calculation of the brake specific fuel consumption (*bsfc*). Brake specific fuel consumption is a normalized value that compares fuel economy among different engine designs (e.g., makes the comparison of a single-cylinder to a multi-cylinder engine feasible). It represents the amount of fuel required to produce a given power output, with a lower value being more advantageous:

$$bsfc = \frac{\dot{m}_f}{P_b} \quad (6)$$

where $\dot{m}_f$ is the mass flow rate of the fuel and P_b is the brake power provided by the engine.

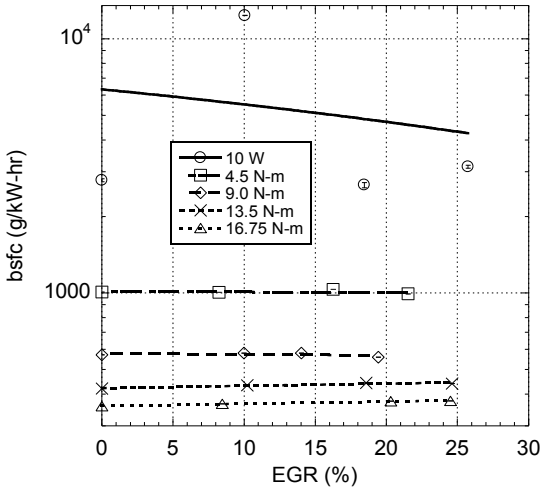

Figure 15. Changes in *bsfc* Resulting from Cooled EGR and Engine Load.

Figure 15 shows that *bsfc* decreases with increasing engine load, indicating that less fuel is required to generate more power. This is because the adiabatic flame temperature increases due to the global equivalence ratio of the engine increasing. This

coincides with more energy released, and higher peak pressures, as shown previously in the pressure plots. Enhanced energy release leads to more "constant volume like" combustion, resulting in faster combustion rates along with greater combustion efficiency. Furthermore, this decreases the ignition delay by increasing the rate of breaking initial hydrocarbon chemical bonds, resulting in earlier combustion facilitating even higher temperatures and pressures. In short, increased engine load creates hotter, faster, and more efficient combustion processes, resulting in a lower *bsfc*. In general, it is difficult to draw conclusions on a brake specific basis for extremely low loads. As previously discussed, *bsfc* ratios of the amount of fuel used to the power output of the engine. With virtually no load applied, the power output, i.e., the denominator, is near zero. In a testing environment, relatively large uncertainties occur at this low power level. In other words, there can be large fluctuations in torque levels because of less than ideal combustion conditions [23]. Hence, there may be data in this situation that does not fit the expected trends. A constant power output of 10 watts was used for the no load case in an attempt to normalize the results, but as shown in the figures, the irregularities cannot always be corrected.

As shown in Figure 15, in general the trends indicate a slightly increasing *bsfc* with the addition of cooled EGR; e.g., a higher fuel flow rate in order to provide the same amount of power. This is because the combustion temperature decreases with increasing EGR addition (explained in depth through the reduction in cylinder pressure). This is similar to the results found by Agrawal et al. who found a slight increase in *bsfc* with EGR addition as discussed in the introduction [4]. One item not discussed regarding the in-cylinder pressure plots is the rate of combustion. On top of the

previously discussed effects (thermal diluent, replaces O_2, and reduces ignition delay), EGR acts to slow the combustion process after initiation. Hence, it acts as a barrier preventing oxidation from occurring and ends up reducing the rate of heat release [11]. Future work in Dr. Depcik's laboratory will include a heat release analysis in order to discuss this effect in more detail.

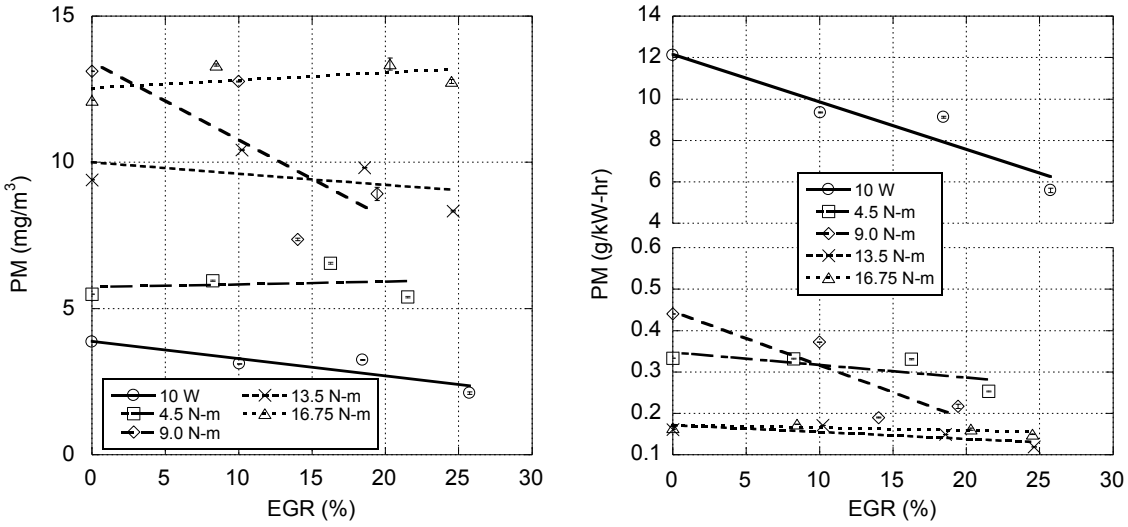

Figure 16. Influence of EGR on PM Emissions on a Concentration Basis (left plot) and from a Brake Specific Analysis (right plot).

As discussed previously, altering run-time properties can lead to a shift in the NO_x-PM tradeoff, an increase in one emission will typically decrease the other. Figure 13 illustrates a decrease in NO_x; hence, there is an expectation of an increase in PM. However, Figure 16 demonstrates a reduction in PM with increasing EGR. When the cooled EGR enters the mixing chamber of Figure 6, it creates turbulent flow of the intake air since they intersect at a 90-degree angle and has a higher pressure than the intake. The enhanced turbulence in the intake, along with a better mixing of EGR and intake air, makes its way to the cylinder and increases turbulence during the combustion process. This increases the level of homogeneity of the mixture creating a more

uniform combustion process. In specific, the heterogeneity of in-cylinder direct injection is the primary cause of the production of PM [24]. Hence, any increase in the mixing process will lead to reduced PM levels [15]. Therefore, with respect to the trend as a function of EGR, opening the throttle valve causes a greater percentage of the exhaust to flow back into the intake, rather than out of the exhaust pipe. This will increase the level of mixing while also allowing a second chance to re-burn some of PM produced the first time through the cylinder. Therefore, even though combustion temperatures are decreasing, which would act to decrease PM oxidation levels, it appears that the influence of mixing is the dominant factor. Future work presents itself for modeling the turbulence inside the mixing chamber, in order to help determine the influence of mixing and turbulence on PM.

Observing the PM trends across all loads in Figure 16 illustrates that PM emissions on a concentration basis largely increase with load. Initial thoughts are that this is opposite to what should occur. Since combustion temperatures are increasing, the level of oxidation of PM should increase along with combustion efficiency. While this is indeed true as indicated by the growing pressures with load in Figure 11, this figure also shows that combustion phasing does not change dramatically when adding more fuel. In particular, the rise in maximum pressure between no load and full load (no ozone) is around 6 bar while combustion starts within a few degrees of 3° ATDC in all cases. Instead, the width of the combustion pressure profile increases with load. Because of the mechanical injector system employed on the engine, at higher loads, fuel is not sent into the engine earlier toward TDC for more power (most likely to keep NO_x emissions low), instead more fuel is sent in later during the expansion process. In

this situation, the piston expands the working fluid causing lower pressures and temperatures. In other words, the engine is sending in more fuel during a less optimal time for combustion. Moreover, more fuel with similar initiation characteristics leads to a similar premixed burn fraction that subsequently increases the level of diffusion burn, which is now occurring under relatively lower expansion temperatures. Hence, PM emissions will increase with load for this particular engine design. Calculating PM on a brake specific basis demonstrates no definite trend after removing the no load values. This relates to the change in the volumetric efficiency and the influence of differing airflow levels as a function of load. Hence, when the airflow changes, the mass flow of fuel adjusts accordingly, subsequently resulting in the total mass flow rate of exhaust gases changing as well, influencing this trend.

In order to assist further in the explanation of the PM results, the combustion efficiency (η_c) is a beneficial performance parameter to calculate. Combustion efficiency is the amount of fuel energy released during the combustion process. In essence, it is a measure of the conversion of fuel chemical energy into potential thermal energy useful for power (not resultant power, potential for power). Included in the analysis are heating values of the fuel and exhaust constituents:

$$\eta_c = \left[1 - \frac{\sum_{j=1}^{n} \dot{m}_j \cdot Q_{lhv,j}}{\dot{m}_f \cdot Q_{lhv,f}} \right] \times 100 \qquad (7)$$

where $\dot{m}_j$ is the mass flow rate of the exhaust constituents, $Q_{lhv,j}$ is the corresponding lower heating values, $\dot{m}_f$ is the fuel mass flow rate, and $Q_{lhv,f}$ is the lower heating value of the fuel. Hydrogen is a common exhaust constituent necessary for accurate

combustion efficiency calculations, as it has a significant lower heating value (120 MJ/kg). Unfortunately, the ability to measure hydrogen was not available for these tests. However, the amount of hydrogen can be estimated by assuming similar molar ratios of H_2O:CO_2 and H_2:CO [13, 23, 25]. Note that for this calculation, the lower heating value used for HC emissions was estimated at 44,700 kJ/kg-K [13, 23], and PM is estimated to have a lower heating value equal to carbon at 32,810 kJ/kg-K [26] since this species is its primary constituent.

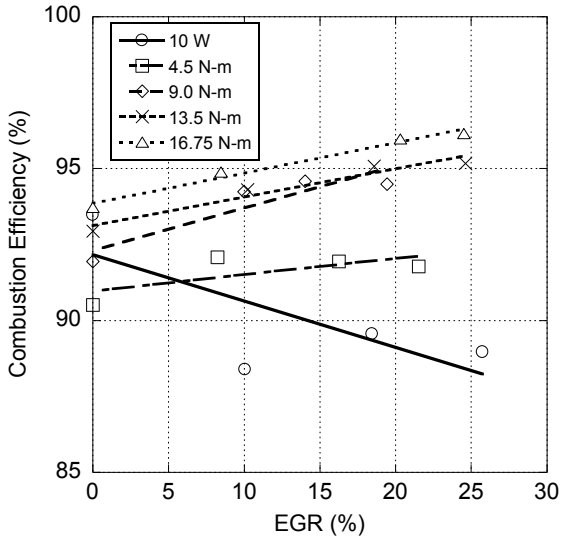

Figure 17. Combustion Efficiency as a Function of EGR and Engine Load.

As shown in Figure 17, the combustion efficiency increases with both cooled EGR and engine loading, except for the no load case that is difficult to quantify for reasons previously stated. As shown for the in-cylinder pressure profiles, an increase in EGR creates a lower temperature and pressure combustion. This generates a slower combustion process and drifts away from an ideal situation. Hence, the assumption would be that this decreases the combustion efficiency. As stated before, the fuel mass flow rate increases with the an increase in EGR causing greater available energy content that can act to reduce the combustion efficiency. Furthermore, the reducing PM

levels with EGR illustrate an enhanced mixing component. In essence, increased homogeneity will lead to a more complete burn. Therefore, it appears that the increased level of mixing outweighs the influence of slower combustion rates and reduced temperatures. In addition, combustion efficiency increases with engine load. Higher loads result in larger combustion temperatures and pressures (Figure 11), leading to greater energy released from the fuel and higher combustion efficiency.

Another useful calculation from the experimental data is the fuel conversion efficiency (η_f) which measures the efficiency of useful (aka shaft) work resulting from added fuel energy:

$\eta_f = \frac{P}{\dot{m}_f \cdot Q_{lhv,f}} \times 100$	(8)

where *P* is the output power of the engine, $\dot{m}_f$ is the mass flow rate of the fuel, and $Q_{lhv,f}$ is the lower heating value of the fuel. Computation of this parameter allows one to calculate the thermal efficiency of the engine (η_t):

$\eta_t = \frac{\eta_f}{\eta_c} \times 100$	(9)

from the combustion efficiency. The thermal efficiency tells the researcher how effective the engine is in converting the potential thermal power into actual power. In simplistic terms, it provides a relative measure of how “constant volume like" combustion is. The more that the combustion becomes like the constant volume process, the more instantaneous the heat release promoting the highest temperatures and pressures (e.g., constant volume combustion, or the Otto cycle, which is the theoretical maximum thermal efficiency of an engine).

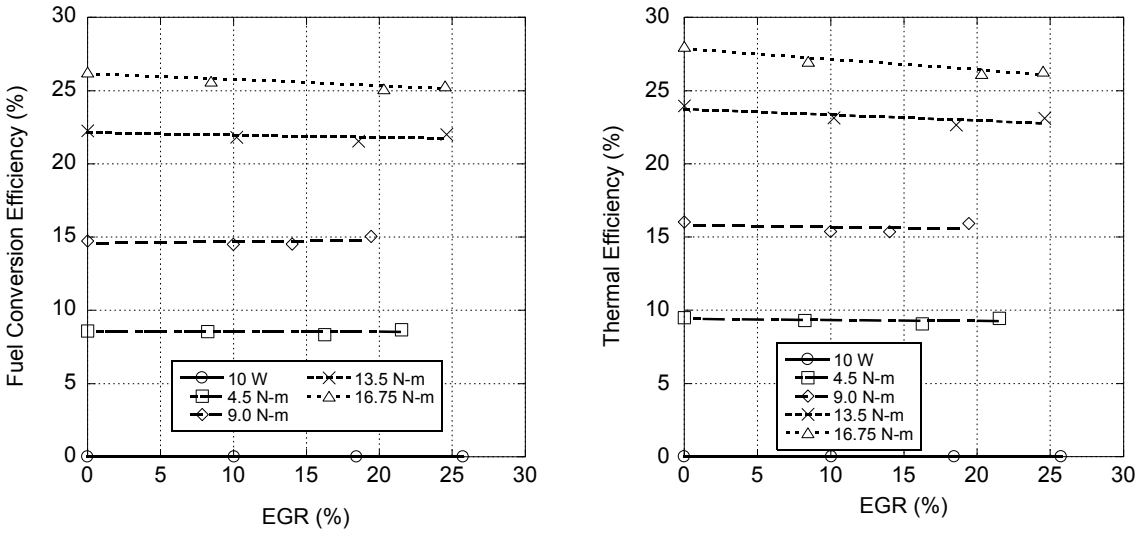

Figure 18. Calculations of Fuel Conversion and Thermal Efficiencies as a Function of EGR and Engine Load.

Observing the trends with an increase in EGR, the fuel conversion efficiency generally decreases, especially at higher loads. While mixing levels increase along with combustion efficiency, EGR acts as a thermal diluent, replaces O_2, reduces ignition delay, and slows the combustion rate. Hence, fuel conversion efficiency will decrease (also evident through a rise in *bsfc*) as shown in Figure 18. After removing the combustion efficiency influence through calculation of the thermal efficiency, the influence of EGR beyond mixing becomes more readily apparent. With respect to load, the more fuel that is added, the larger the energy released and the faster the heat release rate. Hence, higher temperatures and quicker combustion leads to better thermal efficiencies. Combined with enhanced combustion efficiencies this leads to a better fuel conversion efficiency.

Along with the influence of PM upon human health, carbon monoxide levels are a concern for any engine investigation since they are also harmful to the respiratory system. Carbon monoxide is a result of partial combustion; therefore, it should directly correlate with EGR since it influence the combustion event. Figure 19 illustrates that

an increase in cooled EGR assists in the reduction of CO for all EGR fractions tested. Based on the reduction in combustion temperatures and heat release rate, a lower level of oxidation should occur leading to greater CO emissions. However, the re-circulation of engine exhaust facilitates a second chance for combustion. Moreover, the reduced temperatures resulting from EGR lead to less dissociation which decreases the production of CO from CO_2 (analogous to NO_x from N_2 in the thermal NO mechanism). In addition, the mixing from the EGR and intake path creates a more homogeneous charge and more complete burn, as shown by the increasing combustion efficiency, which can act to decrease CO emissions. Hence, the cumulative effect of these influences causes a reduction in CO emission with increasing EGR.

With respect to CO emission decreasing with load, the previous discussion illustrates that higher combustion temperatures lead to an increased formation of CO from dissociation. However, this also increases the level of oxidation in the cylinder, subsequently reducing CO emission as seen through the combustion efficiency results. Moreover, as the NO_x discussion mentions, the engine operates more efficiency resulting in the use of less fuel for a required power increase. Hence, since the results are presented on a brake specific basis, the overall trend with load is a decrease in CO emission.

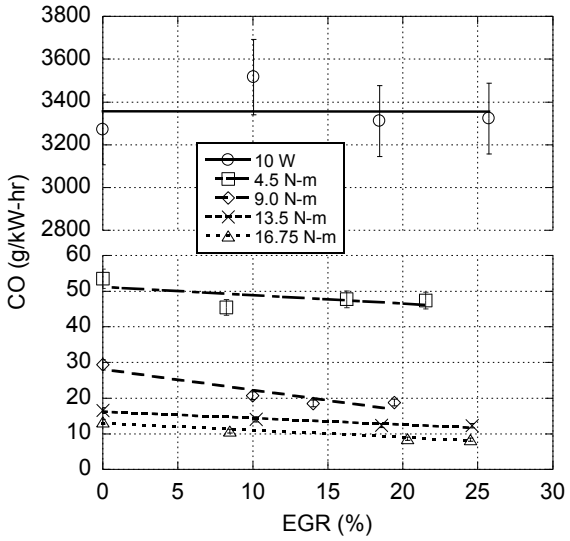

Figure 19. Effect of Cooled EGR on CO Emissions as a Function of EGR Level and Load.

Hydrocarbons (HC) are another harmful effluent requiring analysis when determining if an emission reduction method is viable. Hydrocarbons are generally created due to incomplete combustion or post-flame oxidation [5]. Hence, understanding that HC form due to lower temperatures and incomplete combustion, the researchers anticipated that an increase in cooled EGR would result in an increase in HC emission. However, Figure 20 illustrates that hydrocarbons decrease with the addition of cooled EGR. Similar to PM and CO, the mixing influence of EGR appears to outweigh its subsequent reduction in temperature and heat release rates. Furthermore, the trend with load follows the discussion involving CO while omitting the influence of dissociation.

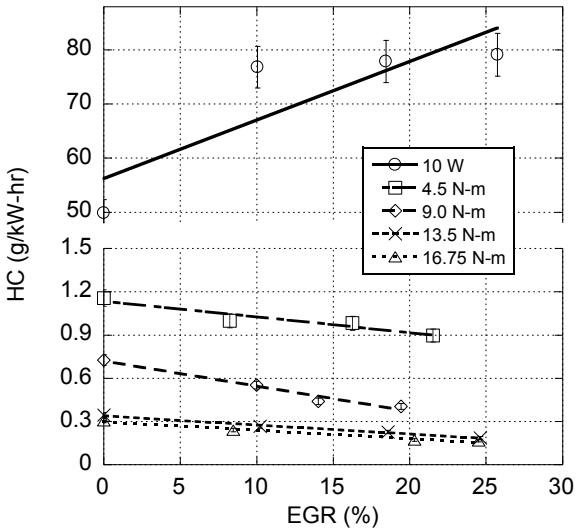

Figure 20.HC Emissions Resulting from Cooled EGR and Engine Load.

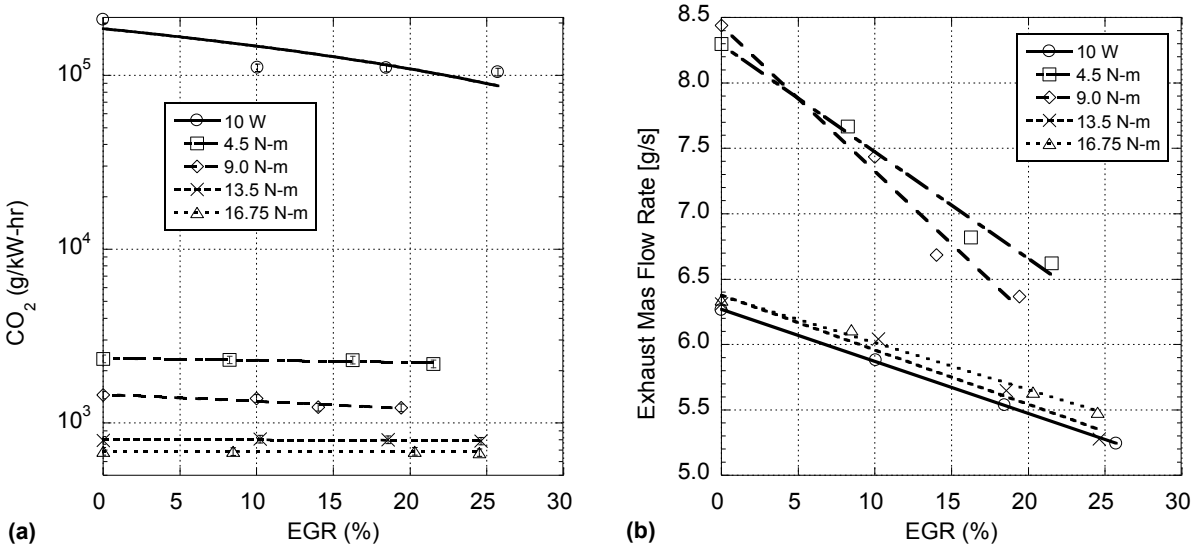

Figure 21. Changes in (a) CO_2 and (b) Exhaust Mass Flow Rate Resulting from Cooled EGR and Load.

Figure 21 presents the resulting carbon dioxide emissions from this study. With regard to engine loading, CO_2 levels decrease as load is applied. This correlates directly to the *bsfc* plot with engine load (Figure 15). The engine becomes more efficient as load is applied; thus, a reduction in CO_2 per power generated. With respect to EGR, plotting the exhaust mass flow rate in Figure 21(b) assists in the understanding of trends. As previously shown, the addition of EGR causes the fuel flow rate to

increase as seen through an increasing *bsfc* because the power is held constant. Hence, more fuel added, which means more carbon added, the more CO_2 that results. The researchers saw this influence in the experiments from the increasing *concentration level* of CO_2 in the exhaust. However, the total flow rate (equal to the sum of air and fuel) leaving the engine decreases with increasing EGR. Therefore, while the concentration of CO_2 in the exhaust increases, on a mass flow basis, it actually decreases since EGR cycles through the engine (a closed loop) displacing air.

2.7 Conclusion

The mandated emission reductions on diesel engines, set forth by the EPA, have led to significant research into reducing NO_x through Exhaust Gas Recirculation. The literature illustrates that most manufacturers provide cooled EGR before it enters the cylinder since it offers a dual benefit of NO_x reduction through its diluent properties without creating a subsequent thermal intake temperature rise as hot EGR. Since current engine test cell capabilities at the University of Kansas do not include a cooled EGR loop, this warranted the need for the implementation of such a system. This work describes its installation including the calculation of EGR percentage using CO_2 sensors located in the intake and exhaust ports of the engine. The setup employs a heat exchanger with dual cooling fans in order to reduce the hot exhaust gas temperature to match (within a few degrees Kelvin) the ambient temperature of the test cell. Testing a range of EGR from approximately 0-25% among five separate engine loads provided clear trends for emissions, as well as performance parameters and combustion efficiencies.

Matching results from the literature, increasing the levels of cooled EGR was successful in reducing brake specific NO_x emission. Additionally, the increased mixing level that resulted in higher turbulence causes a reduction in PM helping alter the NO_x-PM trade-off. In particular, the cooled EGR flow intersects the ambient air intake flow at a higher pressure and 90-degree angle, forcing better mixing of air and EGR while increasing turbulence levels. This contributes to better combustion, which leads to less PM along with reduced CO and HC levels. However, while emissions generally improved, brake specific fuel consumption increased. This is because EGR slows the heat release rate while additionally delaying combustion later into the expansion phase away from ideal thermal efficiencies.

2.8 Acknowledgements

This study was supported by the US Department of Transportation, Office of the Secretary, Grant No. DTOS59-10-G00109. The intellectual guidance and support of Dr. Christopher Depcik of Mechanical Engineering made this work possible. Additional assistance included efforts from Michael Mangus of Mechanical Engineering with engine testing and analysis.

References

1. Zheng, M., G.T. Reader, and J.G. Hawley, *Diesel engine exhaust gas recirculation—a review on advanced and novel concepts.* Energy Conversion and Management, 2004. **45**(6): p. 883-900.
2. Abd-Alla, G., *Using exhaust gas recirculation in internal combustion engines: a review.* Energy Conversion and Management, 2002. **43**(8): p. 1027-1042.
3. McGeehan, J.A., et al., *API CI-4: the first oil category for diesel engines using cooled exhaust gas recirculation.* 2002.
4. Agrawal, A.K., et al., *Effect of EGR on the exhaust gas temperature and exhaust opacity in compression ignition engines.* Sadhana, 2004. **29**(3): p. 275-284.
5. Heywood, J.B., *Internal Combustion Engine Fundamentals*1988, New York: McGraw-Hill, Inc.
6. MACHACON, H., et al. *Simultaneous Reduction of Soot and NOx by Intake Gas Variation*. 2000.
7. Murayama, T., et al., *Simultaneous reductions of smoke and NOx from a DI diesel engine with EGR and dimethyl carbonate.* SAE TRANSACTIONS, 1996. **104**: p. 1887-1896.
8. Tomazic, D. and A. Pfeifer, *Cooled EGR-A Must or an Option for 2002/04.* SAE TRANSACTIONS, 2002. **111**(3): p. 1650-1658.
9. Bosch, R., *Bosch Automotive Handbook*. 8th ed2011.
10. Zelenka, P., et al., *Cooled EGR-A key technology for future efficient HD diesels.* SAE paper, 1998. **980190**.
11. Kim, D.S. and C.S. Lee, *Improved emission characteristics of HCCI engine by various premixed fuels and cooled EGR.* Fuel, 2006. **85**(5): p. 695-704.
12. Kawano, D., et al., *Effect of Exhaust Gas Recirculation on Exhaust Emissions from Diesel Engines Fuelled with Biodiesel.* SAE Technical Paper, 2007: p. 24-0128.
13. Cecrle, E., et al., *An Investigation of the Effects of Biodiesel Feedstock on the Performance and Emissions of a Single-Cylinder Diesel Engine.* Energy & Fuels.
14. Krüger, U., et al., *High Performance Cooling and EGR Systems as a Contribution to Meeting Future Emission Standards.* SAE Int. J. Engines, 2008. **1**(1): p. 756-769.
15. Lim, G., et al., *Effects of HPL and LPL EGR Gas Mixed Supply on Combustion and Emissions in Automotive Diesel Engine.* SAE International, 2011.
16. Sutela, C., N. Collings, and T. Hands, *Fast Response CO~ 2 Sensor for Automotive Exhaust Gas Analysis.* SAE TRANSACTIONS, 1999. **108**(4): p. 1383-1391.
17. Sutela, C., et al., *Real time CO2 measurement to determine transient intake gas composition under EGR conditions*2000: Society of Automotive Engineers.
18. Schwarz, F. and U. Spicher, *Determination of residual gas fraction in IC engines.* 2003.
19. Welling, O. and N. Collings. *UEGO Based Measurement of EGR Rate and Residual Gas Fraction*. 2011.
20. Bihari, B., et al., *Diagnostics for Combustion Metrics in Natural Gas Fuelled Reciprocating Engines.* 2011.

21. Yoshimura, T., M. Miyai, and H. Nakamura, *Transient Exhaust Gas Recirculation Ratio Measurement Utilizing Heated NDIR Method*, 2012, SAE International.
22. Nasser, S.H., S. Morris, and S. James, *A Novel Fuel-Efficient and Emission-Abatement Technique for Internal-Combustion Engines.* SAE TRANSACTIONS, 1998. **107**: p. 1410-1425.
23. Cecrle, E.D., *Controls and Measurements of KU Engine Test Cells for Biodiesel, SynGas, and Assisted Biodiesel Combustion.* 2011.
24. Dec, J.E., *Advanced compression-ignition engines--understanding the in-cylinder processes.* Proceedings of the Combustion Institute, 2009. **32**(2): p. 2727-2742.
25. Mangus, M.D., *Design, Construction, and Validation of an In-Cylinder Pressure Recording System for Internal Combustion Engine Analysis.* 2012.
26. Serrano, D.P., J. Dufour, and D. Iribarren, *On the feasibility of producing hydrogen with net carbon fixation by the decomposition of vegetable and microalgal oils.* Energy Environ. Sci., 2012.

Chapter 3: The Influence of Ozone on Combustion in a Single-Cylinder Diesel Engine

Christopher Depcik[1], Michael Mangus[1], Edward Peltier[2], Colter Ragone*[1]

[1] University of Kansas, Department of Mechanical Engineering

[2] University of Kansas, Department of Civil, Environmental and Architectural Engineering

1530 W. 15th Street, Lawrence, KS 66045-4709

* Corresponding author: colterragone@gmail.com

3.1 Abstract

This work analyzes the effects of ozone-assisted combustion for a single-cylinder, direct-injection diesel engine. It begins by first summarizing the literature in this field in order to determine prior findings. Then, a simplified combustion model helps analyze these earlier trends and leads to experimentation with the authors' laboratory. The resulting outcomes indicate that the addition of ozone leads to a decrease in ignition delay, slightly higher temperatures in the cylinder due to ozone decomposition, augmented production of nitrogen oxides and reduction in particulate matter through radial atomic oxygen chemistry. Of additional importance, hydrocarbon levels decrease but carbon monoxide emissions increase. Furthermore, the results indicate a negligible difference in brake specific fuel consumption as a function of ozone addition. This work illustrates that, similar to others, beyond a certain level of assistance (20 ppm) adding more ozone has a negligible influence on combustion and emissions. This occurs because high concentrations of ozone facilitates its own destruction during the compression process through the corresponding reaction rate in the reverse direction.

3.2 Introduction

Stricter emission regulations from the Environmental Protection Agency (EPA) have led to the development of technologies intended to reduce the hazardous emissions emitted from Compression Ignition (CI) or diesel engines. Of primary importance for regulation of the CI engine is the reduction of both nitrogen oxides (NO_x) and particulate matter (PM). This is because the direct injection design and lean burning environment (excess air) of these engines creates a stratified charge within the engine forming NO_x in the high temperature zones and PM in the rich fuel core [2]. Exposure to these emissions will yield adverse effects on people's respiratory systems and can cause bronchitis. Moreover, NO_x can react with free radicals in the atmosphere, subsequently turning into acid rain when captured by moisture in the air. As a result, these pollutants can severely affect certain ecosystems and even parts of the economy, such as including crops spoiled by acid rain.

Therefore, engine manufacturers and researchers are working to meet the EPA's regulatory requirements by altering engine run-time properties in order to modify the combustion process. For example, Kawano et al. investigated the effects of Exhaust Gas Recirculation (EGR) on CI engines and documented the reduction of NO_x [1]. Increasing EGR levels (e.g., fraction of the intake mixture that is re-circulated exhaust gas) lowers in-cylinder temperatures, which causes a reduction in NO_x emission through the thermal NO mechanism [2]. However, these lower combustion temperatures and pressures lead to an increase in PM from reduced oxidation levels and an increase in brake specific fuel consumption from less output work during a thermodynamic cycle. In fact, the adjustment between high and low combustion temperatures and pressures

leads to a NO_x and PM tradeoff where a decrease in one pollutant typically increases the other pollutant. This balance of emission levels demonstrates the difficulty and importance of finding a strategy that has the ability to reduce both NO_x and PM at the same time while maintaining a low brake specific fuel consumption [2].

Another common run-time adjustment is injection timing. The modification of injection timing allows the operator to control the phasing of in-cylinder combustion. Early injection timing provides more time in order to premix air and fuel, which subsequently creates less PM through an increased level of homogeneity. However, an extended mixing period results in an elevated combustion temperature causing a higher emission of NO_x species. This is due to greater combustion efficiency from better mixing, along with an earlier phasing of combustion. In particular, earlier injection often results in combustion closer to the end of the compression process, or Top Dead Center (TDC), which has the highest pre-combustion temperatures. As an example, Bhusnoor and Babu investigated the effects of altering injection timing on different blends of biodiesel. By adjusting the injection timing, their results displayed the trade-off between the increase and decrease of NO_x and PM emissions, respectively [2, 3].

Other efforts geared toward reducing NO_x and PM include using alternative fuels, such as biodiesel, in order to modify the chemistry of the combustion process [4-8]. An extensive amount of literature demonstrates that using biodiesel, as compared to ultra low sulfur diesel (ULSD), will typically yield a decrease in unburned hydrocarbons (HC), PM, and carbon monoxide (CO). However, the NO_x and PM tradeoff is still evident as NO_x emissions generally increase with the use of biodiesel [4, 6-18]. In this area, Cecrle et al. demonstrate the influence of several different biodiesels on NO_x and PM

emissions [7]. Their results illustrate how the different chemical characteristics of biodiesel, such as unsaturated fraction, can modify this tradeoff. However, the use of biodiesel only shifts this tradeoff without truly defeating it.

A completely different tactic taken by some is to investigate ozone (O_3) as an exhaust aftertreatment or combustion modifier in order to meet EPA requirements and potentially address the NO_x-PM tradeoff. In order to set the stage for ozone usage, most of the NO_x leaving the CI engine is in the form of nitric oxide (NO) because the high oxygen concentrations and temperatures ensuing from diesel combustion result in high NO formation rates [2]. According to Koebel et al., NO_x emissions for diesel engines are typically comprised of approximately 90% NO [19]. Current catalytic exhaust aftertreatment devices used for NO_x reduction, such as Selective Catalytic Reduction (SCR) and Lean NO_x Trap (LNT), prefer nitrogen dioxide (NO_2) because of its stronger oxidative and surface adsorption abilities [20-23]. In most exhaust systems, oxidation of NO to NO_2 occurs in a Diesel Oxidation Catalyst (DOC), of which NO_2 is then absorbed in a zeolite-structure (SCR) or over an alkali earth metal (LNT). NO_2 is preferred because it reacts faster with HC, hydrogen (H_2), and carbon monoxide (CO) in order to produce carbon dioxide (CO_2), water (H_2O), and nitrogen (N_2) [24]. It is important to note that, SCR devices use urea as an ammonia carrier that requires NO_2 levels above exhaust output levels (typically a 50-50 split of NO/NO_2) for conversion with ammonia into N_2 within an O_2 rich environment [25].

In order to oxidize NO to NO_2 for aftertreatment device usage in the exhaust, several researchers conclude that ozone is effective for this NO oxidation process [20, 25-30]. In particular, Mohammadi et al. studied the emissions reduction of diesel fuel

exhaust by using high-frequency dielectric barrier discharge plasma in order to inject ozone into the exhaust. Their aim was to develop a plasma-assisted aftertreatment device for the reduction of both NO_x and PM. Their study revealed that ozone can efficiently oxidize NO into NO_2 [29]. Moreover, the resulting NO_2 from the plasma-assisted conversion allows for continuous regeneration of PM in a Diesel Particulate Filter (DPF), which stores PM for periodic regeneration [31, 32], resulting in enhanced PM reduction. Shortly after, Okubo et al. investigated a similar approach by pairing nonthermal plasma (NTP) with DPF. They discussed several studies displaying the successful use of NTP as a low temperature PM oxidizer and incinerator [25]. Furthermore, Nakada et al. investigated NO removal by ozone injection and developed a NO control system [20]. They used the discharge plasma method to inject ozone into the exhaust. The ozone oxidized NO to form NO_2, subsequently removed by a water scrubber containing an alkaline solution. They looked to develop an economical NO control system without the use of expensive NO_x sensors by altering the discharge power of an ozone generator. Their results indicated up to a 50% NO concentration reduction (in the form of NO_2) with 350 ppm O_3 injection over three separate loads. The decrease of NO concentration with an increase in ozone injection showed a linear correlation across all loads.

As opposed to utilizing ozone in the exhaust system, other researchers find that supplementing the intake air with ozone can influence the combustion process and resultant emissions. Ozone will assist the combustion event due to its thermal decomposition leading to the production of active species. These species then initiate radical chain reactions by attacking the parent fuel leading to an accelerated ignition

[33]. In 1984, Westbrook and Dryer demonstrated the decomposition of ozone during combustion. They explained the oxidizing capabilities of ozone and how it contains more chemical potential energy than oxygen, resulting in significantly higher product pressures and temperatures [34].

The first experimental work in this area was by Tachibana et al. who used pure oxygen as the source carrier in order to create ozone for assisted combustion [33]. Using a Cooperative Fuel Research (CFR) engine, they determined that the addition of ozone increased the effective Cetane Number (CN), subsequently causing a decrease in ignition delay. Of importance, the CN is a dimensionless number given to fuels as an indicator of the time delay between injection and ignition of the fuel with a higher CN number corresponding to a shorter ignition delay [35]. During their experiments, they found that the emission levels of CO and HC decreased along with the amount of PM. However, the addition of 1000 ppm of ozone increased total NO_x emissions by approximately 100 ppm. They concluded that the variation in emissions resulted from changes in the combustion process. In particular, the combustion temperature increased as combustion occurred closer to TDC and ozone's influence was, therefore, similar to the injection timing discussion presented earlier. Their efforts employed constant fuel injection timing in order to isolate the effect of ozone on ignition delay.

In 1993, Clothier et al. presented their findings on how ignition promoters work with diesel fuel in order to increase the CN of the resulting mixture. Their main concern was cold starting engines where the cylinder walls could be around -20°C upon startup. By adding a concentration of 10 ppm ozone, the ignition delay was found to decrease by about 12 percent. This reduction correlates to an increase of CN by 5 to 10 units

after ozone treatment [35]. By reducing the ignition delay, more complete combustion will occur on startup, as well as heating the cylinder walls at a faster rate. The engine used for testing was a Spark Ignition (SI) engine with one cylinder converted into diesel mode by replacing the spark plug with a fuel injector. The compression ratio was 7.5, which is drastically lower than a typical CI engine. Due to the uniqueness of their engine test methodology, they found the cylinder pressures to be lower by a factor of two to three over conventional CI engines. As a result, their approach may not have been the most applicable to CI engines; however, the trend in ozone's influence on the ignition delay appears to be pertinent.

A few years later, Faison studied the influence of ozone on diesel PM precursors through a numerical process using the Fortran computer program Senkin. Acetylene (C_2H_2) is a PM precursor known to be the dominant growth species due to its high concentration [36]. Faison found that ozone injection can reduce C_2H_2 concentration, but not on a linear basis. In particular, the highest injection concentration of ozone at 1000 ppm only yielded a 20% decrease in C_2H_2 concentration as compared to a 25 ppm injection. Faison concluded that 25 ppm was an efficient amount of ozone for the reduction of PM precursors. Note that demonstrating a low concentration of ozone is sufficient for PM reduction is beneficial as 25 ppm of ozone is more readily attainable and will require less energy (the production of ozone is endothermic) to produce than 1000 ppm.

In 1998, Nasser et al. injected ozone into the intake of a 1.6L Ford direct injection CI engine coupled to a Froud hydraulic dynamometer. Their results showed a reduced ignition delay (similar to Tachibana et al. and Clothier et al.) that led to an improvement

in combustion performance, subsequently decreasing CO and HC emissions [37]. This resulted in an increase in CO_2 emission through enhanced CO oxidation, as well as an increase in NO_x emissions due to the resultant higher combustion temperatures. They concluded that improvements in fuel economy and emission characteristics resulted from the increase of oxygen and ozone radicals mixing in the pre-combustion air. However, they did not measure PM in their study. In the same year, Golovitchev and Chomiak investigated the effects of several ignition improvers for methane. One of the promoters studied was ozone which they found to decrease the ignition delay [38]. They attribute the ignition acceleration characteristics mainly to the atomic oxygen (O) radicals generated from the decomposition of ozone.

In 2005, Yamada et al. investigated the effects of adding methanol and ozone to a homogeneous charge compression ignition (HCCI) engine with dimethyl ether (DME). Similar to the previously reviewed literature, ozone increased the heat release rate during the cool ignition phase resulting in an decrease in fuel consumption [39]. Concluding that the accelerated ignition due to the addition of ozone, they developed a chemical kinetic model in order to verify their results. Discussion of this model will occur in a later section. There was no emission analysis conducted for these experiments, but they found an increase in combustion pressure, temperature, and heat release. From combustion kinetics and the previous discussion herein, these types of conditions typically lead to an increase in NO_x emission paired with a decrease in PM.

Using a Premixed Charge Compression Ignition (PCCI) natural-gas engine, in the following year, Mohammadi et al. studied the effects of the addition of ozone on the combustion process. Since PCCI is controlled largely by chemical kinetics requiring

accurate temperature control during compression, stability of ignition is accomplished through modifications of the compression ratio, intake temperature, or internal EGR [40]. The researchers stated that each of these methods could increase the stability of ignition; however, a combination of the various techniques may be required. As a result, the non-linearity that ensues using all techniques would make it difficult to maintain consistent ignition. Therefore, the goal of their study was to create stable ignition using varying levels of ozone at different intake temperatures. Operating at an equivalence ratio of 0.24, ozone concentrations lower than 40 ppm, yielded high HC and CO emissions along with a low combustion efficiency. Their data showed that CO emissions peaked around 40 ppm ozone injection. The low equivalence ratio resulted in relatively cold combustion, which led to increased amounts of CO, and HC emissions (reduced levels of oxidation). When the concentration of ozone rose above 80 ppm, the combustion efficiency increased to 70% and the HC and CO emissions drastically decreased. At 80 ppm, they saw a marked decrease in ignition delay to more of an optimal state of combustion timing resulting in better combustion. This subsequently led to a higher rate of oxidation of HC and CO before exiting the cylinder, resulting in a decrease in those emissions. Their results demonstrated that ozone injection greater than 80 ppm produced little effect as the level of improvement was effectively saturated; hence, they considered 80 ppm to be the ideal condition.

As the literature demonstrates, adding ozone to the intake mixture of a CI engine can influence both combustion and emissions through modifications to the combustion process along with chemical kinetic reactions. In particular, ozone appears to have the following effects:

- Reduced ignition delay [33, 35, 37, 38]
- Reduction in PM precursors [36]
- Faster combustion process [39]

Moreover, the addition of an extra oxygen compound can change the global and local air-to-fuel ratios in the cylinder making it effectively a leaner combustion process. As a result, it is important to separate the different outcomes of ozone in order to understand its role regarding the NO_x and PM tradeoff. The following section reviews ozone kinetics in preparation for a relatively simple combustion simulation study using CO and H_2. This study will reveal that ozone can survive the compression process of an engine and contribute to combustion and emissions via three pathways; i.e., increasing temperature through its exothermic nature during decomposition, advancement of combustion timing by promoting initial CO and H_2 oxidation, and through radical species chemistry. Finally, this work builds on these outcomes through an experimental study using a single-cylinder engine in order to discuss these routes further using in-cylinder pressure data.

3.3 Ozone Kinetics

The first step in creating a combustion model using ozone is to determine the correct ozone reaction kinetics to employ. In this area, a literature review illustrates that there are over 40 kinetic expressions for the decomposition and interaction of O_3 with other species in the combustion process [34, 37, 39-51]. This review begins here with Benson and Axworthy in 1957 when they conclude that the pyrolysis of ozone can be represented adequately by reactions (1) and (2) [52]:

$O + O_3 \Leftrightarrow O_2 + O_2$	(1)
$O_3 + M \Leftrightarrow O + O_2 + M$	(2)

For the second reaction, M is a third body species that could be, but is not limited to CO or NO. Moreover, the reversible arrow for both reactions illustrates that they can proceed in either the forward or the reverse direction. Benson and Axworthy conducted four experiments using two different reaction vessels filled with ozone and oxygen. As the ozone decomposes, the partial pressure of the vessel will drop, yielding a method to measure the rate of decomposition between ozone and oxygen.

Jones and Davidson followed this work in 1961, where they studied the thermal decomposition of ozone in a shock tube. They confirmed the conclusions of Benson and Axworthy through the use of diluted mixtures of ozone in argon or nitrogen with hydrogen or helium driver gases [44]. Similar to the work of by Jones and Davidson, Myers and Bartle conducted similar shock tube studies, with more extreme temperature ranges [48]. Their findings confirmed the previous efforts, leading to the same core reactions for ozone decomposition. In 1968, Johnston established an extensive review of all theoretical and experiment work completed in the field of ozone decomposition [53]. His analysis falls in line with the previous authors mentioned, defining reactions (1) and (2) as the primary equations required for a thorough analysis of the decomposition of ozone. His work was later cited and confirmed by Center and Kung in 1974 through their studies of thermal decomposition of ozone in shock tubes [42].

During the investigation of chemical kinetic modeling of hydrocarbon combustion, Westbrook and Dryer discussed the oxidation kinetics considered for a comprehensive mechanism. They mentioned the importance of ozone in combustion environments, because it is an oxidizer that carries an elevated potential energy as compared to ordinary oxygen. From its increased energy content, ozone provides significantly higher

pressures and temperatures than oxygen. Ozone is a strong oxidizer that contains a larger amount of chemical potential energy as compared to oxygen. When ozone oxidizes other species, its decomposition is an exothermic process, which adds energy to combustion events. As a result, a mixture of ozone and oxygen will propagate a higher laminar flame speed resulting in faster combustion [34]. Coinciding with previously discussed literature, they stated the simplest detailed mechanism consisting of the necessary features is through reactions (1) and (2).

In 1991, Chang et al. presented a thorough discussion of the corona, or silent, discharge process first proposed by Siemens in 1857 [45]. A section of the work included analysis of the generation of ozone by ionic processes. They indicated that ozone generation in a corona discharge is a two-step process. The first includes oxygen generation through free radicals by ionic processes, and the second is the generation of ozone by free radicals, as shown in the reverse of reaction (2) [43]. Gas temperatures significantly influence the reaction rate of ozone generation, as the rate decreases with increasing temperature. This will be an important factor to consider when pairing ozone injection with the combustion process, as temperature is a difficult variable to control and will affect the results.

Kitayama and Kuzumoto conducted theoretical and experimental investigations in 1997 using oxygen as a source gas for ozone generation while altering the gap lengths for discharge. Coinciding with other researchers, Kitayama and Kuzumoto used the reverse of reaction (1) as their ozone generation reaction for theoretical calculations [45]. They tested gap lengths from 0.05 to 0.2 mm for ceramic plate electrodes and 0.5 to 1.0 mm for glass tube electrodes. Through experimental results, they determined that

the gap lengths did influence the concentration of ozone generation while the change in materials had no effect. The resulting ozone concentration from altering gap lengths was minimal for lower specific energies, while an increase in specific energy made the differences in production more visible. This is important to note because, if a low concentration of ozone is required for a given application, the production difference for varying gap lengths is minimal, which can lead to choosing a more economical ozone generator. Concurring with the results as found by Chang et al., Kitayama and Kuzumoto concluded that temperature had a significant effect on the ozone generation process. They completed this work in 1999, illustrating that the model for ozone generation improves by altering the gas pressures across a narrow discharge gap. They determined that, for the production of a high concentration of ozone, an optimized high gas pressure for a narrow gap width is beneficial [46]. Moreover, of continued importance was that these high pressures suppress the potential of nitrogen oxide generation from N_2 and the rise in gas temperature.

Three years later, Westbrook studied the chemical kinetics of ozone addition to an HCCI engine. It was determined that, with the addition of 10 ppm ozone, the ignition delay was reduced from 14 to 9 ms after TDC [51]. He discussed further the decomposition of ozone via reaction (2), resulting in O atoms that interact with fuel molecules. These additional decompositions contain high activation energies that facilitate the decreased ignition delay.

As previously stated, in 2005 Yamada et al. investigated methods of controlling ignition timing with the addition of ozone in an HCCI process using dimethyl ether. They utilize a hydrocarbon chemical kinetic mechanism including ozone reactions. Initially,

they incorporate five ozone reactions; however, ozone decomposition reaction (2) was determined to be the most significant [39]. As a result, calculations using only reaction (2) as compared to simulations including all reactions provided no difference in pressure, temperature, or concentration profiles for major chemical species. As a result, they concluded that the alternative reactions were of negligible influence.

Furthermore, Mohammadi et al. conducted a kinetic study prior to their PCCI engine testing using CHEMKIN [40]. They included twelve reactions in their model in order to verify their experimental data including reactions (1) and (2). However, they did not include any discussion regarding the significance of each reaction. They validated their experimental data through a chemical kinetic analysis, resulting in an accurate model for their application as previously discussed. Finally, recent efforts by Ombrello et al. in 2010 investigated the thermal and kinetic effects of ozone on flame propagation using a dielectric barrier plasma discharge. They separated out ozone and measured it quantitatively with absorption spectroscopy. For the kinetic mechanism, sixteen reactions involving ozone were included; however, they explicitly stated that the most important reactions were the decomposition and three body recombination reaction of ozone, as shown in reactions (1) and (2), respectively [49]. Based on their analysis, they determined that ozone significantly influences the propagation speeds of propane lifted flames.

In 2006, Nishida and Tachibana studied the effects of ozone addition to a HCCI engine. They used natural gas as the fuel with the intake gas ozonized. Through experiments, a reduction in ignition timing was found with the addition of ozone [54]. To further their understanding, they conducted a numerical analysis on the effects of ozone

and determined that the influence of ozone on ignition delay was approximately the same as an injection of an O radical.

Based on the literature, reactions (1) and (2) are found to be the most prevalent and utilized herein this paper in order to create a reduced mechanism [34, 39, 40, 42-50, 52, 55]. Summarizing the previous discussion, according to Westbrook and Dryer, this is the simplest mechanism that has all of the requisite features in comparison to others that might be more detailed [34]. This conclusion was validated by Yamada et al. and Luther et al. who found that the sensitivities of other reactions were negligible [39, 47]. Moreover, Yamada et al. tested this simple model with a large detailed kinetic mechanism and found no significant difference in pressure, temperature, and profiles of the major species. Future work should investigate the impact of the individual reactions mentioned in the literature survey; however, for this study the simple mechanism is sufficient.

The forward reaction rates for these mechanisms are expressed in Arrhenius format as:

$R_1 = k_1 T^{m_1} \exp\left(-\frac{E_1}{R_u T}\right) C_O C_{O_3} = A_1 C_O C_{O_3}$	(3)
$R_2 = k_2 T^{m_2} \exp\left(-\frac{E_2}{R_u T}\right) C_{O_3} C_M = A_2 C_{O_3} C_M$	(4)

where k is the pre-exponential, T is the temperature, m indicates the temperature dependency, E is the activation energy (energy barrier) for the reaction to occur, R_u is the universal gas constant, and C are the respective molar concentrations of the species. The choice of using CHEMKIN to solve the kinetic expressions, discussed later, does not require the derivation of reverse reactions since they are computed from equilibrium [56]. The literature dictates that one specific value for these terms (k, m, E)

does not match all of the experimental data. In specific, Figure 1 illustrates the papers that provide values of these components for both R_1 [36, 50, 52, 53, 57-60] and R_2 [39, 40, 42] expressions.

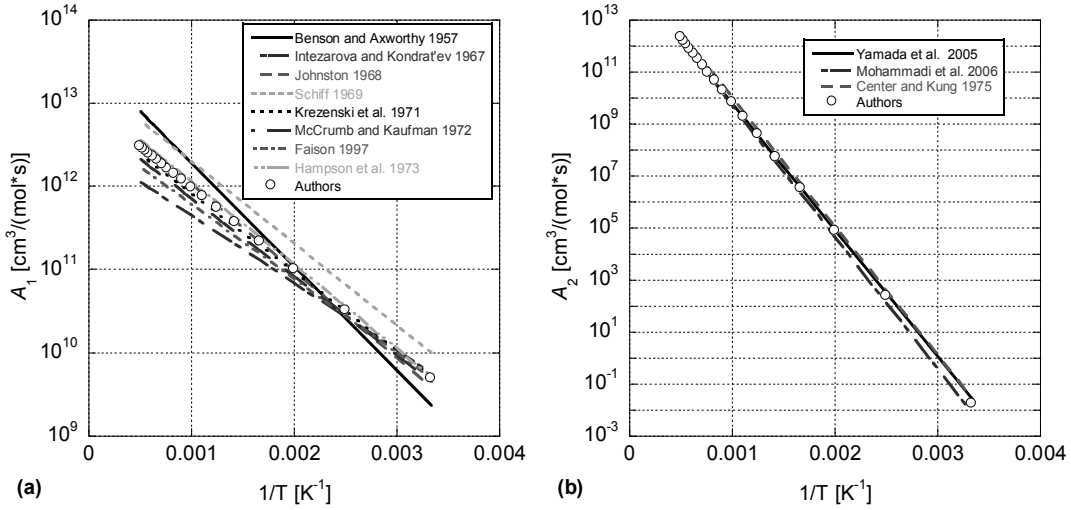

Figure 1. Literature Arrhenius Expressions for the Ozone Reactions of (a) R_1 and (b) R_2 including Averaged Expressions.

Since the kinetic constants do vary across the different papers, the choice becomes whether to select a certain researcher's values or calculate an average set of parameters. This work utilizes the second option, and Figure 1 illustrates how the following values correspond to the literature:

$R_1 = 9.325\times10^{12} T^0 \exp\left(-\frac{4.495}{R_u T}\right) C_O C_{O_3}$	(5)
$R_2 = 6.286\times10^{14} T^0 \exp\left(-\frac{22.691}{R_u T}\right) C_{O_3} C_M$	(6)

While the ozone assisted combustion literature mentions that O_3 does contribute to the combustion process, the relative amount of involvement is still an unknown. This is because under high temperatures, O_3 decomposes relatively fast [61]. Hence, it is possible that a significant amount of injected ozone is lost during the compression process depending on the compression ratio of the engine. As a result, use of a zero-

dimensional (0D) engine simulation code allows exploration of the impact of O_3 decomposition during the compression and expansion processes. For simplicity, the model neglects heat loss to the walls and blow-by past the piston, and is only useful from Intake Valve Closing (IVC) until Exhaust Valve Opening (EVO) when there is not any additional mass entering or exiting (neglecting the fuel injection event). The following paragraphs provide the governing differential equations of the model, with a full derivation based on the conservations equations of mass, energy, species, and cylinder volume change [2] available upon request.

For this simple model, computation of the cylinder volume change (V) is a function of the bore (*b*),

$$\frac{d\mathbb{V}}{dt} = -\frac{\pi b^2}{4}\frac{dx}{dt} \quad (7)$$

and change in the distance between the crank and piston pin axis as a function of time:

$$\frac{dx}{dt} = \left(-a\sin\theta - \frac{a^2\sqrt{2}\cos\theta\sin\theta}{\sqrt{2\ell^2 - 2a^2\sin^2\theta}} \right)\frac{d\theta}{dt} \quad (8)$$

where *a* is the crank radius, ℓ is the connecting rod length and θ is the crank angle. Calculation of the change in crank angle is a function of the engine speed (*N*) in revolutions per minute as follows:

$$\frac{d\theta}{dt} = \frac{2\pi N}{60} \quad (9)$$

From the conservation of mass, the change in density (ρ) is a function of time equals:

$$\frac{d\rho}{dt} = -\frac{\rho}{\mathbb{V}}\frac{d\mathbb{V}}{dt} \quad (10)$$

Utilizing the conservation of species equation while substituting continuity recovers:

$$\frac{d\mathbf{Y}}{dt} = \frac{\dot{\boldsymbol{\omega}}\mathbf{W}}{\rho} \quad (11)$$

for the change in species via mass fractions (**Y**) as a function of reaction rates $(\dot{\omega})$ and molecular weights (**W**) where bold indicates a vector of species. Reaction rates, R_1 and R_2, are incorporated in this equation in order to solve for the change in species as a function of time.

The governing equation of energy simplifies to the change in temperature as a function of time:

$$c_v \frac{dT}{dt} = -\sum_{j=1}^{L} \frac{e_j \dot{\omega}_j W_j}{\rho} - \frac{p}{\mathbb{V}\rho} \frac{d\mathbb{V}}{dt} \quad (12)$$

where c_v is the constant volume specific heat, e is the internal energy of the individual species (j is the individual species indicator) and p is the pressure. Since this is a compressible gas solver, the ideal gas law must be included in differential format as:

$$\frac{dp}{dt} = \rho R \frac{dT}{dt} + \rho T \frac{dR}{dt} + RT \frac{d\rho}{dt} \quad (13)$$

which solves for the change in pressure as a function of time.

In order to complete the solver, the differential change in the gas constant, mixture molecular weight (W_{mix}), and mole fractions are required, respectively:

$$\frac{dR}{dt} = -\frac{R_u}{W_{mix}^2} \frac{dW_{mix}}{dt} \quad (14)$$

$$\frac{dW_{mix}}{dt} = \sum_{j=1}^{L} W_j \frac{dX_j}{dt} \quad (15)$$

$$\frac{dX_j}{dt} = \left[\frac{1}{W_j} \frac{dY_j}{dt} \sum_{i=1}^{L} Y_i / W_i - \frac{Y_j}{W_j} \sum_{i=1}^{L} \frac{1}{W_i} \frac{dY_i}{dt} \right] \Bigg/ \left(\sum_{i=1}^{L} Y_i / W_i \right)^2 \quad (16)$$

where X are the mole fractions of the species. This series of equations was solved using the ordinary differential equation solver DVODE [62] while incorporating CHEMKIN to handle the chemical species reactions. CHEMKIN curve-fits of the thermodynamic properties were included in order to account for the resulting mixture composition.

Using this model and the average O_3 reaction kinetics, an ozone addition sweep was completed from 0 to 1500 ppm in the intake of the modeled Yanmar single-cylinder CI engine (full engine specifications provided in Table 1 later in this document) undergoing a motoring event using atmospheric pressure and temperature at IVC (101325 Pa and 300 K, respectively). Representation of air occurs through a molar ratio of 3.76 N_2 to O_2 while a reduction of both N_2 and O_2 via this ratio happens when adding O_3 to the intake mixture. In other words, this simulation effort holds the fractional composition of modeled air constant as O_3 simply displaces both N_2 and O_2.

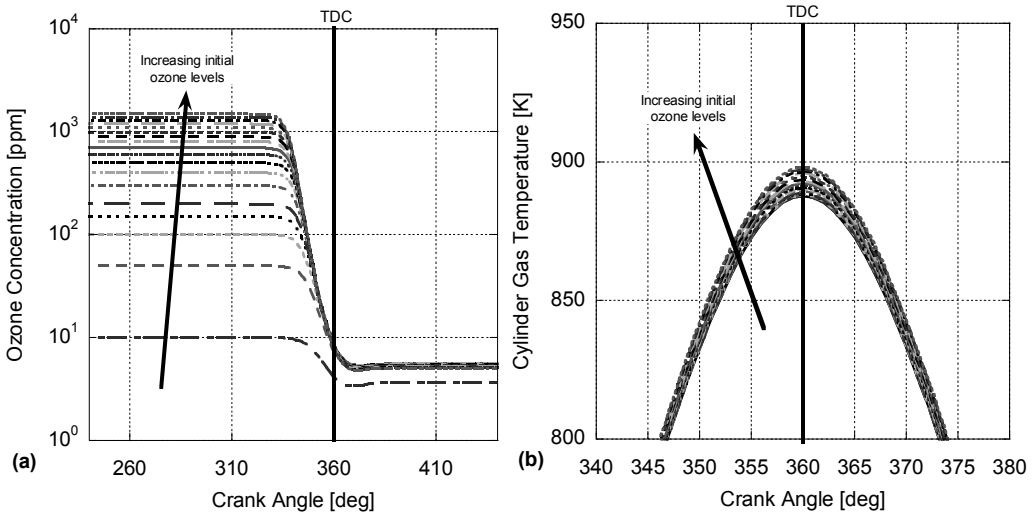

Figure 2. Zero-dimensional Motoring Engine Simulation of (a) Ozone Concentration and (b) In-cylinder Temperature as a Function of Initial Ozone Concentration.

The results of this sweep in Figure 2 illustrate that ozone will be present during the combustion process for this particular engine since it has a measurable concentration at TDC. However, it appears that adding high concentrations of ozone to the intake is not practical. This is because the reaction rates of both Eqns. (3) and (4) increases significantly via their ozone concentration dependency. Beyond adding 10 and 50 ppm ozone to the intake (approximately 4 and 7 ppm respectively at TDC), all

increased concentration results asymptote to around 8 ppm at TDC. On a related note, recall that Faison found through the acetylene studies that high levels of ozone are not useful for PM reduction [36]. Therefore, this may indicate an intake ozone concentration that provides the largest influence for the minimum of expense (e.g., energy it takes to convert O_2 to O_3).

Furthermore, because creating ozone is endothermic, as ozone decomposes, it undergoes an exothermic reaction. This results in an increasing gas temperature in the cylinder as presented in Figure 2b that can lead to additional NO_x production through the thermal NO mechanism. Therefore, Figure 2 demonstrates that ozone will contribute to NO_x production through a purely thermal impact; however, this impact is small when the ozone added is relatively low (e.g., 10 ppm = 0.02 K, 50 ppm = 0.23 K, 1500 ppm = 10.41 K at TDC over 0 ppm added). The small dip and rise in the ozone concentration that results after TDC is a function of the reverse reactions promoting ozone production as atomic oxygen, molecular oxygen and other radicals react to create ozone at increased temperatures [49]. The next section will consider these results when modeling a simplified combustion mechanism. This will help further distinguish the influence of ozone on combustion phasing and NO_x chemistry through radical species.

3.4 Simplified Combustion Kinetic Mechanism

As discussed in the introduction, the primary issue of CI engines is the NO_x versus PM tradeoff. The historical recap of ozone-assisted combustion mentions that it influences this tradeoff through different mechanisms. As a result, in order to determine the complete impact of ozone upon NO_x, modeling the combustion process including

thermal and prompt NO mechanisms is required. Typical diesel fuel is a blend of hundreds of species that belongs to several groups of hydrocarbons like alkanes, alkenes, aromatics and cycloalkanes [63-67]. It has a mean chemical formula with carbon and hydrogen constituents in a certain range (e.g., $C_{13.4\ -15}\ H_{24.8-27.1}$) depending on the fuel manufacturer, location, and time of the year. In order to understand the impact of ozone upon diesel combustion, one approach is to simulate the entire combustion process including the fuel spray atomization and vaporization along with the ensuing kinetic mechanism for combustion. This requires a significant amount of computational overhead in setting up the numerical simulation while additionally taking time to generate the results.

Following the thoughts of Warnatz [68], hydrocarbon combustion can be approximately described as the combustion of CO and atomic hydrogen (H) with these compounds created by the radical pyrolysis of the initial fuel. In fact, Ó Conaire et al. mention that hydrocarbon oxidation kinetic mechanisms begin with the development of hydrogen (H_2) oxidation mechanisms followed by CO chemistry [69]. As a result, the authors simplify the simulation of diesel fuel combustion for this effort into CO and H_2 constituents as follows:

$C_{14.2}H_{25.543} + a\left(O_2 + 3.76N_2\right) \rightarrow bCO + dH_2 + eN_2 + fO_2$	(17)

where 14.2 was taken as the average molar constituent of carbon from the previously mentioned values from the literature, and an analysis of latest batch of diesel tested in Dr. Depcik's laboratory found the H:C molar ratio equal to 1.799. The authors chose this avenue rather than combustion of a complete hydrocarbon fuel in order to eliminate

the influence of radical pyrolysis. Future efforts should extrapolate the results here to a full simulation including a representative hydrocarbon fuel.

This reaction expression effectively creates a surrogate fuel (syngas) that contains the right amount of carbon and hydrogen as the diesel fuel tested in Dr. Depcik's lab. It allows for the use of fundamental oxidation kinetic mechanisms in a 0D simulation reducing numerical run time and complexity. It is important to mention that this purely theoretical study will not provide the same results as complete diesel combustion simulations including fuel injection; however, the trends of adding ozone to the mixture will provide insight on the different mechanisms.

Continuing this pathway, incorporating ozone into the intake of a virtual engine results in the simplified reaction equation:

$C_{14.2}H_{25.543} + a\left(O_2 + 3.76N_2 + cO_3\right) \rightarrow bCO + dH_2 + eN_2 + fO_2 + gO_3$	(18)

Since the simulated fuel consists of the species CO and H_2, the reaction equation effectively passes O_3 through to the syngas-equivalent side. It is important to mention that when introducing O_3 into the intake, it displaces a small amount of air as indicated in the parenthesis. Therefore, these calculations lower the relative amount of fuel in order to remain consistent with respect to the air-to-fuel (and equivalence) ratio in Eqn. (17). Since combustion temperatures and emissions are largely dependent on the relative ratio of fuel to air [2], it is important to be consistent when analyzing the impact of ozone. In other words, the ozone-added results maintain the exact same air-to-fuel ratio as the baseline results. This will change the relative amount of oxidizer, as more oxygen is now present in the form of ozone. Another route could be to maintain the

same C:O and H:O ratios with respect of fuel to oxidizer; however, this is left to future work.

With respect to the choice of kinetic mechanisms, a recent paper by Konnov [70] investigates past H_2 oxidation mechanisms while postulating an updated pathway. His paper states that the models of Li et al. [71] and Ó Conaire et al. [69] are the most extensively validated; hence, the Ó Conaire et al. mechanism was chosen for this paper based on its widespread usage. In order to validate the correct programming of this initial reaction mechanism, hydrogen oxidation data from Mueller et al. [72] in a constant pressure reactor was simulated as indicated in Figure 3. This is done using a zero-dimensional constant pressure model, similar to the 0D engine simulation, with the fundamentals of its derivation available upon request. The results of the model follow the experimental results with good accuracy under both low pressure (Figure 3a) and relatively high-pressure (Figure 3b) situations at different air-to-fuel ratios indicating correct implementation of the numerical solver and initial combustion kinetic mechanism.

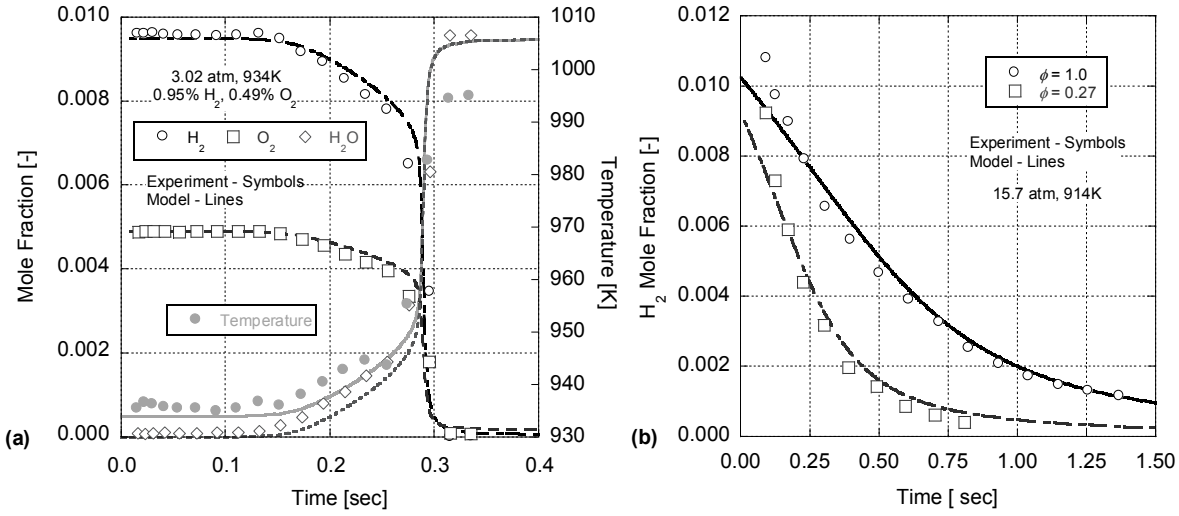

Figure 3. Constant Pressure Reactor Simulations of Mueller et al. [72] using Ó Conaire et al. [69] Hydrogen Oxidation Mechanism for (a) Low Pressures and (b) High Pressures.

In order to complete the kinetic mechanism, Konnov mentions that Saxena and Williams [73] made updates in the H_2/CO sub-mechanism that were in good agreement with experimental tests; hence, this work includes these specific CO oxidation components. For thermal NO production, the model includes a recently updated mechanism by Goswami et al. [74] that was validated with available literature. For prompt NO, Konnov investigated and modified this component of NO_x production [75]. However, in order for this mechanism to proceed, an initiation step is required to form the prerequisite CH that forms the major pathway to prompt NO formation. This initiation step was taken from Konnov's detailed reaction mechanism in another paper [76]:

$CH + O \Leftrightarrow CO + H$	(19)

It is important to mention that the prompt NO route will be more prevalent when using a hydrocarbon fuel rather than syngas. Hence, this work mainly explores the influence of ozone on the thermal NO mechanism.

At this stage, the kinetic model includes CO and H_2 oxidation chemistry, the two-reaction ozone mechanism along with the main pathways to NO_x production through thermal and prompt routes. It is important to note that this effort does not calibrate the combined mechanism to experimental data similar to the GRI mechanism for natural gas combustion [77]. Accomplishing this would ensure that the model results will accurately reproduce exact values for heat release and emissions. This paper does not intend that the simplified combustion and NO_x mechanism provide this type of result. Instead, by running parametric studies, the trends of adding ozone will be determined for a surrogate diesel fuel. This will lead to a better understanding of the mechanisms involved during actual engine testing presented later.

In the previous section, the in-cylinder kinetics study of ozone incorporating the compression event of the engine found that, at TDC, the temperature in the cylinder is 887.76K and the pressure is 5.284×10^6 Pa when ozone is not included. This is the starting point of a parametric fuel sweep over air-to-fuel ratios for a constant volume combustion event. This allows investigation of the ignition delay of the fuel surrogate along with NO_x production in a controlled manner. For this study, all ozone added is available at TDC in order to investigate only the impact of ozone on ignition delay while not including the influence of ozone destruction during the compression event. Similar to previous efforts, the authors formulated a 0D constant volume combustion simulation with the model equations available upon request.

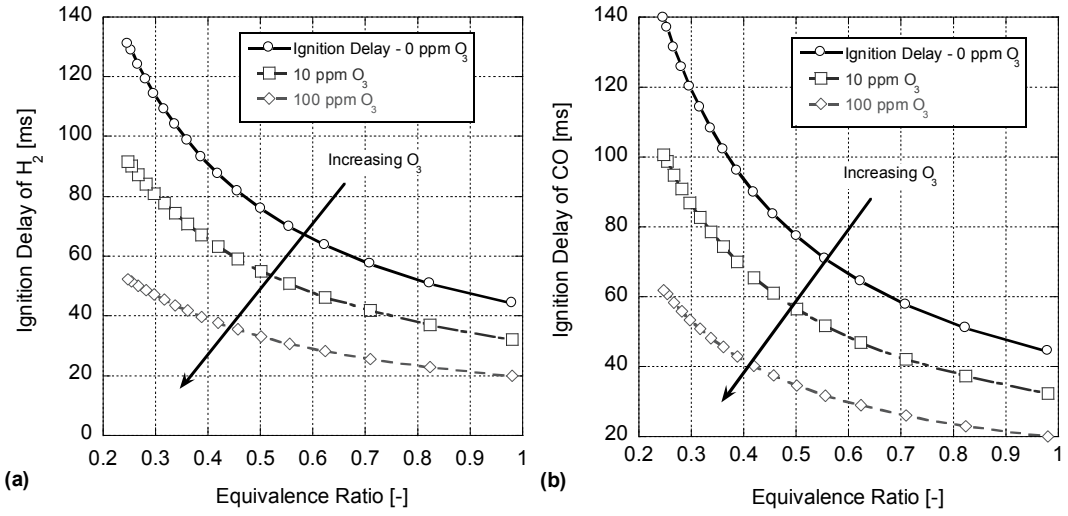

Figure 4. Ignition Delay of (a) Hydrogen and (b) Carbon Monoxide as a Function of Increasing Ozone Levels for a Constant Volume Simulation at Top Dead Center Conditions.

Figure 4a and Figure 4b present the results of this parametric sweep on ignition delay as a function of different ozone levels for hydrogen and carbon monoxide, respectively. Introducing ozone into a mixture of H_2 and CO causes it to react immediately because of its highly radical nature. As a result, this initiates the combustion process resulting in a reduced ignition delay that this study defines as the 10% mass fraction burned amount of H_2 and CO. Therefore, with respect to an internal combustion engine, since there will be some ozone present after the compression process (Figure 2), this will act to advance combustion to earlier in the thermodynamic cycle (Figure 4). This result is supported by the literature through findings of a reduced ignition delay when O_3 is added [33, 35, 37, 38, 40, 49, 54, 78].

Notice that the ignition delay of both H_2 and CO are significant in magnitude; i.e., greater than a few milliseconds. This is longer than findings in engine research for the ignition delay of diesel-like fuels. Since H_2 and CO have relatively strong chemical bonds that must be broken, their ignition delay is somewhat longer. In fact, Das

believes that hydrogen cannot be ignited through compression alone because of this detail [79]; e.g., the engine rotates too fast for these longer ignition delays. In comparison, since diesel fuel contains large chains of carbon and hydrogen bonds, thermal cracking is easier leading to heat release that propagates through more bonds breaking and further combustion. The important takeaway of Figure 4 is the relative trend of ignition delay when adding O_3 instead of the magnitude.

The final simulation analysis involves a comparison of NO_x emissions; however, this work must address the results of the change in ignition delay in Figure 4 since it will shift the relative time of production of the different species. Because reaction kinetics are a time-dependent phenomena, just comparing the NO_x predictions as a function of equal simulation time would be erroneous as less NO_x would be produced in general for the zero added O_3 case; e.g., combustion happens later, so NO_x production would be delayed, showing up as a lower value at the same simulation time. As a result, the authors' time-adjusted the O_3 added results in order to equate the 50% mass fraction burned time between all simulations.

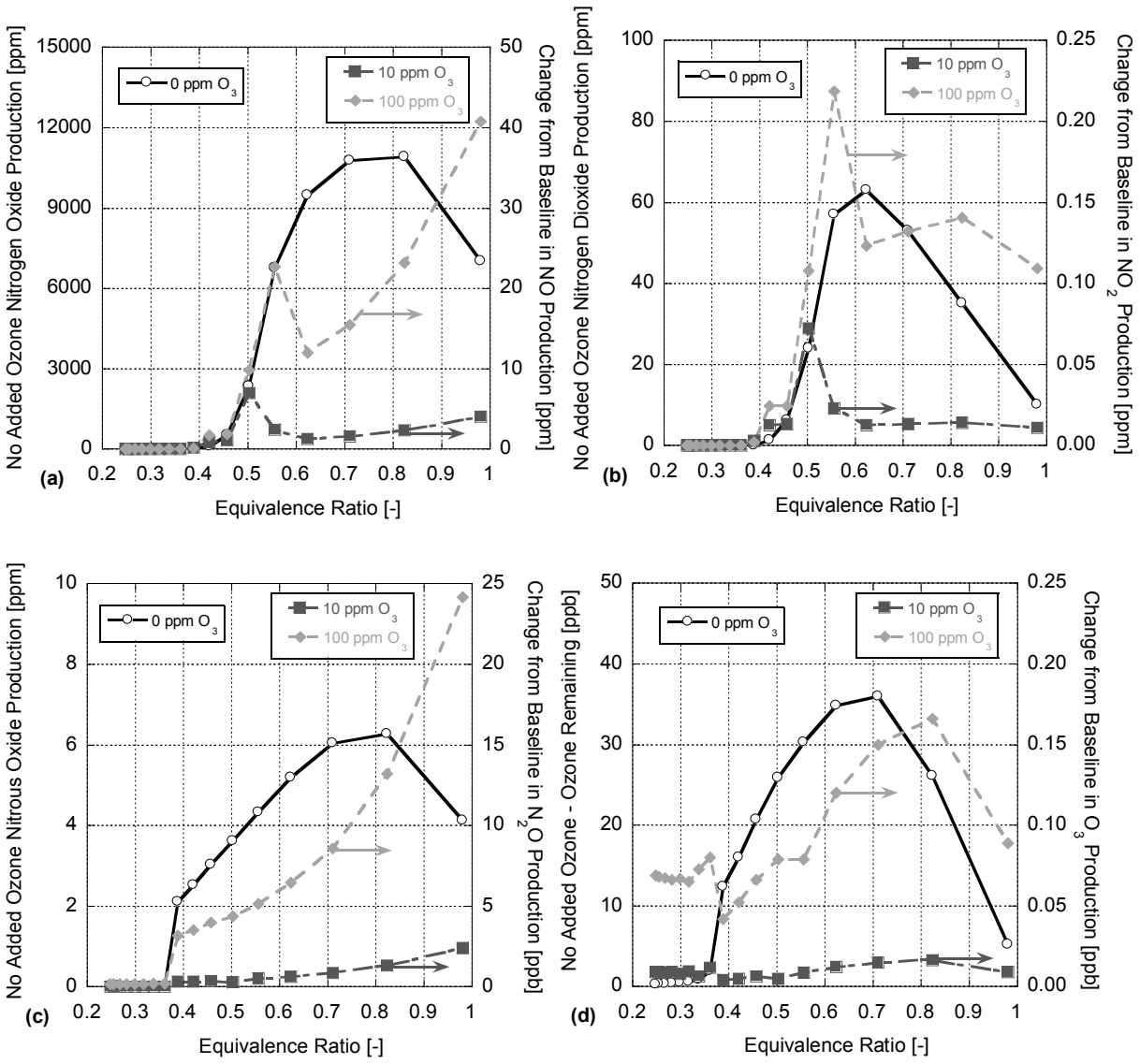

Figure 5. Comparison of (a) NO, (b) NO_2, (c) N_2O and (d) O_3 Levels when Adding 10 and 100 ppm O_3 to a Zero-dimensional Constant Volume Simulation.

Investigating the results in Figure 5, NO_x production follows the requirement of both high temperatures and excess oxygen in order to create the nitrogen-based species. When adding 10 ppm O_3, the second *y*-axis on the plots illustrates the production of a relatively small amount of NO and NO_2 over the zero ppm O_3 case (average of 2 ppm and 0.02 ppm, respectively). For N_2O and O_3, the change is nearly negligible since its magnitude is less than or equal to one part per billion. However, when 100 ppm O_3 is utilized in the model, the change is more significant with ample NO

and NO_2 production. Moreover, the change in N_2O is also significant; whereas, the relative amount of O_3 remaining at the end of the combustion process does not increase appreciably. As a result, the simulation studies indicate that adding ozone can increase NO_x and N_2O emissions while not considerably adding to the ozone emissions leaving the engine.

It is important to mention that (as discussed before) adding O_3 to the mixture does increase the temperature after combustion slightly due to its exothermic impact; 10 and 100 ppm O_3 increased the maximum temperatures on average 0.04 K and 0.33 K, respectively. To account for this impact, the simulations were re-run by adjusting the initial temperature of the ozone added cases (temperature at IVC) in order to match the maximum temperature after combustion. However, the results are not included here because the change in species production was negligible. Moreover, the trends with equivalence ratio were not analyzed (dip around an equivalence ratio of 0.6 for NO and NO_2) because the model was not calibrated, nor could be compared to experimental data; hence, exploration of the radical chemistry and postulation of non-linear effects would be purely hypothetical at this point. Instead, the goal was to investigate the trend change in NO_x and N_2O production through adding differing levels of ozone.

With respect to this change, the following pathways influence nitrogen radical species generation. As indicated in Eqn. (2), adding ozone to the mixture increases the level of atomic oxygen (O) within the mixture (verified via the numerical model). As a result, this leads to an increased amount of NO and N through the Rate Determining Step of the thermal NO mechanism:

$O + N_2 \Leftrightarrow NO + N$	(20)

Even though atomic oxygen is present on the parts per billion basis, the fact that N_2 is of a significant magnitude (around 70% by volume when including the fuel), this is significant enough to warrant an increase in NO on the ppm level. Furthermore, increasing levels of atomic oxygen lead to more atomic hydrogen via the chain combustion reactions of H_2 and O_2:

$H + O_2 \Leftrightarrow O + OH$	(21)
$O + H_2 \Leftrightarrow H + OH$	(22)
$OH + H_2 \Leftrightarrow H + H_2O$	(23)
$O + H_2O \Leftrightarrow OH + OH$	(24)

while additionally leading to more hydroxyl (OH) production. This increase in OH further helps the combustion process, along with O and H, illustrating why the ignition delay decreases.

The increased atomic oxygen level enhances atomic hydrogen production that subsequently promotes HO_2 creation [69]:

$H + O_2 + M \Leftrightarrow HO_2 + M$	(25)

With the combined influence of higher NO levels, this creates more NO_2 [2]:

$NO + HO_2 \Leftrightarrow NO_2 + OH$	(26)

However, because reversion back to NO can occur,

$NO_2 + O \Leftrightarrow NO + O_2$	(27)

with the increased atomic oxygen component, NO_2 does not increase significantly and the gain in NO_x occurs mainly because of increased NO levels through Eqn. (20).

With respect to the small increase in N_2O, Löffler et al. [80] investigated a reduced mechanism in its production as part of the thermal NO mechanism. They illustrated that atomic oxygen influences both the forward and reverse pathways (included in the Goswami et al. [74] kinetics modeled):

$N_2 + O + M \Leftrightarrow N_2O + M$	(28)
$N_2O + O \Leftrightarrow NO + NO$	(29)
$N_2O + O \Leftrightarrow N_2 + O_2$	(30)

From the simulation results presented, it appears that the addition of ozone enhances the production of N_2O over its destruction.

As a result, the impact of ozone in an internal combustion engine can be broken into three different facets that influence nitrogen oxides:

- The exothermic ozone decomposition reaction will increase the cylinder temperature: $T\uparrow$ $NO_x\uparrow$
- The destruction of ozone and radical production of atomic oxygen promotes NO_x creation pathways: $O\uparrow$ $NO_x\uparrow$
- Ozone promotes reduced ignition delays advancing combustion towards TDC resulting in higher combustion pressures and temperatures in an engine: $ID\downarrow$ $NO_x\uparrow$

In the next section, experiments will shed further light regarding the influence of ozone on engine combustion and emissions and help confirm the simulation results. Since the engine under study does not allow for dynamic adjustment of injection timing, the previously mentioned analysis (literature and simulation) postulates that the experiments should result in a reduced ignition delay resulting in higher in-cylinder temperatures along with greater NO_x emissions.

3.5 Experimental Setup

In order to generate reliable and repeatable results, this effort employs a single-cylinder engine for testing. The use of a single-cylinder engine eliminates the non-linearity in fluid mechanics and heat transfer of multi-cylinder engines allowing for a

clearer identification of trends from ozone injection. The single-cylinder engine for this experiment is a direct-injected Yanmar L100V diesel engine (see Table 1 for specifications). A Dyne Systems, Inc. Dymond Series 12 horsepower air-cooled regenerative Alternating Current (AC) dynamometer acts as the load upon the engine with a maximum speed of 7500 RPM while utilizing a Dyne Systems, Inc. Inter-Loc V OCS controller. A FUTEK rotary torque sensor (model #TRS-605) connected between the engine and dynamometer shafts provide torque readings for the system and can measure from 0-200 N-m. This range of readings eliminates any limiting factors from the torque sensor on the engine, including signal saturation due to torque spikes, while allowing for possible future testing under a higher power output.

Table 1. Engine and Dynamometer Specifications [7]

Engine	Value
Manufacturer and Model	Yanmar L100V
Type	Vertical Direct-Injection Compression Ignition
Engine Intake	Naturally Aspirated
Cooling	Air-Cooled
Cycle	4-Stroke
Displacement	435 cc
Number of Cylinders	1
Number of Valves	1 Intake, 1 Exhaust
Bore	86 mm
Stroke	75 mm
Connecting Rod Length	0.118 m
Crank Radius	0.038 m
Clearance Volume	2.1611×10^{-5} m^3
Cylinder Head/Piston Area	0.0058088 m^2
Compression Ratio	21.2
Injection Timing	15.5 (+/- 0.5) degrees BTDC
Intake Valve Close	122 degrees BTDC
Exhaust Valve Open	144 degrees ATDC
Continuous Rated Output	8.3 hp SAE

	6.2 kW
Rated Speed	3600 RPM
Injector Pressure	19.6 MPa
Aftertreatment	None
Engine Oil Used	Shell 15W-40
Dynamometer	
Manufacturer and Model	Dyne Systems, Inc.Dymond Series 12
Continuous Torque	21.1 ft-lbs
Continuous Power	12 hp
Speed Range	0-7500
Voltage	480 V
Phase	Three-phase
Frequency	60 Hz
Controller	Dyne Systems, Inc. Inter-Loc V OCS

Instrumentation for the engine includes thermocouples for ambient air temperature, engine intake temperature, exhaust port temperature, and downstream exhaust temperature. A Kistler 6052C piezoelectric transducer measures the pressure inside the cylinder of the diesel engine and measures from 0 to 250 bar with a minimal error of 0.5%. The setup utilizes a Kistler 2614B1 encoder in correlation with the transducer bolted directly to the flywheel of the engine. The encoder sends an analog signal that is converted to digital crank angle and TDC signals via a signal converter (model #2614B2). Employing a Kistler pulse multiplier (model #2614B4) allows adjustment of the encoder angle resolution from 0.1º to 6º. A National Instruments-based data acquisition system using LabView records these digital crank angle and pressure signals. This allows for highly accurate pressure readings at 0.5 degree increments. A Micro-Motion Coriolis flow meter (model #CMF010M) provides the mass flow and density measurements of the fuel. A Merriam laminar flow element (model #50MW20-2) paired with an Omega differential pressure transducer (model #PX277-

30D5V) calculates the airflow readings. Additional sensors include ambient and exhaust pressure along with the relative humidity of the test cell environment.

Measurement of ozone concentration at the engine intake, which is downstream of the injection point, was done using a 2B Technologies Ozone Concentration Monitor (model #106-M). The range of this monitor is accurate to 2% of the reading for the range of 0-1000 ppm O_3. This will allow for accurate measurements during a full ozone sweep of low to high concentrations. Ozone supply to the engine intake involves the use of an ozone generation system with the ability to produce concentrations up to 430 ppm O_3. This system includes an Absolute Ozone ATLAS 30 Ozone Generator that provides 30 g/hr maximum ozone output with 14% ozone concentration by weight. An AirSep Onyx Plus Oxygen Concentrator supplies pure oxygen as a source for the ozone generator. Using oxygen as a source gas eliminates nitrogen, argon, and other gases from the air supply in order to create the purest generation of ozone possible. This leads to results stemming directly from the addition of ozone, rather than nitrogen and other gases in the air. Figure 6 shows the ozone sampling and injection line positions in the intake.

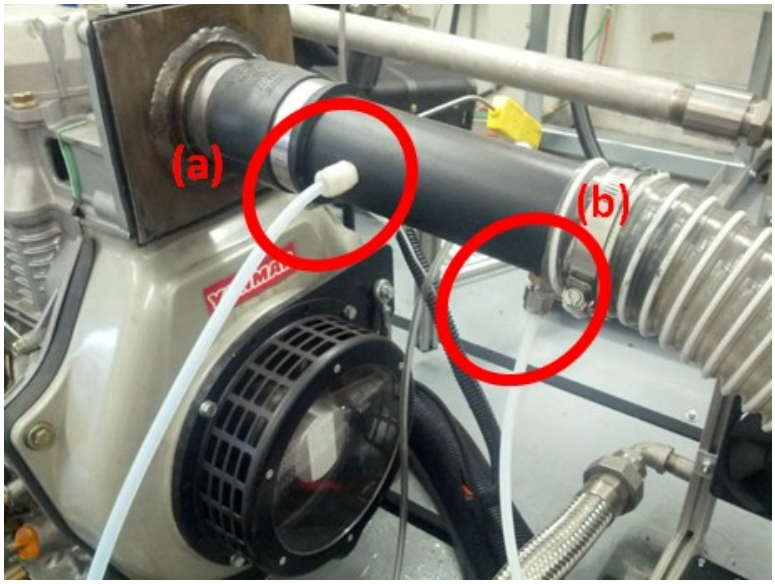

Figure 6. Picture of the (a) Ozone Sample Line and (b) Ozone Injection Line Port on the Intake of the Single Cylinder Engine.

Emission analysis includes an AVL SESAM Fourier Transform Infrared Spectroscopy (FTIR) in order to measure a wide range of emissions. Of interest for this study are water (H_2O), carbon dioxide (CO_2), oxygen (O_2), carbon monoxide (CO), nitrogen oxide (NO), nitrous oxide (N_2O), and nitrogen dioxide (NO_2). The device utilizes a probe in the exhaust of the Yanmar to retrieve the gas sample. The hot gas flows through a heated prefilter in order to eliminate particulates from the exhaust gas stream. Following the heated prefilter, the sample stream flows through heated lines at 191°C in order to prevent condensation build up. At this point, the sample stream diverges into three separate components for measurement. These components consist of the FTIR analyzer, the Flame Ionization Detector (FID) for total hydrocarbon measurements, and the Magnos 106 for measuring oxygen.

Measurement of particulate matter takes place using an AVL 415S Variable Sampling Smoke Meter. Through a probe built into the exhaust of the Yanmar, the

device samples a volume of exhaust. Calculation of an effective length happens by drawing this volume through a filter paper with subsequent measurement using an orifice flow meter. Detection of the blackening of the filter paper due to PM occurs through usage of an optical reflectometer head. From the filter paper blackening and effective length values, the operator is provided a Filtration Soot Number (FSN) and soot concentration in mg/m^3. Note that the operator adjusts the sample time according to the level of filter paper blackening. This is because different run-time conditions of the engine can produce a wide range of PM measurements. If the sampling volume remains constant for all conditions, the filter paper may blacken completely, resulting in inaccurate data. Ideal operating conditions specified by the manufacturer lie in-between the range of one to six for respective filter paper blackening. For repeatability, the paper blackening number remained at four for this set of testing. Figure 7 presents the test cell with all components indicated.

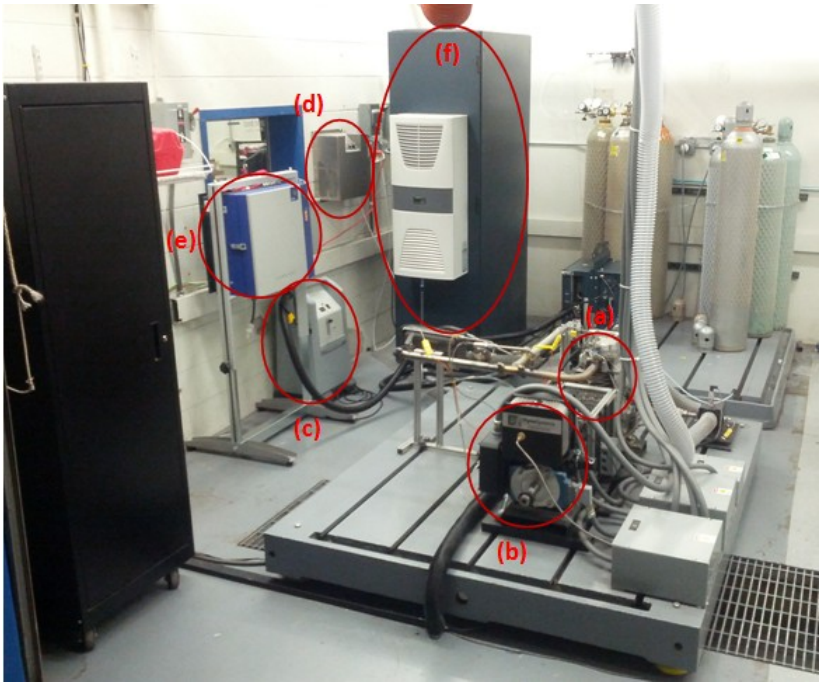

Figure 7. The University of Kansas Single Cylinder Engine Test Cell including (a) Yanmar Engine, (b) AC Dynamometer, (c) Oxygen Concentrator, (d) Ozone Generator, (e) AVL Smoke Meter, and (f) AVL FTIR.

3.5 Test Strategy

The effects of ozone on combustion and emissions included testing five distinct engine loads during the same day at the same engine speed (3600 rpm); 0.5 N-m, 4.5 N-m, 9.0 N-m, 13.5 N-m, and 16.75 N-m. Note that the current engine equipment limits engine speed to 3600 RPM because of the mechanical unit injector system and speed governor employed. Future efforts include replacing this system with a rail injection system for complete control of the injection event for testing under different engine speeds. In order to produce comparable results for the no load cases, this effort utilized a minimal load of 0.5 N-min order to provide corresponding values for brake specific fuel consumption (*bsfc*) and emission data in g/kW-hr. Other researchers employ this methodology as a viable option for low load situations [37]. As mentioned in the prior section, an AC dynamometer applied the load during each test. Capture of the

experimental data occurs once the engine reached steady-state, which was determined when the temperature of the downstream exhaust port changed less than one percent per minute. Collection time for emissions on each load was five minutes, with a sample rate of one sample per second. Sample time for particulates varied between 30 and 120 seconds. In particular, in order to produce accurate and repeatable results, the investigators targeted a blackening number of four. Hence, the adjustment of sample times for different engine loads to achieve the desired blackening number. Sampling commenced only when reaching steady-state of the engine under each load and specific ozone addition. Taking engine performance metrics for two minutes during the emission testing at a rate of ten samples per second provided low experimental error. Moreover, the LabView setup records in-cylinder pressure traces concurrently to the performance and emissions data. The sample rate for pressure readings occurred at a 0.5-degree crank angle resolution and the results presented later comprise of the average of 60 thermodynamic cycles. Experimental error analysis includes calculation of the relative standard error for each data point and a root mean squared analysis for each subsequent performance parameter calculation. Furthermore, the plots within the results and discussion section provide linear trend lines, in some circumstances, in order to help with the visual identification of the trends indicated.

3.6 Results and Discussion

The initial goal of testing was to employ ozone intake concentrations at 0, 20, 50, 100, and 200 ppm levels. However, ozone generation is significantly hindered by temperature and humidity [20]. As a result, the maximum consistent output possible with the given conditions on the designated test day was approximately 125 ppm.

Hence, Figure 8 presents the in-cylinder pressure profiles for increasing ozone concentrations at different loads with the average ozone concentration during the test indicated in the legend. Moreover, Figure 8 only plots the crank angle between -10° to +15° after TDC (ATDC) since visual indication of ignition delay is located in this region. Observation of these plots confirm the results found in literature and through the combustion modeling that ozone injection will decrease ignition delay with the most dramatic effect occurring at lower loads [33, 35, 37, 38, 40, 49, 54, 78]. In particular, comparing the results amongst all engine loads, the change in ignition delay from 0 ppm ozone injection to 20 ppm is the most significant. As previously discussed, both Faison and the model simulations describe that increasing levels of ozone beyond this concentration are not meaningfully advantageous. The reasoning comes from the model predictions that simulate an increase in ozone destruction at higher concentrations during the compression event.

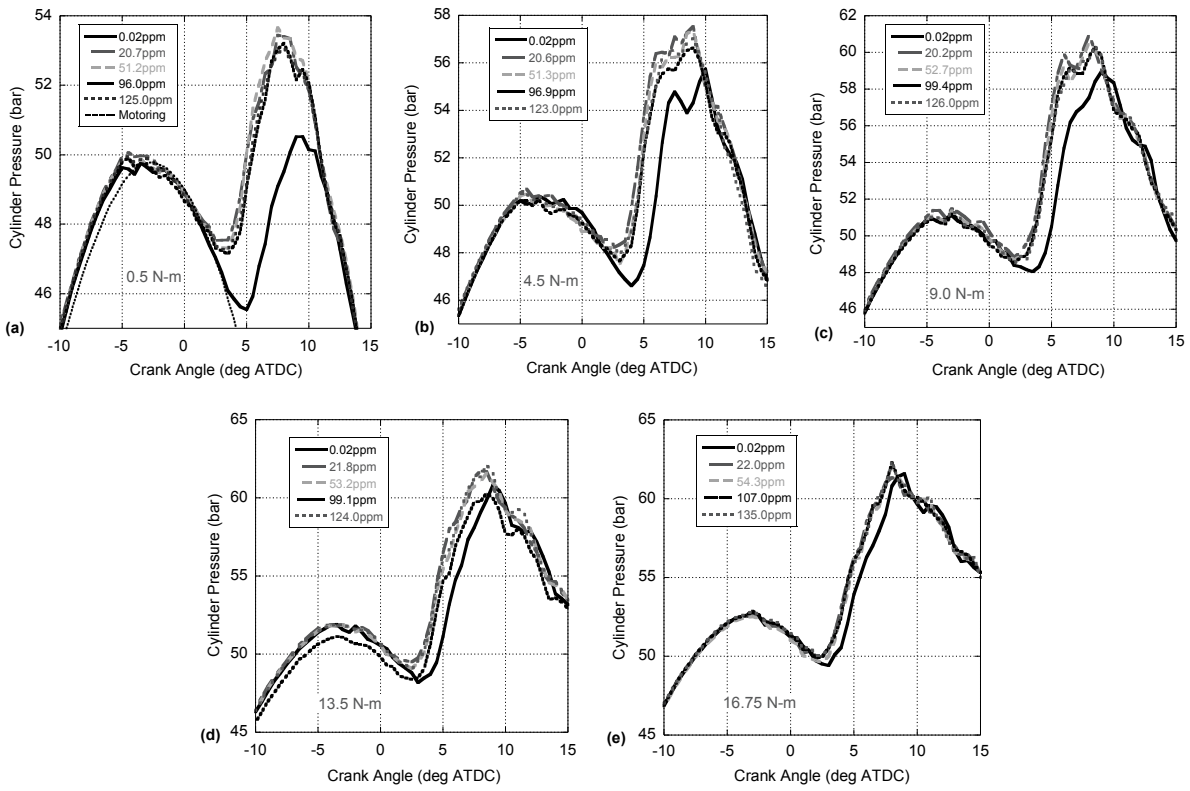

Figure 8. In-cylinder pressure traces at (a) 0.5 N-m, (b) 4.5 N-m, (c) 9.0 N-m, (d) 13.5 N-m, and (e) 16.75 N-m as a Function of Increasing Ozone Levels.

Investigating the influence of ozone on the intake charging process requires calculation of the volumetric efficiency of the engine. This parameter indicates the effectiveness of the amount of air brought into the engine in relation to the volume displaced by the piston. An increase in volumetric efficiency would be the result of the engine pulling in a given amount of air, and then displacing the piston a greater amount than previously with the same amount of air. The calculation of volumetric efficiency (η_v) follows as:

$$\eta_v = \frac{\dot{m}_a}{2 \cdot \rho_a \cdot N \cdot V_d} \times 100 \qquad (31)$$

where $\dot{m}_a$ is the air mass flow rate, ρ_a is the ambient air density, N is engine speed, and V_d is the engine displacement volume. Use of the ideal gas law allows for calculation of the ambient air density:

$$\rho_a = \frac{p_{amb}}{R_{air} \cdot T_{amb}} \quad (32)$$

where p_{amb} is the ambient pressure of the test cell, R_{air} is the gas constant specific to air, and T_{amb} is the ambient air temperature of the test cell. Furthermore, from the bore and stroke of the engine, one can compute the displacement volume from the bore (*b*) of the engine and its stroke (*s*):

$$V_d = \frac{\pi b^2}{4} s \quad (33)$$

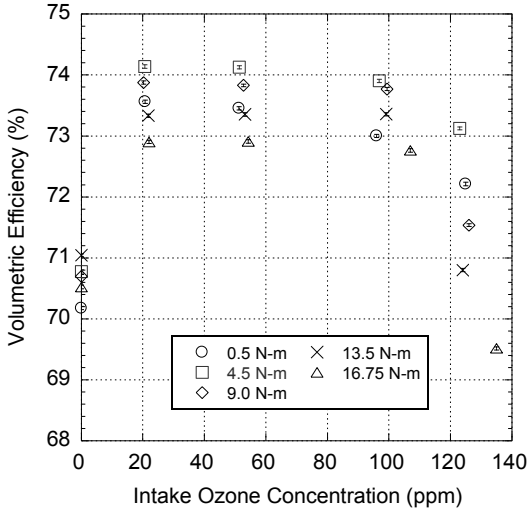

Figure 9.Volumetric efficiency as a function of ozone concentration and engine load.

As Figure 9 illustrates, it appears that the volumetric efficiency of the engine increases initially from the addition of 20 ppm ozone. Past this concentration, increasing amounts of ozone are not beneficial from a volumetric efficiency standpoint. Initial logic dictates that this is because of the fact that the addition of ozone displaces some air (effectively nitrogen); however, generation of ozone only happens in small

concentrations that would not lead to as dramatic of a volumetric efficiency rise. Instead, the oxygen concentrator employed in the experimental setup feeds ozone and oxygen to the engine. Hence, it adds a small flow rate of oxygen that shows up in the volumetric efficiency calculations. Of importance, the ozone generator produced approximately 15% ozone by weight at low concentrations but only 11% at full production (approx. 125 ppm). As a result, some of the improvement in combustion in Figure 8 relates to an enhancement of oxygen by the ozone generation system in general; e.g., oxygen flow rate in addition to ozone components. Nevertheless, the literature illustrates that ozone will act to reduce the ignition delay of the engine and plays a primary role.

Neglecting the 0.5 N-m load experiments that result in less stable combustion and more fluctuations in airflow and subsequent measurements, the volumetric efficiency decreases with load. This is because the temperature of the engine is increasing from hotter combustion events. Therefore, the cylinder walls heat up along with the air inside the engine (reduction in density through ideal gas law influences the mass flow rate of air through the engine) reducing the air charging potential of the cylinder. Moreover, as the cylinder walls increase in temperature this will aid in the convective heat transfer to the working fluid facilitating a lower ignition delay with load, also seen in Figure 8 as combustion phases closed towards TDC.

As previously discussed, NO_x emissions are a major concern for CI engines and Figure 10 displays the resulting influence of ozone injection on these emissions. Of importance, presentation of results on a brake specific basis (e.g. emissions per power output) allows for comparison with other CI engines of different sizes. The advanced

combustion caused by ozone injection results in increased combustion temperatures; e.g., increase in combustion pressures through Figure 8 coupled with the ideal gas law. Higher combustion temperatures promote both NO and NO_2 formation through the thermal NO mechanism. Moreover, the previous discussion revolving around the radial production of oxygen (literature and simplified combustion model) illustrates that ozone can act through chemistry to increase NO_x. The most significant increase in NO_x between ozone concentrations is from 0 ppm to 20 ppm with erratic trends seen at higher ozone levels. This result follows from the discussion regarding its destruction during the compression process. It is important to note that N_2O concentrations only consist of approximately 0.002-0.005% of the NO_x emissions. In additions, the concentrations were so low that the FTIR had issues obtaining accurate readings resulting in an uncertainty level of about 20%. Hence, the authors cannot conclude any findings about N_2O emissions.

The trend of decreasing NO_x emissions with load relates to two phenomena. Adding more fuel in order to increase the power output releases more energy, subsequently raising the combustion pressure and temperature (see Figure 8). This will lead to additional NO_x production through the thermal NO mechanism. However, the combustion and thermal efficiency of the engine increases with load leading to a more efficient process (results presented later in this section). This, in turn, will reduce the relative amount of fuel per unit power decreasing the normalized values of NO_x. Hence, the results in Figure 9 illustrate that the improvement in fuel economy outweighs the relative gain in NO_x from higher temperatures.

Heywood states that NO_x emissions for diesel engines typically are comprised of between 10 to 30 percent NO_2 [2]. The formation of NO_2 happens through the oxidation of NO at high temperatures in the flame front. If the temperature in the cylinder remains relatively high, NO_2 quickly decomposes back to NO. However, it remains in the form of NO_2 when the periphery of the flame front is cooled relatively fast from the surrounding turbulent air. This illustrates why the lower loads in Figure 10 (d), which have a relatively colder burning mixture, have a higher fraction of NO_2. From the experiments, ozone does not appear to have any appreciable increase in the NO/NO_x ratio as found through the numerical simulations. The plot does illustrate increasing trend lines at the lower loads when ozone has a relatively bigger influence; however, the authors cannot confirm definitively if this is the influence of ozone.

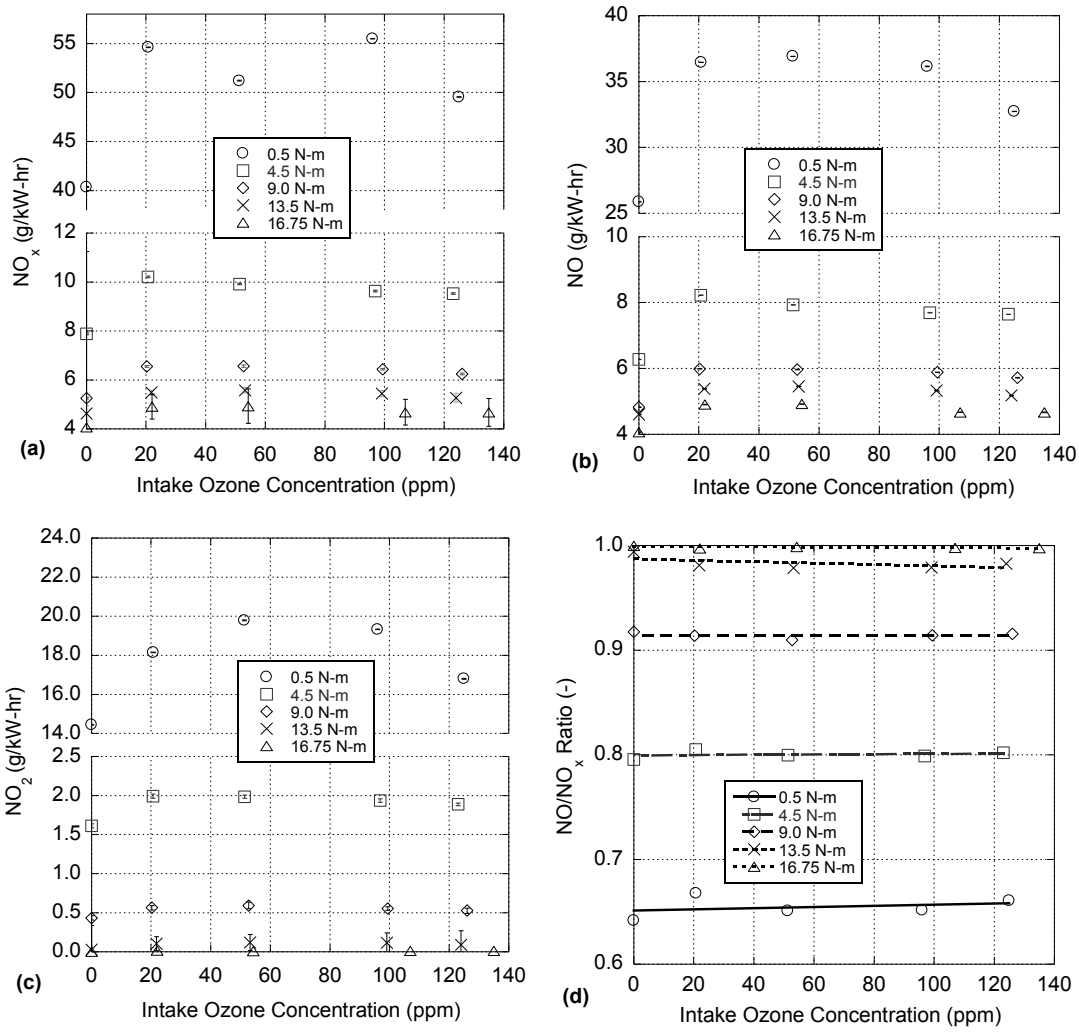

Figure 10. The Influence of Ozone Addition on (a) NO_x, (b) NO, (c) NO_2 Emissions, and (d) Ratio of NO/NO_x.

As previously discussed, the NO_x and PM tradeoff is an important aspect to discuss when addressing methods for altering CI emissions. Particulates typically form in rich fuel to air regions within the cylinder. Their production is most prevalent near the injector nozzle, as the equivalence ratio changes drastically from lean to rich in a relatively small area. The reduction in ignition delay with ozone injection will lead to higher pressures and temperatures promoting a hotter burn. However, a reduction in ignition delay increases the relative amount of diffusion burn for a given amount of fuel injected (less premixed combustion, more diffusion burn). Extended diffusion burn

phases lead to increased PM production because of combustion happening around a rich fuel core [81, 82]. Moreover, ozone is a highly radical species and reduces acetylene, a precursor to PM production. Finally, increasing the oxidizer level in the cylinder through replacement of nitrogen with ozone can act to reduce locally the equivalence ratio around the injector nozzle leading to a leaner burn. The trends in Figure 11 illustrate that the influence of ozone acts to reduce PM with ignition delay and ozone chemistry assumed here to be the dominant effects. It is important to note that no significant trend under the no load case is seen because of the relatively low levels of fuel injected and the less stable combustion; e.g., a small amount of fuel creates less PM under a wider range of crank angles for initiation of combustion. Again, the most significant reduction in PM occurred from 0 ppm to 20 ppm in ozone concentration. With increasing ozone concentrations from that point, the effects on PM are unclear (similar to NO_x).

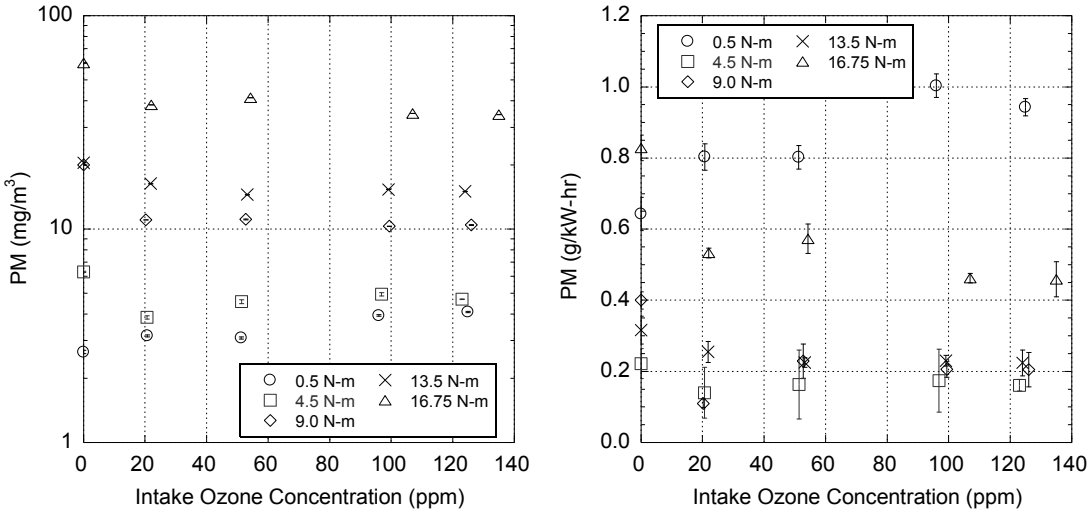

Figure 11. PM Concentration Levels Resulting from Ozone Injection on a Concentration and Brake Specific Basis.

Observing the PM trends across all loads in Figure 11 illustrates that PM emissions on a concentration basis increase with load. Initial thoughts are this is an

opposite trend as to what should occur since combustion temperatures are increasing, the level of oxidation of PM should increase along with combustion efficiency. While this is indeed true as indicated by the growing pressures with load in Figure 8, this figure also shows that combustion phasing does not change dramatically when adding more fuel. In particular, the rise in maximum pressure between no load and full load (no ozone) is around 10 bar while combustion starts within a few degrees of 5° ATDC in all cases. Instead, the width of the combustion pressure profile increases with load. Because of the mechanical unit injector system employed on the engine, at higher loads fuel is not sent earlier into the engine towards TDC for more power (most likely to keep NO_x emissions low), instead more fuel is sent in later during the expansion process. In this situation, the piston expands the working fluid causing lower pressures and temperatures. In other words, the engine is sending in more fuel during a less optimal time for combustion. Moreover, more fuel with similar initiation characteristics leads to similar premixed burn fraction that subsequently increases the level of diffusion burn, which is now occurring under relatively lower expansion temperatures. Hence, PM emissions will increase with load for this particular engine design. Calculating PM on a brake specific basis additionally finds this trend after removing the no load values.

In order to assist in the explanation of the PM results, the combustion efficiency (η_c) is a beneficial performance parameter to calculate. Combustion efficiency is the amount of fuel energy released during the combustion process. In essence, it is a measure of the conversion of fuel chemical energy into potential thermal energy useful for power (not resultant power, potential for power). Included in the analysis are heating values of the fuel, as well as exhaust constituents:

$$\eta_c = \left[1 - \frac{\sum_{j=1}^{n} \dot{m}_j \cdot Q_{lhv,j}}{\dot{m}_f \cdot Q_{lhv,f}} \right] \times 100 \qquad (34)$$

where $\dot{m}_j$ is the mass flow rate of the exhaust constituents, $Q_{lhv,j}$ is the corresponding lower heating values, $\dot{m}_f$ is the fuel mass flow rate, and $Q_{lhv,f}$ is the lower heating value of the fuel. Hydrogen is a common exhaust constituent necessary for accurate combustion efficiency calculations, as it has a significant lower heating value (120 MJ/kg). Unfortunately, the ability to measure hydrogen was not available for these tests. However, the amount of hydrogen can be estimated by assuming similar molar ratios of H_2O:CO_2 and H_2:CO [7, 8, 83]. Note that, for this calculation, the lower heating value used for HC emissions was estimated at 44,700 kJ/kg-K [7, 83] and PM is estimated to have a lower heating value equal to carbon at 32,810 kJ/kg-K [84] since this species is its primary constituent.

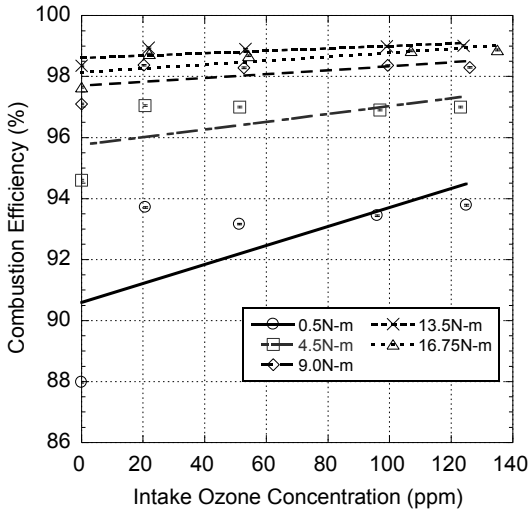

Figure 12. Combustion Efficiency Calculations Resulting from Ozone Injection and Engine Loading.

As shown in Figure 12, combustion efficiency generally increases with both the application of ozone and load. An increase in combustion efficiency correlates to more

of the chemical energy from the fuel converted into potential thermal energy. With a higher amount of thermal energy, a hotter and more complete combustion will occur, resulting in the destruction of PM and other partial combustion emissions. With respect to ozone, an increase in combustion efficiency results from the shorter ignition delays as seen in Figure 8. In addition, combustion efficiency increases with engine load. Higher loads result a greater energy released leading to higher combustion temperatures and pressures. The exception to this trend is at the highest loading where combustion efficiency decreased slightly as compared to the combustion efficiency at 13.5 N-m. This is because the engine is reaching its mixing (smoke) limit with respect to air finding fuel during the injection process. This smoke limit is further evident from the rise in PM emissions at this load (Figure 11). At the upper loads, the efficiencies are upwards of 98%, leaving minimal to no room for further improvement due to ozone injection. Hence, ozone injection has a larger influence at lower loads when combustion efficiency is relatively lower.

In addition to PM, hydrocarbon emissions are equally a concern for people's health along with negative environmental effects such as smog. In order to reduce the complexity of the analysis in this paper, the HC analysis only includes total HCs. Future work will explore the individual components and build off the results presented here. As shown in Figure 13, ozone injection does not significantly influence total hydrocarbons with linear trend lines indicating a slight decrease due to ozone injection. Recalling from earlier discussions, ozone acts as follows:

- Reduces ignition delay leading to a hotter burn and better combustion efficiencies: HC↓

- Influences HC chemistry to reduction in acetylene; hence, assume that ozone will reduce other HC components: HC↓
- Increases the level of diffusion burn that can lead to more HC emissions: HC↑

Since combustion efficiency is already high for CI engines resulting in less potential for reduction, HC emissions only decrease slightly with ozone injection.

Increasing load results in decreasing HC emissions. As seen in the pressure traces, the peak pressure increases approximately 10 bar from the no load case to the 16.75 N-m test (with no ozone). The increasing combustion levels with load facilitate higher temperatures along with higher combustion efficiencies leading to a reduction in HC emissions. The difference between PM increasing and HC decreasing with load involves their resulting production and destruction process. In a generalized sense, PM forms during combustion; whereas, HC oxidizes. Hence, while they are both partial oxidation components, increasing load of the engine substantially increases the amount of carbon entering that facilitates more potential for PM growth [2].

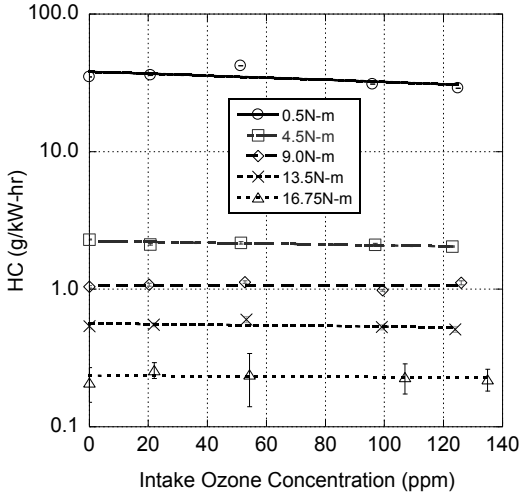

Figure 13. Total Hydrocarbons Measured as a Function of Ozone Concentration and Engine Load.

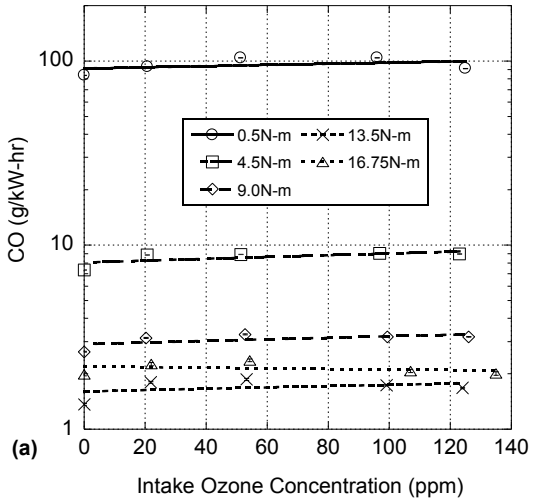

Figure 14. The Influence of Ozone and Engine Load on (a) CO and (b) CO_2 Emissions.

Carbon monoxide emissions are additionally worth noting, since it is harmful to the respiratory system, and contributes to the destruction of tropospheric ozone. As shown in Figure 14, CO increases with the injection of ozone. Without including the no load conditions, the CO emissions increase the most under 0 ppm to 20 ppm and remain fairly constant throughout the remaining concentrations of ozone. The increase in CO with the addition of ozone is similar to the results calculated by Faison's combustion model [36]. In particular, Faison finds that the formation of CO is five times greater than CO_2 during the oxidation of hexane. Since the authors' simplified combustion model does not include radical hydrocarbon chemistry, this result is not evident. Further work should explore the pyrolysis of hydrocarbon fuels and what leads to this increase of CO. The trends of CO with load follow the analysis of HCs since they are both partial oxidation components. Of importance, higher loads can slightly increase CO production due to dissociation effects at greater temperatures.

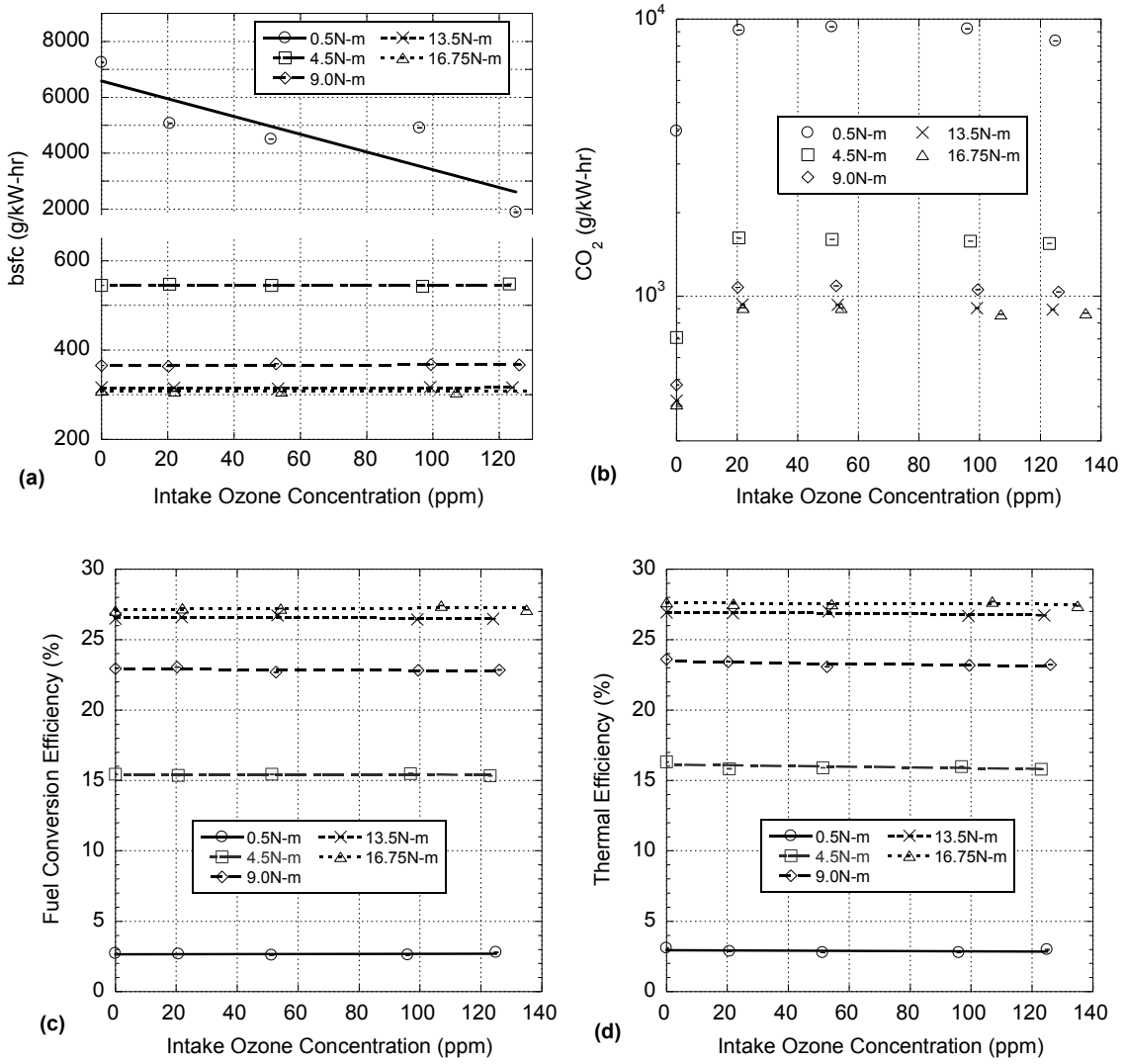

Figure 15. Effects of Ozone on (a) bsfc, (b) CO_2, (c) Fuel Conversion Efficiency, and (d) Thermal Efficiency.

Fuel consumption plays a critical role in the investigation of assisted combustion and alteration of run-time properties. This effort calculates the brake specific fuel consumption (bsfc) from the measured fuel mass flow rate and the power calculated through the torque transducer and the speed from the dynamometer. Figure 15 illustrates that the no engine load values are significantly higher. Since the engine is effectively under idle, there is a minimal power output for the engine resulting in high bsfc values (small denominator in the calculation). It should be noted that the

uncertainty for the no load case is not included on this plot. Because the load on the engine is minimal, any small change in power output during the test results in significant uncertainty values. At this load, it is evident that the fuel consumption decreases with the injection of ozone. For the remaining loads, the trends are close to the uncertainty of the measurements and calculations; hence, the authors cannot come to a generalized result.

In order to investigate the fuel consumption further, analysis of CO_2 emissions, fuel conversion and thermal efficiencies in Figure 15 helps indicate fuel usage as a function of ozone assistance. Figure 12 demonstrates that combustion efficiency increases that would act to facilitate the production of CO_2. Looking at the trends, there is an initial jump in CO_2 results from 0 to 20 ppm ozone helping illustrate further how ozone helps promote complete combustion. However, CO_2 emissions alone cannot help with the analysis of brake specific trends at higher loads due the addition of ozone since CO_2 levels remain constant after this jump.

Fuel conversion efficiency (η_f) measures the efficiency of useful (aka shaft) work resulting from added fuel energy:

$$\eta_f = \frac{P}{\dot{m}_f \cdot Q_{lhv,f}} \times 100 \quad (35)$$

where *P* is the output power of the engine, $\dot{m}_f$ is the mass flow rate of the fuel, and $Q_{lhv,f}$ is the lower heating value of the fuel. Since the dynamometer holds power constant for each load, and the lower heating value of the fuel remains constant, the only differing value is the mass flow rate. Observing Figure 15 (c), fuel conversion efficiency stays approximately constant within experimental accuracy with the addition of ozone.

The final calculation involves thermal efficiency of the engine (η_t):

$\eta_t = \frac{\eta_f}{\eta_c} \times 100$	(36)

The thermal efficiency demonstrates the effectiveness of the engine as it converts the potential thermal power into actual power. A high efficiency would result in a more "constant volume" like combustion where the heat release is more instantaneous, resulting in the highest temperatures and pressures possible. Moreover, high thermal efficiency might also result when the mixture is more advantageous chemically from a ratio of specific heats perspective. In other words, if the mixture contains a higher ratio of specific heats (like air), its expansion work increases as the area underneath the pressure-volume curve grows.

In Figure 15 (d), with respect to ozone addition, thermal efficiency apparently decreases with ozone addition (also calculated by the authors separately through pressure-volume work that additionally demonstrated this same decrease). This is counterintuitive to earlier results via advanced combustion through a decreased ignition delay that would promote more ideal combustion timing. Since thermal efficiency removes the dependency of combustion efficiency (increases), it appears that adding ozone adversely influences the rate of combustion after initiation and/or modifies the ratio of specific heats of the mixture. CO emissions do increase indicating that ozone has an influence on hydrocarbon radical chemistry. However, further work is required investigating the combustion process in order to come to a definitive conclusion as to ozone's influence on fuel economy. Finally, as load increases, fuel consumption levels decrease as discussed prior (along with increases in fuel conversion and thermal efficiencies): more energy released leads to higher temperatures, earlier combustion

through a subsequent reduction in ignition delay (hotter chamber plus more energy released), and faster combustion rates leading to more constant volume like combustion.

3.7 Conclusion

One considered method for defeating the common NO_x-PM tradeoff in CI engines is through the addition of ozone. This work discussed previous efforts in this field illustrating that ozone will reduce ignition delay and participate in the combustion process. In order to elaborate on the findings, this effort includes a simplified combustion model including ozone kinetics that simulates ozone injection for a single cylinder Yanmar CI engine. This model illustrates the decomposition rate of ozone is low enough that ozone will survive the compression process and contribute to combustion events. In particular, ozone does act to reduce ignition delay. Beyond a certain level of ozone addition, the destruction of ozone increases illustrating a sweet spot of production versus usage depending largely on the compression event and subsequent temperatures. Furthermore, there will not be an increase in ozone emissions from the engine, since it will not survive combustion. Moreover, the decomposition of ozone is an exothermic process that leads to a slight increase in temperature in the cylinder. However, this increase is approximately a few degrees Kelvin; hence, it is small in comparison to combustion events. Overall, the model indicates that NO_x and N_2O emissions will increase with the addition of ozone.

In order to elaborate on the model results, experiments illustrate that the injection of ozone will reduce the ignition delay leading to an earlier and more complete combustion. Moreover, as the model predicts, there is a certain level of ozone that is

beneficial and beyond this level, no change in the results is seen. This increase in temperature and pressure inside the cylinder facilitates the formation of NO_x (no perceivable trend in N_2O) while simultaneously reducing the amount of PM. Hence, the NO_x-PM tradeoff is evident with the addition of ozone. Furthermore, hydrocarbon emissions decrease but carbon monoxide emissions increase. The result is that the authors cannot confirm any significant trend with brake specific fuel consumption within experimental accuracy.

After observing the results from ozone injection, one major influence of ozone is on the ignition timing. This leads to future work in this area for determining if the effects of ozone on combustion and emissions are resulting from the kinetic processes related to ozone, or strictly a decrease in ignition delay. Since 20 ppm appears to be the most perceptible concentration for injection, future efforts will advance the injection timing in order to match that of an ozone injection of 20 ppm. The process of installing a rail injection system on the Yanmar has begun, so this testing will be possible in the near future. Analyzing the NO_x-PM tradeoff and *bsfc* of this study would bring a conclusion to whether or not the trends seen are due to injection advance, or the chemical phenomena set forth by ozone. This would determine if ozone injection is a viable method for emission regulation on CI engines and defeats the common NO_x-PM tradeoff.

Furthermore, the authors chose to use syngas in the model rather than combustion of a hydrocarbon-based fuel in order to eliminate the influence of radical pyrolysis. Future efforts can extrapolate the results here to a full simulation including a representative hydrocarbon fuel. It is important to mention that the prompt NO route will

be more prevalent when using a hydrocarbon fuel rather than syngas. Hence, future work can explore the influence of ozone on the prompt NO mechanism. Finally, follow-up efforts are underway at exploring the individual HCs monitored by the FTIR.

3.7 Acknowledgements

This study was supported by the US Department of Transportation, Office of the Secretary, Grant No. DTOS59-10-G00109 and Emission Control Solutions, LLC.The intellectual guidance and support of Dr. Christopher Depcik of Mechanical Engineering made this work possible. Dr. Peltier provided emissions expertise critical to the success of the study. Additional assistance included efforts from Michael Mangus of Mechanical Engineering with engine testing and analysis.

References

1. Kawano, D., et al., *Effect of Exhaust Gas Recirculation on Exhaust Emissions from Diesel Engines Fuelled with Biodiesel.* SAE Technical Paper, 2007: p. 24-0128.
2. Heywood, J.B., *Internal Combustion Engine Fundamentals*1988, New York: McGraw-Hill, Inc.
3. Bhusnoor, S.S., M.K.G. Babu, and J. Subrahmanyam, *Studies on performance and exhaust emissions of a CI engine operating on diesel and diesel biodiesel blends at different injection pressures and injection timings.* SAE Technical Paper, 2007: p. 01-0613.
4. Balat, M., *Potential alternatives to edible oils for biodiesel production–A review of current work.* Energy Conversion and Management, 2011. **52**(2): p. 1479-1492.
5. Pinto, A.C., et al., *Biodiesel: an overview.* Journal of the Brazilian Chemical Society, 2005. **16**(6B): p. 1313-1330.
6. Duncan, A.M., et al., *High-pressure viscosity of biodiesel from soybean, canola, and coconut oils.* Energy & Fuels, 2010.
7. Cecrle, E., et al., *An Investigation of the Effects of Biodiesel Feedstock on the Performance and Emissions of a Single-Cylinder Diesel Engine.* Energy & Fuels.
8. Mangus, M.D., *Design, Construction, and Validation of an In-Cylinder Pressure Recording System for Internal Combustion Engine Analysis.* 2012.
9. Adi, G., et al., *Soy-Biodiesel Impact on NO x Emissions and Fuel Economy for Diffusion-Dominated Combustion in a Turbo− Diesel Engine Incorporating Exhaust Gas Recirculation and Common Rail Fuel Injection.* Energy & Fuels, 2009. **23**(12): p. 5821-5829.
10. Ban-Weiss, G.A., et al., *A numerical investigation into the anomalous slight NO< sub> x</sub> increase when burning biodiesel; A new (old) theory.* Fuel processing technology, 2007. **88**(7): p. 659-667.
11. Benjumea, P., J.R. Agudelo, and A.F. Agudelo, *Effect of the degree of unsaturation of biodiesel fuels on engine performance, combustion characteristics, and emissions.* Energy & Fuels, 2011.
12. Enweremadu, C. and H. Rutto, *Combustion, emission and engine performance characteristics of used cooking oil biodiesel--A review.* Renewable and Sustainable Energy Reviews, 2010. **14**(9): p. 2863-2873.
13. Knothe, G., *"Designer" Biodiesel: Optimizing Fatty Ester Composition to Improve Fuel Properties†.* Energy & Fuels, 2008. **22**(2): p. 1358-1364.
14. Knothe, G., J.H. Van Gerpen, and J. Krahl, *The biodiesel handbook*2005: Amer Oil Chemists Society.
15. McCormick, R.L., et al., *Impact of biodiesel source material and chemical structure on emissions of criteria pollutants from a heavy-duty engine.* Environmental Science & Technology, 2001. **35**(9): p. 1742-1747.
16. McCormick, R.L., et al., *Effects of Biodiesel Blends on Vehicle Emissions: Fiscal Year 2006 Annual Operating Plan Milestone 10.4*, 2006, National Renewable Energy Laboratory (NREL), Golden, CO.
17. Mueller, C.J., A.L. Boehman, and G.C. Martin, *An experimental investigation of the origin of increased NOx emissions when fueling a heavy-duty compression-ignition engine with soy biodiesel.* SAE paper, 2009: p. 01-1792.

18. Zhang, Y. and A.L. Boehman, *Impact of biodiesel on NO x emissions in a common rail direct injection diesel engine.* Energy & Fuels, 2007. **21**(4): p. 2003-2012.
19. Koebel, M., M. Elsener, and M. Kleemann, *Urea-SCR: a promising technique to reduce NOx emissions from automotive diesel engines.* Catalysis today, 2000. **59**(3–4): p. 335-345.
20. Nakada, K., et al., *Automatic Control of NO Removal by Ozone Injection Method.* Proceeding of International Journal of Plasma Environmental Science & technology, 2006. **1**(1).
21. Depcik, C., D. Assanis, and K. Bevan, *A one-dimensional lean NOx trap model with a global kinetic mechanism that includes NH3 and N2O.* International Journal of Engine Research, 2008. **9**(1): p. 57-77.
22. Smith, M.A., et al., *Modeling of SCR NH[sub 3] Storage in the Presence of H[sub 2]O.* ASME Conference Proceedings, 2011. **2011**(44427): p. 727-738.
23. Smith, M.A., et al. *NO Reaction Pathways With NH on an Fe-Zeolite SCR Catalyst*. 2011. ASME.
24. Yanying, W., S. Raman, and J.W. Grizzle. *Dynamic modeling of a lean NO_x trap for lean burn engine control*. in *American Control Conference, 1999. Proceedings of the 1999*. 1999.
25. Okubo, M., et al. *Total diesel emission control system using ozone injection and plasma desorption*. 2005. IEEE.
26. Fujishima, H., et al., *Improvement in NOx Removal Performance of the Pilot-Scale Boiler Emission Control System Using an Indirect Plasma–Chemical Process.* Industry Applications, IEEE Transactions on, 2010. **46**(5): p. 1722-1729.
27. Shoyama, T. and Y. Yoshioka, *Theoretical study of methods for improving the energy efficiency of NOx removal from diesel exhaust gases by silent discharge.* Electrical Engineering in Japan, 2007. **161**(3): p. 1-9.
28. Yamamoto, T., et al., *PM and NOx Removal for Diesel Engine Emission Using Ozonizer and Chemical Hybrid Reactor.* Industry Applications, IEEE Transactions on, 2008. **44**(5): p. 1431-1435.
29. Mohammadi, A., et al., *A study on diesel emission reduction using a high-frequency dielectric barrier discharge plasma.* SAE TRANSACTIONS, 2003. **112**(4): p. 1524-1531.
30. Levendis, Y.A. and C. Larsen, *Use of ozone-enriched air for diesel particulate trap regeneration.* 1999.
31. Depcik, C., *Simulating the Concentration Equations and the Gas-Wall Interface for One-Dimensional Based Diesel Particulate Filter Models.* Journal of Engineering for Gas Turbines and Power, 2010. **132**: p. 032803.
32. Depcik, C. and D. Assanis, *Simulating Area Conservation and the Gas-Wall Interface for One-Dimensional Based Diesel Particulate Filter Models.* Journal of Engineering for Gas Turbines and Power, 2008. **130**: p. 062807.
33. Tachibana, T., et al., *Effect of ozone on combustion of compression ignition engines.* Combustion and flame, 1991. **85**(3-4): p. 515-519.
34. Westbrook, C.K. and F.L. Dryer, *Chemical kinetic modeling of hydrocarbon combustion.* Progress in energy and combustion science, 1984. **10**(1): p. 1-57.

35. Clothier, P., et al., *How do diesel-fuel ignition improvers work?* Chemical Society Reviews, 1993. **22**(2): p. 101-108.
36. Faison, I.L., *The Effect of Ozone on Diesel Soot Precursors*, 1997, Virginia Polytechnic Institute and State University.
37. Nasser, S.H., S. Morris, and S. James, *A Novel Fuel-Efficient and Emission-Abatement Technique for Internal-Combustion Engines.* SAE TRANSACTIONS, 1998. **107**: p. 1410-1425.
38. Golovitchev, V.I. and J. Chomiak, *Evaluation of Ignition Improvers for Methane Autoignition.* Combustion Science and Technology, 1998. **135**(1-6): p. 31-47.
39. Yamada, H., et al., *Controlling mechanism of ignition enhancing and suppressing additives in premixed compression ignition.* International Journal of Engine Research, 2005. **6**(4): p. 331-340.
40. Mohammadi, A., et al., *Study on Combustion Control in Natural-Gas PCCI Engines with Ozone Addition into Intake Gas.* 2006.
41. *Kinetics Database Resources*. 2000 [cited 2011 7/5]; Available from: http://kinetics.nist.gov/kinetics/rpSearch?cas=10028156.
42. Center, R. and R. Kung, *Shock tube study of the thermal decomposition of O3 from 1000 to 3000 K.* Journal of Chemical Physics, 1975. **62**: p. 802-807.
43. Chang, J.S., P.A. Lawless, and T. Yamamoto, *Corona discharge processes.* Plasma Science, IEEE Transactions on, 1991. **19**(6): p. 1152-1166.
44. Jones, W.M. and N. Davidson, *The Thermal Decomposition of Ozone in a Shock Tube1.* Journal of the American Chemical Society, 1962. **84**(15): p. 2868-2878.
45. Kitayama, J. and M. Kuzumoto, *Theoretical and experimental study on ozone generation characteristics of an oxygen-fed ozone generator in silent discharge.* Journal of Physics D: Applied Physics, 1997. **30**: p. 2453.
46. Kitayama, J. and M. Kuzumoto, *Analysis of ozone generation from air in silent discharge.* Journal of Physics D: Applied Physics, 1999. **32**: p. 3032.
47. Luther, K., K. Oum, and J. Troe, *The role of the radical-complex mechanism in the ozone recombination/dissociation reaction.* Phys. Chem. Chem. Phys., 2005. **7**(14): p. 2764-2770.
48. Myers, B. and E. Bartle, *Shock Tube Study of the Radiative Processes in Systems Containing Atomic Oxygen and Carbon Monoxide at High Temperature.* The Journal of Chemical Physics, 1967. **47**: p. 1783.
49. Ombrello, T., et al., *Flame propagation enhancement by plasma excitation of oxygen. Part I: Effects of O3.* Combustion and flame, 2010. **157**(10): p. 1906-1915.
50. McCrumb, J. and F. Kaufman, *Kinetics of the O+O Reaction.* The Journal of Chemical Physics, 1972. **57**: p. 1270.
51. Westbrook, C.K., *Chemical kinetics of hydrocarbon ignition in practical combustion systems.* Proceedings of the Combustion Institute, 2000. **28**(2): p. 1563-1577.
52. Benson, S.W. and A.E. Axworthy Jr, *Mechanism of the gas phase, thermal decomposition of ozone.* The Journal of Chemical Physics, 1957. **26**: p. 1718.
53. Johnston, H.S., *Gas phase reaction kinetics of neutral oxygen species*, 1968, DTIC Document.

54. Nishida, H. and T. Tachibana, *Homogeneous charge compression ignition of natural gas/air mixture with ozone addition.* Journal of propulsion and power, 2006. **22**(1): p. 151-157.
55. Viner, A.S., et al., *Ozone generation in DC-energized electrostatic precipitators.* Industry Applications, IEEE Transactions on, 1992. **28**(3): p. 504-512.
56. Kee, R.J., et al., *Chemkin-III: A Fortran Chemical Kinetics Package for the Analysis of Gas-Phase Chemical and Plasma Kinetics*, 1996, Sandia National Laboratories.
57. Hampson, R.F., et al., *Survey of Photochemical and Rate Data for Twenty eight Reactions of Interest in Atmospheric Chemistry.* Journal of Physical and Chemical Reference Data, 1973. **2**: p. 267.
58. Intezarova, E. and V. Kondrat'ev, *Thermal decomposition of ozone.* Russian Chemical Bulletin, 1967. **16**(11): p. 2326-2331.
59. Krezenski, D.C., R. Simonaitis, and J. Heicklen, *The reactions of O (3P) with ozone and carbonyl sulfide.* International Journal of Chemical Kinetics, 1971. **3**(5): p. 467-482.
60. Schiff, H., *Neutral reactions involving oxygen and nitrogen.* Canadian Journal of Chemistry, 1969. **47**(10): p. 1903-1916.
61. Molina, M.J. *The Nobel Prize in Chemistry 1995*. 1995 [cited 2012; Available from: http://molina.hitunic.com/1.htm.
62. Hindmarsh, A.C. *Serial Fortran Solvers for ODE Initial Value Problems*. [Internet] 2002 August 5, 2002 [cited 2006 April 18]; Available from: http://www.llnl.gov/CASC/odepack/.
63. Han, M., *Speciation of diesel fuel.* 2006.
64. Mati, K., et al., *The oxidation of a diesel fuel at 1-10 atm: Experimental study in a JSR and detailed chemical kinetic modeling.* Proceedings of the Combustion Institute, 2007. **In Press, Corrected Proof**.
65. Pereira, C., et al., *Liquid Fuel Reformer Development: Autothermal Reforming of Diesel Fuelt.* U.S. Department of Energy 2000 Hydrogen Program Technical Review San Ramon, California, 2000.
66. Jonaitis, T.J., *Final Analytical Report*, 2005, Paragon Laboratories Inc.
67. Tsolakis, A. and S.E. Golunski, *Sensitivity of process efficiency to reaction routes in exhaust-gas reforming of diesel fuel.* Chemical Engineering Journal, 2006. **117**(2): p. 131-136.
68. Warnatz, J., *Experimental and computational study of ignition and flame propagation in internal combustion engines.* Endeavour, 1996. **20**(1): p. 31-36.
69. Ó Conaire, M., et al., *A Comprehensive Modeling Study of Hydrogen Oxidation.* International Journal of Chemical Kinetics, 2004. **36**(11): p. 603-621.
70. Konnov, A.A., *Remaining uncertainties in the kinetic mechanism of hydrogen combustion.* Combustion and Flame, 2008. **152**(4): p. 507-528.
71. Li, J., et al., International Journal of Chemical Kinetics, 2004. **36**: p. 566-575.
72. Mueller, M.A., et al., *Flow reactor studies and kinetic modeling of the H-2/O-2 reaction.* International Journal of Chemical Kinetics, 1999. **31**(2): p. 113-125.
73. Saxena, P. and F.A. Williams, *Testing a small detailed chemical-kinetic mechanism for the combustion of hydrogen and carbon monoxide.* Combustion and Flame, 2006. **145**(1-2): p. 316-323.

74. Goswami, M., et al., *Updated Kinetic Mechanism for NO_x Prediction and Hydrogen Combustion*, 2008, Technische Universiteit Eindhoven: Eindhoven, The Netherlands.
75. Konnov, A.A., *Implementation of the NCN pathway of prompt-NO formation in the detailed reaction mechanism.* Combustion and Flame, 2009. **156**(11): p. 2093-2105.
76. Konnov, A.A., *Development and validation of a detailed reaction mechanism for the combustion of small hydrocarbons*, in *28th Symposium (Int.) on Combustion*2000: Edinburgh.
77. Smith, G.P., et al. *GRI-MECH 3.0*. 2008 [cited 2008 September 7]; Available from: http://www.me.berkeley.edu/gri_mech/
78. Yamada, H., M. Yoshii, and A. Tezaki, *Chemical mechanistic analysis of additive effects in homogeneous charge compression ignition of dimethyl ether.* Proceedings of the Combustion Institute, 2005. **30**(2): p. 2773-2780.
79. Das, L.M., *Hydrogen engines: A view of the past and a look into the future.* International Journal of Hydrogen Energy, 1990. **15**(6): p. 425-443.
80. Löffler, G., et al., *NOx formation in natural gas combustion—a new simplified reaction scheme for CFD calculations.* Fuel, 2006. **85**(4): p. 513-523.
81. Dec, J.E., *A conceptual model of DI diesel combustion based on laser-sheet imaging.* SAE, 1997. **1997**(412).
82. Dec, J.E., *Advanced compression-ignition engines--understanding the in-cylinder processes.* Proceedings of the Combustion Institute, 2009. **32**(2): p. 2727-2742.
83. Cecrle, E.D., *Controls and Measurements of KU Engine Test Cells for Biodiesel, SynGas, and Assisted Biodiesel Combustion.* 2011.
84. Serrano, D.P., J. Dufour, and D. Iribarren, *On the feasibility of producing hydrogen with net carbon fixation by the decomposition of vegetable and microalgal oils.* Energy Environ. Sci., 2012.